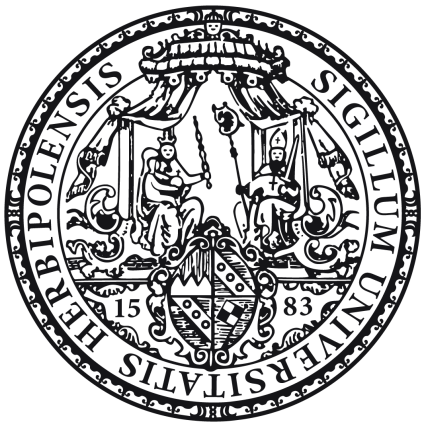

Differential parathyroid hormone receptor signaling directed by adaptor proteins

Steuerung differenzieller Signalgebung des Parathormon Rezeptors durch Adapterproteine

Doctoral thesis for a doctoral degree
at the Graduate School of Life Sciences,
Julius-Maximilians-Universität Würzburg,

Section Biomedicine

submitted by
Alexander Emami-Nemini
from
Braunschweig

Würzburg 2012

Submitted on: ……..……..

Members of the *Promotionskomitee*:

Chairperson:	Michael Sendtner
Primary Supervisor:	Martin J. Lohse
Supervisor (Second):	Caroline Kisker
Supervisor (Third):	Thomas Müller
Supervisor (Fourth):	Antje Gohla

Date of Public Defense: ……

Date of receipt of Certificates: ……..

In 'modern' bio-molecular research, we are merely trying to uncover principles that had the beginning four billion years ago; at the start of life.

Dedication

I would like to dedicate this work to three special persons; my parents, Lucja and Hossein, who are of value beyond words for me. They transmitted me their life values and I owe a perpetual debt of gratitude to them for their support since 28 years. My heartfelt thanks go to my girlfriend Rebecca. Thank you for five wonderful years and our special relationship.

Widmung

Ich möchte diese Arbeit drei einzigartigen Personen widmen; meinen Eltern, Lucja und Hossein, die von unbeschreiblichem Wert für mich sind. Sie gaben mir ihre Werte des Lebens mit auf den Weg und ich schulde Ihnen große Dankbarkeit für ihre Unterstützung seit 28 Jahren. Meine vom Herzen kommende Dankbarkeit gilt meiner Freundin Rebecca. Danke, für fünf wundervolle Jahre und unsere einzigartige Beziehung.

Summary

The superfamily of G protein-coupled receptors (GPCR) regulates numerous physiological and pathophysiological processes. Hence GPCRs are of significant interest for pharmacological therapy. Embedded into cytoplasmic membranes, GPCRs represent the core of large signaling complexes, which are critical for transduction of exogenous stimuli towards activation of downstream signaling pathways.

As a member of the GPCR family B, the parathyroid hormone receptor (PTHR) activates adenylyl cyclases, phospholipases C β as well as mitogen-activated protein kinase-dependent signaling pathways, thereby mediating endocrine and paracrine effects of parathyroid hormone (PTH) and parathyroid hormone-related peptide (PTHrP), respectively. This regulates, calcium homeostasis, bone metabolism and bone development. Paradoxically, PTH is able to induce both catabolic and anabolic bone metabolism. The anabolic effect of PTH is successfully applied in the therapy of severe osteoporosis. Domination of anabolic or catabolic bone-metabolism is entailed by temporal and cell-type specific determinants. The molecular bases are presumably differential arrangements of adaptor proteins within large signaling complexes that may lead to differential activation of signaling pathways, thereby regulating physiological effects. The molecular mechanisms are largely unclear; thus, there is significant interest in revealing a better understanding of PTHR-related adaptor proteins.

To identify novel adaptor proteins which direct PTHR signaling pathways, a proteomic screening approach was developed. In this screening, vav2, a guanine-nucleotide exchange factor (GEF) for small GTPases which regulates cytoskeleton reorganization, was found to interact with intracellular domains of PTHR. Evidence is provided that vav2 impairs PTH-mediated phospholipase C β (PLCβ) signaling pathways by competitive interactions with G protein α_q subunits. Vice versa, PTH was shown to regulate phosphorylation and subsequent GEF activity of vav2. These findings may thus shed new light on the molecular mechanisms underlying the effects of PTH on bone metabolism by PLC-signaling, cell migration and cytoskeleton organization.

In addition to the understanding of intracellular molecular signaling processes, screening for ligands is a fundamental and demanding prerequisite for modern drug development. To this end, ligand binding assays represent a fundamental technique. As a substitution for expensive and potentially harmful radioligand binding, fluorescence-based ligand-binding assays for PTHR were developed in this work. Based on time-resolved fluorescence, several assay variants were established to facilitate drug development for the PTHR.

Zusammenfassung

Die Superfamilie der G-Protein-gekoppelten Rezeptoren (GPCRs) reguliert eine Vielzahl von physiologischen und pathophysiologischen Prozessen, was sie bedeutend für die Pharmakotherapie macht. Eingebettet in die Zytoplasmamembran sind GPCRs das Zentrum von Signalkomplexen, die eine Transduktion äußerer Stimuli zur Aktivierung von nachgeschalteten Signalwegen ermöglichen.

Der zur Familie B der GPCRs gehörige Parathormon-Rezeptor (PTHR) aktiviert Adenylyl-Zyklasen-, Phospholipasen Cβ- und Mitogen-aktivierte Proteinkinase (MAPK)-abhängige Signalwege, wodurch endokrine und parakrine Wirkungen des Parathormons (PTH) und des Parathormon-ähnlichen Peptides (PTHrP) vermittelt werden. Dies ermöglicht die Regulation der Calcium-Homöostase, des Knochenmetabolismus und der Knochenentwicklung. Paradoxerweise kann PTH sowohl katabole als auch anabole Effekte auf den Knochenstoffwechsel induzieren. Den anabolen Effekt von PTH nutzt man erfolgreich in der Therapie der schweren Osteoporose. Ob ein anaboler oder kataboler Knochenmetabolismus überwiegt, wird durch zeitliche und Zelltyp-spezifische Faktoren bestimmt. Dem zugrunde liegt vermutlich unter anderem eine differenzielle Anordnung verschiedener Adapterproteine innerhalb der Signalkomplexe, die zur differenziellen Aktivierung von Signalwegen führen und so eine Steuerung bestimmter physiologischer Effekte ermöglichen. Die molekularen Mechanismen sind jedoch noch weitgehend unklar, weshalb großes Interesse besteht, ein besseres Verständnis über die PTHR-assoziierten Adapterproteine zu entwickeln.

Zur Identifizierung neuer Adapterproteine, die PTHR-Signalwege beeinflussen, wurde in dieser Arbeit ein auf dem Proteom-basierender Screening-Ansatz entwickelt. Dieser führte zur Entdeckung einer Interaktion von intrazellulären Domänen des PTHR mit vav2, einem Guanin-Nukleotid Austauschfaktor (GEF) für kleine GTPasen, der die Zytoskelett-Reorganisation steuert. Des Weiteren wurde nachgewiesen, dass vav2 über kompetitive Interaktionen mit G Protein α_q Untereinheiten PTH-vermittelte Phospholipase Cβ (PLCβ)-abhängige Signalwege beeinflusst. Umgekehrt wurde gezeigt, dass PTH die Phosphorylierung und damit die GEF Aktivität von vav2 reguliert. Diese Befunde können Aufschluss über molekulare Mechanismen geben, die den Wirkungen von PTH auf den Knochenstoffwechsel durch PLC-Signalwege, Zellmigration und Zytoskelett-Reorganisation zugrunde liegen.

Neben dem Verständnis über molekulare Prozesse der intrazellulären Signalgebung ist die Suche nach Liganden eine herausfordernde Grundvoraussetzung für die aktuelle Arzneistoffentwicklung. Liganden-Bindungs-Experimente stellen dafür elementare Techniken dar. Zur Substitution kostenintensiver und potentiell gesundheitsschädlicher Radioliganden-Bindungen, wurden in dieser Arbeit Fluoreszenz-basierte Liganden-Bindungs-Experimente für den PTHR entwickelt. Basierend auf Zeit-aufgelöster Fluoreszenz wurden mehrere Varianten dieser Experimente etabliert, um die Arzneistoffentwicklung am PTHR zu unterstützen.

Table of Contents

1. Introduction

1.1. Background

Living cells were defined as the basic functional and autonomic unit of organisms by Rudolf Ludwig Karl Virchow (1821-1902). This hypothesis emerged to be the basis for modern physiology and pathophysiology. Nowadays, biomedical research focuses on smaller structures such as molecules and molecule complexes; nevertheless, cellular states are fundamental readouts for investigations on the level of molecules. Autonomy of cells claimed by Rudolf Virchow is well applied to cell division and metabolism, but in complex organisms one hundred trillion cells and over two hundred cell-types need to be well-orchestrated for proper organ function and consequent viability of the organism. As it is true for civilizations, communication is a critical skill within organisms. In organisms, transmitters enable cell-cell communication over short distances via interstitial fluids, or long distances via the blood. These signals need to be recognized on the cell surfaces, therefore a variety of cell surface proteins evolved. The largest family of cell surface receptors is represented by G protein coupled-receptors (GPCRs) [1].

1.2. G protein-coupled receptors

The capability of G protein-coupled receptors to bind guanine nucleotide-binding proteins (G proteins) was the first common characteristic found and therefore became eponymous. Also common for GPCRs is the signature of seven trans-membrane domains, composed of alpha-helices which penetrate the lipid bilayer of membranes. Consequently, GPCRs are anchored in the cytoplasmic membrane and transduce chemical stimuli (hormones, peptides, ions, lipids, and neurotransmitter) as well as sensory stimuli (light and odors) in quality and quantity into the cell. This diversity of stimuli is recognized by more than 800 different G protein-coupled receptors [2]. GPCRs are a prerequisite for numerous physiological and pathophysiological processes. Remarkably, approximately one third of currently used drugs target GPCRs, thus GPCRs represent the major segment of drug targets in pharmacological treatment of pathophysiological states [3].

1.2.1. Signal transduction via G proteins

Recognition of hormones like adrenalin or acetylcholine takes place at the trans-membrane regions of GPCRs. This recognition is a close, non-covalent molecule interaction, simply named as binding, which leads to conformational changes of the receptor. The change of conformation, which primarily depends on the kind of the ligand, leads to signal transduction to cytosolic signaling proteins. The most studied cytosolic signaling proteins for GPCRs are heterotrimeric G proteins, which consist of α, β and γ subunits. Several steps are involved in the activation process and the recycling of G proteins. The inactive form of Gα subunits is GDP-bound and exhibits high affinities to the Gβ and Gγ subunits. Interactions with intracellular domains of activated GPCRs catalyze GDP/GTP exchange thereby activating Gα. The affinity of active Gα to Gβγ is reduced and subsequently leads to dissociation of α- and βγ-subunits [4]. Dissociated and active G protein subunits then transduce the signal to further downstream effectors, such as adenylyl cyclases (AC). One receptor is capable of activating numerous G proteins, and in turn activated G proteins trigger generation of second messengers. Thus, generation of second-messenger represents a mechanism for multiplying signals of GPCRs. Finally, the intrinsic GTPase of Gα hydrolyzes GTP and thereby renders the G protein to ground state.

Multiple mammalian genes encode for G protein subunits; Sixteen genes encode for Gα, 5 genes for Gβ, and Gγ is encoded by 12 genes [5]. This variation of subunits is capable of activating or inhibiting various downstream effectors [2]. Gα subunits can be divided into four subfamilies; $G\alpha_s$, $G\alpha_i$, $G\alpha_q$ and $G\alpha_{12}$. $G\alpha_s$ activates AC leading to the generation of 3'-5'-cyclic adenosine monophosphate (cAMP). In contrast to $G\alpha_s$, $G\alpha_i$ subunits inhibit AC activity and regulate G protein-coupled inwardly-rectifying potassium (GIRK) channels [6]. The subfamily of $G\alpha_q$ subunits activates phospholipase Cβ (PLCβ) [2]. Activated PLCβ cleaves phosphatidylinositol-4,5-diphosphate (PIP_2) into the second-messengers diacylglycerol (DAG) and inositol 1,4,5 trisphosphate (IP_3). The family of $G\alpha_{12}$ subunits was found to activate nucleotide exchange factors (GEFs) of the Ras homology gene family (Rho) of small GTPases (GTP hydrolyzing enzymes). Beside the effects of Gα subunits, Gβγ subunits are capable of activating ACII, ACIV and PLCβ 1, 2, 3 [7-9]. Furthermore, Gβγ subunits regulate the function of G-protein coupled receptor kinases (GRK), a family of protein kinases that in turn regulates the function of GPCRs; GIRK channels which are GPCR-regulated potassium channels in the central nervous system and the heart; and phosphoinositol-3-kinases gamma (PI3Kγ) [10-12].

The molecular activation mechanisms of G proteins are currently explained by two competing models, the collision coupling and the precoupling model. In the collision coupling model, G proteins and receptors are believed to collide by free diffusion, thereby inducing the activation of G proteins. Activated receptors display an increased affinity to G proteins. Hereby, different

types of activated receptors may compete for the same G protein pool. However, such a competition would be in conflict with receptor-specific G protein activation. Moreover, collision models do not explain sub-second kinetics that can be observed for GPCR signaling. Consequently, it is questionable whether G protein-GPCR coupling is controlled by simple collision kinetics [13, 14].

In contrast, the precoupling model suggests the G protein to be bound to the receptor prior to agonist binding and receptor activation. Thus, activated receptors directly trigger activation of G proteins without underlying the kinetics of diffusion for a collision. It may be assumed that the precoupling model is more reasonable in terms of signaling kinetics and specificity for the GPCR G protein coupling [15].

Taken together interactions between G proteins and GPCRs enable signal transduction and determine potency of bound ligand. Furthermore, this interaction has influence on the affinity of ligands to GPCRs. This relation is explained by a ternary complex model of GPCRs **(Figure 1)**. The ternary complex model describes the formation of a high affinity complex between GPCR, G protein and ligand [16, 17]. This complex is either formed by coupling of the nucleotide-free G protein to the GPCR followed by binding of the agonist, or vice versa. The ternary complex facilitates the activation of the G protein by the exchange of GDP for GTP which leads to activation of effector proteins. The recently obtained crystal structure of the active ternary complex composed of agonist-bound beta-adrenergic receptor 2 (β_2AR) and nucleotide-free Gα_s shed light on the molecular arrangement of receptor-induced G protein activation [18]. This study identified the N- and C-terminal α-helices of Gα_s as the critical interfaces for receptor interaction. Interactions with the N- and C-terminal α-helices of Gα_s induce conformational changes of the nucleotide-binding pocket, thereby enabling nucleotide exchange [18].

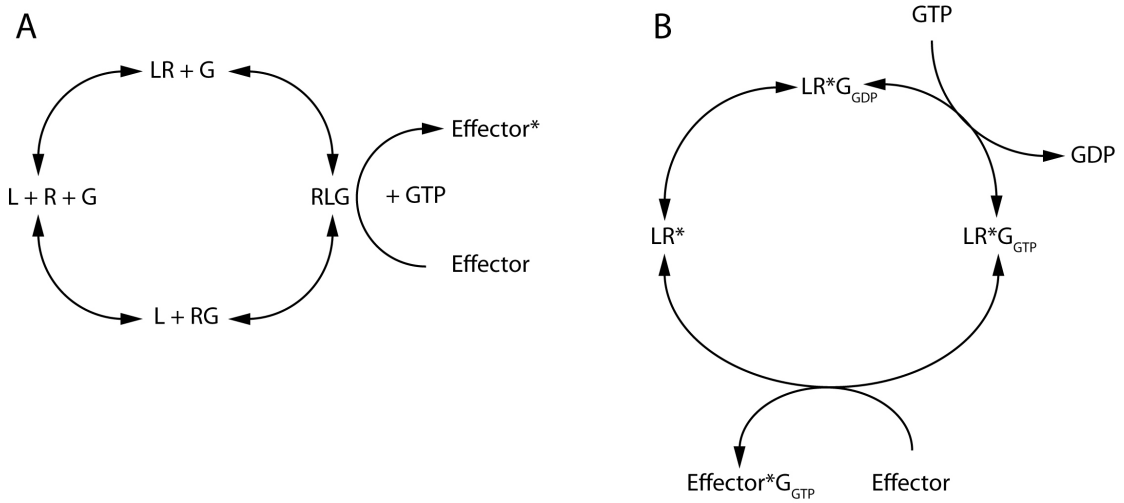

Figure 1. The ternary complex (a) and enzymatic G protein activation model (b) [17]. (a) Receptor (R) binds either agonist ligand (L) or G protein (G) in random order. RG represents a precoupled G protein receptor complex, whereas LR represents an agonist-bound receptor conformation with low-affinity. The agonist-bound receptor or the G protein-precoupled receptor complex subsequently recognizes a G protein or agonist, respectively. Thereby, the high affinity complex RLG is formed. After dissociation of the RLG complex, an effector is activated (Effector*) in the presence of GTP [17]. **(b)** The enzymatic model of G protein activation. Binding of agonists (L) induces the active state of the receptor (R*). Here, R* is taken as enzyme and L as allosteric activator. First, LR* binds G_{GDP} and second, GDP is exchanged for GTP. Thus, LR* catalyzes G protein activation by coupling and exchange of GDP for GTP more efficiently than inactive receptors. GTP-bound G proteins (G_{GTP}) dissociate from the receptor and G protein subunits (α, βγ) induce effector activation. Thus, the enzyme, LR*, is released to activate another G protein. [19, 20].

1.2.2. β-Arrestin

Initially, β-arrestin was found as a cofactor of beta-adrenergic receptor kinase (β-ARK)-induced receptor desensitization [21]. For GPCRs, desensitization represents the process of receptor phosphorylation and subsequent internalization from the plasma membrane to intracellular compartments, thereby inhibiting further recognition of exogenous stimuli. The importance of the desensitization process, which arrests beta-adrenergic signaling, was eponymous for β-arrestin. Further studies demonstrated β-arrestin recruitment to almost all GPCRs. β-arrestin recruitment induces receptor internalization and is triggered by phosphorylation of GPCRs via G protein-coupled receptor kinases [22, 23]. Moreover, the relevance of β-arrestins for receptor signal transduction gained in interest. Nowadays, β-arrestins are known to be multifunctional signal adaptor proteins for signaling pathways independent from G proteins. Four arrestin subtypes are known; arrestin 1 (visual arrestin) is expressed in cone and rod photoreceptor cells, whereas arrestin 4 (cone arrestin) is solely expressed in cone cells. Arrestin 2 and 3, also known as β-arrestin 1 and 2, respectively, are non-visual arrestin and ubiquitously expressed.

1.2.3. G protein-independent signal transduction by GPCRs

Classical GPCR signaling pathways via G proteins and second messengers are not sufficient to explain some well-known effects of GPCRs on cell-growth and differentiation [24, 25]. Numerous studies indicate that GPCRs may activate mitogen-activated protein kinase cascades (MAPK) independent of G protein activation. Several signaling mechanisms are believed to contribute to GPCR-mediated MAPK activation, including transactivation of receptor tyrosine kinases, such as epidermal-growth factor receptor (EGFR), scaffolding by integrin-based focal adhesion and the GPCR-based scaffolding function [26]. Scaffolding induced by GPCRs requires phosphorylation-induced desensitization via β-arrestin. As mentioned above, receptor activation induces phosphorylation and consequently recruitment of β-arrestin. Subsequently, β-arrestin serves as scaffold for Src and the activated receptor, and both are directed to clathrin-coated pits. Thereby, the GPCR/β-arrestin/Src signaling complex likewise transactivates EGFR and subsequently extracellular-signal regulated kinase (ERK) [26].

1.2.4. Biased agonism

Recognition of agonists by GPCRs may drive the signaling activity of a receptor in two directions; increasing or decreasing basal activity. Thus, agonists are entitled positive or inverse agonists. Positive agonists can be classified into partial and full agonists which increase basal activity partially and to the maximum, respectively. The direction and magnitude of agonist efficacy is not constitutive for agonists and may vary between different receptors. In addition, the effects of agonists on different signaling pathways are not inherently linked and can be distinguished [27]. For instance, GPCR-mediated activation of G protein-dependent and β-arrestin-dependent signaling pathways can be separated [28]. Thus, some agonists are able of selectively activating these pathways. This phenomenon was named biased agonism [29]. The detailed underlying molecular mechanism for biased agonism may vary for each ligand or receptor. However, ligand-specific receptor conformations which selectively lead to arrangement of receptor-related signaling complexes might represent a common principle for biased agonism.

The value of biased agonism can be appreciated by considering the hypothesis that in pharmacological treatment one pathway might be responsible for therapeutic effects of drugs, whereas another is mediating adverse effects. Consequently, the principle of biased agonism may contribute to the development of more effective and more tolerant drugs.

1.2.5. Classification of GPCRs

Classification of GPCR is based on sequence homology and functional properties. Four main classes should be mentioned, each class itself is divided into subfamilies with respect to their recognized ligand families. The class A (or 1) were named as rhodopsin-like and represent the largest group with about 85% of all GPCRs. Class A includes, inter alia, adrenergic, acetylcholine, cannabinoid, chemokine and numerous olfactory receptors. The class B (or 2), named the secretin receptor family, is typically targeted by peptide hormones. The class B includes receptors for calcitonin, parathyroid hormone, corticotropin-releasing factor secretin and glucagon. The class C (or 3) includes metabotropic glutamate receptors (mGlu), extracellular calcium-sensing receptor-related (CaSR) and gamma-aminobutyric acid (GABA) receptors [30, 31]. The fourth class, named frizzled family receptors, includes receptors which are targeted by secreted palmitoylated signaling proteins [32]. Taxonomically, two additional classes of GPCRs are known, named cyclic AMP receptors and fungal mating pheromone receptors, which are of minor significance to this day.

1.3. The parathyroid hormone receptor

The parathyroid hormone receptor type 1 (PTHR) was first cloned and characterized in 1991 by Jüppner et al. [33]. As a member of class B GPCRs, the PTHR is conserved in fish, amphibians and mammalians, including humans. In addition to predominant expression in bone and kidney cells, PTHR are expressed in numerous cell types including heart, aorta, brain, cerebellum, breast, skin, spleen, ileum, liver, lung, skeletal muscle, adrenal gland, bladder, ovary, testes, placenta, uterus and stomach [34, 35]. The location of the PTH/PTHrP receptor gene was determined in the region 3p21.1-p24.2 of the short arm of human chromosome 3 [36]. The PTH/PTHrP receptor gene ranges over 22 kb and contains at least 15 exons and 14 introns [37]. Exon U is the most 5’ exon. The next exon, exon S, encodes for the initiator methionine and the signal peptide. Exons E1, E2, E3 and G encode for the large extracellular domain, whereas exons M1-M7 encode for trans-membrane domain. Exon EL2 encodes for the second extracellular loop and the exon T is coding for the large C-terminal tail of the PTHR [37]. In addition to the PTHR, a parathyroid hormone receptor type 2 (PTHR2) was identified in 1995 by Usdin et al. [38]. Particularly expressed in brain and pancreas, the PTHR2 exhibits a more specific tissue distribution than the PTHR1 [38]. PTHR2 signaling was reported to inhibit chondrocyte proliferation and differentiation [39]. To date, the physiological role of the PTHR2 is not clear;

however, a neuroendocrine function is suggested, since abundant expression of PTHR2 in the nervous system was reported [40].

1.3.1. Structure-function relationships of the PTHR

The PTHR cDNA encodes for 593 amino acids. As common for class B GPCRs, the PTHR harbors a large extracellular N-terminal domain of about 191 amino acids. The signal peptide consists of the first 22 amino acids targeting the receptor to the cell membrane [41].

To date, solely the structure of the isolated extracellular domain of the PTHR has been determined by X-ray crystallography [42-44]. The secondary structure of the PTHR extracellular domain is arranged into a three-layer α-β-β-α fold which is held together by three interlayer disulfide bonds thereby forming the ligand-binding pocket **(Figure 3)**. In more detail, the first disulfide bond (C^{48}-C^{117}) links the N-terminal α-helix to the middle layer β-sheet. The second disulfide bond (C^{108}-C^{148}) connects the middle and the bottom β-sheets. The third disulfide bond (C^{131}–C^{170}) links the middle layer of β-sheets with the C-terminal α-helix **(Figure 3)** [42]. However, four disulfide bonds are present within the PTHR **(Figure 2)**. The fourth disulfide bond is formed by cysteine residues between extracellular loops 1 and 2 of the PTHR. This disulfide bond is not described in the crystal structure, although it is assumed to connect the first and the second extracellular loop of the PTHR. In addition, the crystal structure revealed the amino acids encoded by the exon E2 to be disordered [42]. This observation is consistent with findings that a proteolytic cleavage occurs within exon E2 and that this region is dispensable for ligand binding [45, 46]. Notably, this proteolytic cleavage can be avoided by the presence of PTH. N-Glycosylation of the PTHR takes place at asparagine residues 151, 161, 166 and 176, which are encoded in exon G **(Figure 2)** [47]. The role of PTHR glycosylation remains elusive, since non-glycosylated PTHRs are functional in terms of binding, membrane expression and signaling [47].

Three intracellular loops and the large C-terminal tail represent the interface for interactions with signaling and adaptor proteins. At the second intracellular loop, K^{319} has been implicated in $G\alpha_q$ signaling [48]. Residues in the third intracellular loop V^{384} and L^{385} are believed to be responsible for $G\alpha_q$ coupling, T^{387} for $G\alpha_s$ coupling and K^{388} for both, $G\alpha_s$ and $G\alpha_q$ coupling [49]. Activation of the PTHR induces phosphorylation of intracellular serine residues by G protein-coupled receptor kinases (GRKs). This phosphorylation triggers β-arrestin recruitment and subsequently interaction with the clathrin-mediated endocytosis machinery resulting in receptor internalization [50, 51]. At the C-terminal tail, eight serine residues are targets for protein kinases. Mutation of serine residues S^{491}, S^{492}, S^{493}, as well as S^{501} or S^{504} enhanced

coupling to $G\alpha_{q/11}$ and eliminated receptor internalization [52, 53]. Mutations of PTHR, which result in clinically relevant phenotypes, are rare. However, in patients, three mutations have been attributed to Jansen's metaphyseal chondrodysplasia, a disease which is characterized by dwarfism or short stature, disorganized metaphyseal regions, hypercalcaemia and hypophosphatemia [54]. These mutations occur at TM2 (R^{233} to H), TM6 (T^{410} to P) and TM7 (I^{458} to R) and result in cAMP signaling independent of agonists, a phenomenon called constitutive activity [55]. Further studies on Jansen mutations revealed new findings on receptor internalization. The $T^{410}P$ mutation proved T^{410} to be necessary for receptor internalization in addition to cAMP signaling and β-arrestin binding [56, 57]. This finding led to the conclusion that conformational changes are direct requirements for internalization processes [54].

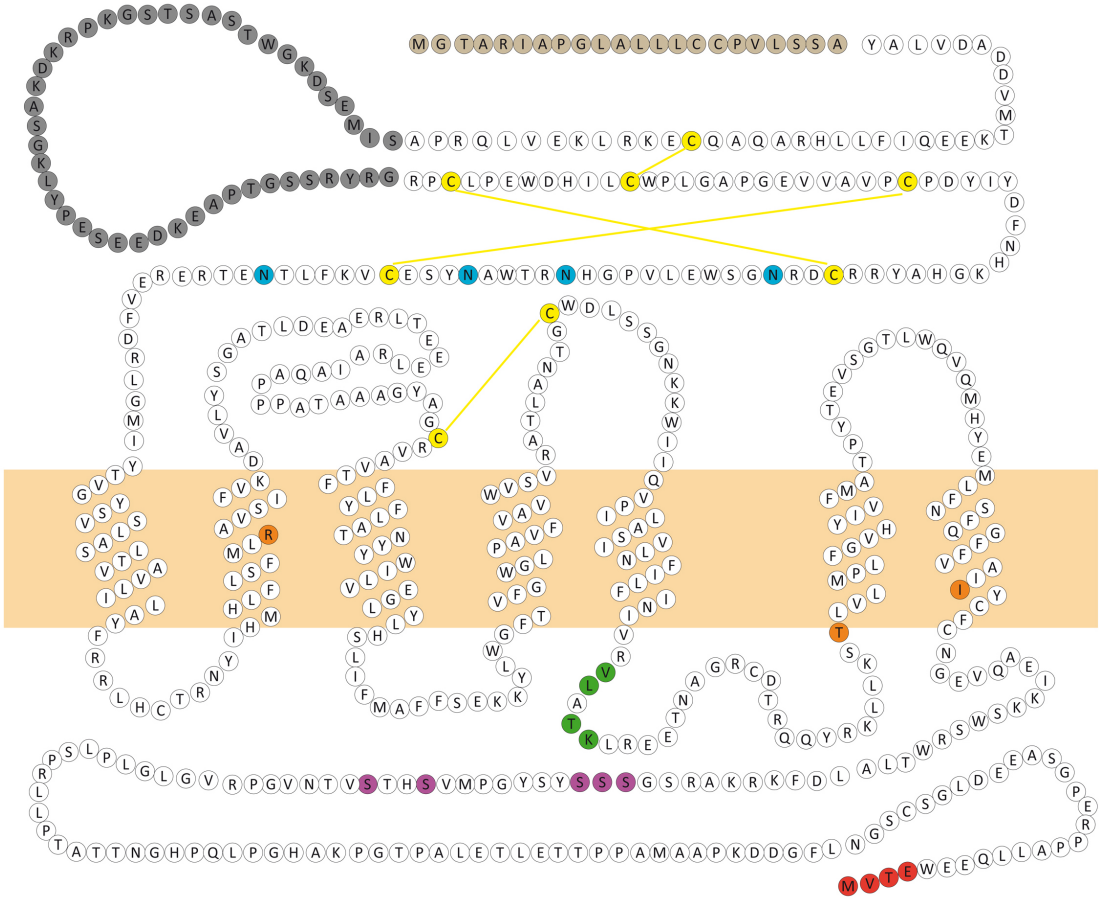

Figure 2. Amino acid sequence and key residues of the PTHR. Functional key residues are colored. The first 22 amino acids represent the signal peptide (light-brown) and residues G^{57} to G^{105} represent exon E2 (grey) [41]. Cysteine residues located on the extracellular side of the receptor (yellow) form disulfide bonds (yellow lines) [42]. Four known N-glycosylation sites are located on exon G of the N-terminal domain (cyan) [47]. V^{384} and L^{385} located at the third intracellular loop are required for PLC-coupling (green). Residue T^{387} is required for AC activation whereas K^{388} is required for AC and PLC activation (green) [49]. Residues at TM2 (R^{233} to H), TM6 (T^{410} to P) and TM7 (I^{458} to R) represent Jansen mutation sites (orange) [55]. Residues 589 to 593 at the C-terminal tail represent the PDZ-binding domain (red) **(ref. 1.4)** [58]. Serine residues S^{491}, S^{492}, S^{493}, S^{501} and S^{504} are important for phosphorylation-induced internalization and $G\alpha_{q/11}$-coupling (magenta). Predicted position of the cytoplasmic membrane is illustrated by a rose bar [52, 53].

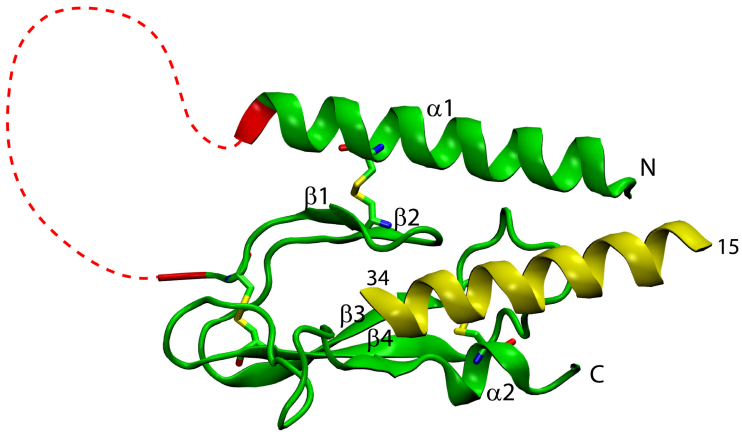

Figure 3. Crystal structure of the extracellular domain of the PTHR bound to a PTH fragment (Pioszak et al. 2008; pdb3C4M) [42]. Conformation of the PTHR extracellular domain derived from X-ray crystallography [42]. The extracellular domain of the PTHR is built up by a three-layer α-β-β-α conformation (green) fixed by three disulfide bonds (yellow sticks). The PTH 15-34 fragment (yellow) is bound to the ligand-binding pocket. Exon E2 is assumed to be disordered, thus having no detectable secondary structure (red dashed line) [42].

1.3.2. Parathyroid hormones

In the early 20th century, the function of parathyroid glands became an object of research. Besides the hypothesis that parathyroid glands are a detoxification organ, MacCallum et al. claimed the control of blood calcium levels as the main function [59]. The critical active components for this homeostasis were assumed to be hormones. The amino acid sequence of parathyroid hormone (PTH) was not determined until the 1970's, because of degradation during isolation from the glands. Finally, PTH was found to be an 84 amino acid peptide [60, 61]. Before secretion through secretory vesicles, PTH exists as a 115 amino acid pre-pro-hormone form, which is processed by two steps. First, 20 N-terminal amino acids are cleaved cotranslationally at the ribosomes, and second, 6 amino acids are cleaved during processing in the Golgi-apparatus. Secretion of PTH is controlled by blood calcium levels, which are recognized by a GPCR, named calcium sensing receptor (CaSR). Activation of the CaSR, which is located at the surface of parathyroid cells, leads to $G\alpha_q$-mediated intracellular calcium increase and subsequently to exocytosis of PTH vesicles. In turn, exocytosis into the blood circulation elicits endocrine actions of PTH on bone and kidney cells.

The major function of PTH is to increase blood calcium levels by actions on bone and kidney cells. In more detail, these actions include the regulation of the proliferation and function of osteoblasts and indirect effects on the activity of osteoclasts, which are critical for calcium homeostasis. Furthermore, PTH regulates the calcium and phosphate resorption as well as

vitamin D levels. After secretion, PTH is further degraded in liver and kidney cells. The resulting C-terminal fragments can be detected in blood, but the physiological relevance of this degradation is not yet clear [62]. Based on the knowledge that degradation of PTH produces active fragments, it was deduced that N-terminal parts of PTH may harbor biological activity. Indeed, PTH 1-34 is sufficient to fully activate PTHR-mediated pathways, such as PLC or AC, and their classical effects on bone metabolism and calcium homeostasis [63-65].

Besides PTH, other endogenous polypeptides with high affinities to the PTHR exist, that are called parathyroid hormone related peptides (PTHrP). Both peptide groups are believed to share an evolutionary origin [66]. For PTHrP, solely one gene in the human genome is assumed, however, splicing variants have been suggested, which lead to multiple mRNA species for PTHrP [66, 67].

PTH and PTHrP display differential endocrine functions and are secreted by different organs. PTH is critical for calcium homeostasis and is produced in and secreted by parathyroid glands. In contrast to PTH, the secretion of PTHrP takes place in various tissues. PTHrP was found to mainly be a paracrine factor playing a role in development of bone, heart, mammary glands and bone metastasis of some tumors [68-70].

PTHrP appears to be more selective in receptor recognition as it binds PTHR, but not PTHR2, whereas PTH is recognized by both, PTHR and PTHR2 [38]. On the contrary, the tuberoinfundibular peptide of 39 residues (TIP39), a hypothalamic peptide, selectively activates the PTHR2, but not the PTHR [54].

1.3.3. Parathyroid hormone receptor activation and signaling

A two-step binding mechanism is assumed to underlie the activation of PTHR. First, the C-terminal segment of PTH 1-34 binds to the extracellular domain of the receptor. Second, the N-terminal segment of PTH 1-34 interacts with the juxtamembrane domain (J-domain) of the PTHR, which represents the membrane-spanning region. Residues 17-31 of PTH, which enable the first binding step, are believed to harbor residues critical for receptor binding affinity [71]. In contrast, PTH 1-14, which mainly interacts with the transmembrane portion of the receptor, has a lower affinity and potency than PTH 1-34, but is sufficient to activate the PTHR [72]. Recent crystal structures of the ligand-bound extracellular domain of the PTHR remarkably confirmed this two-step model **(Figure 3)** [42, 43]. Both steps together, the C-terminal and the N-terminal binding arrangement of PTH, are believed to take about 1 sec [54, 73]. In accordance to the two-step activation mechanism, a two-phase kinetic was reported, consisting of fast

binding to the extracellular domain (rate constant τ = 140 msec) and slow receptor activation kinetics via N-terminal regions of PTH (rate constant τ = 1 sec) [74].

Binding of PTH to the PTHR and subsequent receptor activation leads to activation of downstream signaling molecules. The main downstream signaling molecules are heterotrimeric G proteins. The Gα-subunits of heterotrimeric G proteins, $G\alpha_s$ and $G\alpha_q$, are activated by the PTHR. Subsequently, AC and PLC are activated and trigger downstream signaling cascades involving cAMP/PKA and IP_3/PKC, respectively. In addition, G protein subtype $G\alpha_{i/o}$ is activated by the PTHR leading to AC inhibition, whereas activation of $G\alpha_{12/13}$ by the PTHR leads to PLD and RhoA activation [75-77]. Full-length hormone PTH 1-84 acts as a full agonist on PTHR in terms of PLC and AC activation. As mentioned above, the N-terminal fragment PTH 1-34 is sufficient to also fully activate these pathways and exhibits identical effects on bone metabolism and calcium homeostasis [63, 64]. This full agonism of N-terminal fragments does also apply for PTHrP 1-36 [71]. In contrast to PTH 1-34, PTH 7-34 is assumed to be an antagonist in terms of $G\alpha_s$ and $G\alpha_q$ signaling by the PTHR [78, 79]. Other N-terminally truncated PTH or PTHrP analogues, e.g. 3-34, cause loss in cAMP-signaling efficacy without dramatically diminishing receptor-binding affinity [80]. These observations are consistent with the hypothesis that the N-terminal regions of PTH and PTHrP are involved in receptor-mediated signaling and furthermore in PTHR subtype selectivity [80]. Additional studies on selective signaling of PTH revealed that PTH 1-31, but not PTH 3-34, activates PKC via phospholipase D in renal distal tubule cells whereas in proximal tubule cells PTH 3-34, but not PTH 1-31, stimulates the PLC-mediated pathway [54, 81]. These numerous differential activation patterns of distinct downstream pathways are assumed to be triggered by ligand-selective conformations of the PTHR which induce differential arrangements of proteins within signaling complexes. Moreover, it is suggested that there is a high affinity conformation triggered by certain PTH analogs which does not couple to heterotrimeric G proteins, as the conformation is stable in the presence of GTPγS [82, 83]. This conformation, dissimilar to the RG conformation of the classical ternary complex model **(Figure 1)**, was named R^0 [17]. The R^0 conformation seems to be characteristic for family B GPCRs and has been described for the corticotropin releasing factor 1 (CRF1) receptor as well [84].

Classical models for GPCR-induced cAMP production are described as a process that is exclusively occurring at the plasma membrane. Additionally, internalization induced by receptor activation was believed to be a pure switch-off mechanism leading to dissociation of ligand, receptor and G protein, as well as to cAMP degradation by phosphodiesterases (PDE) [85]. In contrast, mutational studies on PTH analogues revealed ligands which induce prolonged cAMP and Ca^{2+} signaling [86]. These mutated PTH analogues are believed to display enhanced affinities to the R^0 conformation of the PTHR, which leads to sustained cAMP, Ca^{2+} and phosphate responses [86]. Additionally, clinical studies emerged that report PTH 1-34, but not PTHrP 1-36,

to trigger prolonged elevated 1,25-dihydroxyvitamin D and calcium concentrations [70]. These observations can be barely explained by classical receptor desensitization models. Further studies on sustained cAMP generation induced by PTH, but not PTHrP, revealed a novel signaling mechanism for PTHR [87]. Here, evidence is provided that PTHR can generate second messenger after internalization into early endosomes. In these endosomes, a complex consisting of receptor, G proteins and adenylate cyclases was found to signal from intracellular membranes. This finding was also proven by a study on the thyroid stimulating hormone receptor (TSHR) [88].

As unusual as PTH induces second messenger generation after internalization, the antagonist PTH 7-34 is capable of inducing internalization independent of AC or PLC activation [89]. This counter-intuitive observation for antagonistic PTHR ligands suggests a mechanistic dissociation of receptor internalization and activation.

1.3.4. PTH-mediated mitogen-activated protein kinase activation

Activation of MAPK cascades by PTHR is achieved by two independent mechanisms. A transient rapid phosphorylation and activation of ERK1/2 is mediated by $G\alpha_s$ and PKA/PKC, whereas a slower but more persistent activation is mediated through β-arrestin1/2-dependent effects independent of G proteins [90]. These signaling mechanisms for MAPKs can be selectively activated by PTH analogues, suggesting distinct active conformations of PTHR which lead to specific signaling events. [W^1]PTHrP 1-36 selectively activates $G\alpha_s$, while [D-W^{12}, Y^{34}] PTH 7-34 activates β-arrestin signaling without affecting G protein signaling. In addition to MAPK activation by G proteins or β-arrestin, $G\alpha_i$ or $G\alpha_{q/11}$-coupled GPCRs, including PTHR, can transactivate epidermal growth factor receptors (EGFRs) [91]. This transactivation occurs through a proteolytic liberation of membrane-bound EGFR ligands, by this triggering EGRFs activation, auto-phosphorylation and phosphorylation of ERK1/2 [91]. Crosstalk of GPCRs and EGFRs is suggested as the predominant mechanism of GPCR-mediated activation of ERK1/2 in osteoblasts, which may contribute to cell proliferation and cell differentiation [91].

1.3.5. Alternative downstream effects of PTHR signaling

Besides activation of G proteins, β-arrestin or direct transactivation mechanisms, PTH-mediated PTHR activation affects numerous proteins of other signaling cascades. For instance, PTH stimulates PI3K activity involving the downstream effector Akt/PKB, a serine threonine kinase,

in a c-Src-dependent manner [92]. This pathway contributes to PTH-induced MAPK activation. In addition, PTHR was shown to directly interact with the PI3K regulatory subunit p38 and is capable of activating the pro-apoptotic protein Bad by activating PI3K/Akt-mediated signaling cascades [93]. These signaling properties could function as an anti-apoptotic signaling pathway in osteoblasts, therefore being a mechanism how PTH may influence bone metabolism through osteoblasts [93]. Classical activation of phospholipases by PTH is mediated by $G\alpha_q$ and involves subtype C of phospholipases. Nevertheless, there is evidence for PTH-mediated activation of phospholipase D (PLD) in osteoblastic cells (UMR-106) [94]. This activation is dependent on p42/44 MAPK and the small G protein RhoA. Further studies on osteoblastic cells revealed G proteins $G\alpha_{12}$ and $G\alpha_{13}$, but not $G\alpha_s$, to transduce the effects of PTH on activation of PLD mediated by RhoA GTPase **(ref. 1.5)** [76].

1.3.6. Parathyroid hormone-regulated bone metabolism

Physiological effects of PTH on bone metabolism and calcium homeostasis are mediated by two major mechanisms. On the one hand, PTH increases tubular reabsorption of calcium in the kidney and decreases phosphate reabsorption, subsequently elevating serum calcium concentrations. In more detail, a decreased serum phosphate concentration results in increased available calcium, which results from the low solubility product of calcium phosphate. The inhibition of phosphate reabsorption is mediated by PTH-induced internalization and degradation of the sodium-phosphate cotransporter 2 (NPT2), which reabsorbs phosphate and is expressed in proximal tubules of nephrons. On the other hand, PTH increases bone resorption through osteoclast-induced bone degradation, thereby releasing calcium into the blood. Paradoxically, PTH also exhibits anabolic effects on bone metabolism after intermittent PTH-bolus administration once a day. Bolus injections of PTH stimulate a net increase in bone mass, whereas constant physiological PTH levels or continuous infusions stimulate a net loss of bone mass [95, 96]. To elucidate the underlying mechanism of the diverse effects of PTH, coordinated functions of osteoblasts and osteoclasts need to be investigated. Remarkably, PTHRs are expressed in osteoblasts, but not in osteoclasts [63, 97]. Hence, effects of PTH on osteoclasts are mediated by indirect mechanisms. Stimulation of osteoblasts with PTH leads to increased secretion of the cytokine RANKL (receptor activator of nuclear factor kappa B ligand) and decreased expression of osteoprotegerin (OPG), a member of the TNF-receptor family and RANKL inhibitor [98]. RANKL is an important factor for osteoclast development, whereas OPG inhibits osteoclast-development and osteoclast-activity [99, 100]. Consequently, the RANKL/OPG expression ratio is a surrogate for bone resorption and serves for indirect

regulation of osteoclasts by PTH. Interestingly, RANKL/OPG ratios increase with increasing PTH concentration and duration. Therefore, RANKL/OPG expression may mediate the catabolic effects of PTH versus the paradox anabolic effects of intermittently administrated PTH. In addition to indirect effects of PTH on osteoclasts, a direct proliferative, differentiating and anti-apoptotic function of PTH on PTHR-expressing osteoblasts is well accepted [101]. These direct effects on osteoblasts are believed to be mediated via PTHR signaling pathways and cAMP generation. Therefore, the periodicity and duration of cAMP signaling is suggested to be a critical parameter. PTH analogues, which induce prolonged cAMP responses and exhibit higher affinity to R^0 conformations of the PTHR, were reported to increase bone mineral density (BMD) to a greater extent than PTH 1-34 [86].

Besides $G\alpha_s$-mediated signaling via cAMP, there is evidence for involvement of $G\alpha_q$ signaling pathway in osteoanabolic effects of PTH [102]. A recent study examined the bone metabolism of $G\alpha_q$ and $G\alpha_{11}$ single and double knockout mice. These mice exhibit normal bone volume and turnover, whereas upon PTH treatment double knock-out, but not single knock-out mice, had increased bone volume and turnover compared to wild-type mice [102]. This finding indicates an inhibitory effect of $G\alpha_q$ signaling on PTH-mediated osteoanabolic effects. Since bone volume is unaffected when $G\alpha_q$ or $G\alpha_{11}$ is present, a redundant functionality of $G\alpha_q$ and $G\alpha_{11}$ was assumed. Furthermore, PTH-induced PKCδ membrane translocation was associated with the presence of $G\alpha_q$ in primary osteoblasts, indicating a connection between $G\alpha_q$-mediated inhibition of PTH-induced osteoanabolic effects and PKCδ [102].

On the other hand, evidence was provided that β-arrestin-biased signaling presents a selective pathway for bone formation [103, 104].

In sum, mechanisms by which PTH exhibits catabolic and paradoxical anabolic effects on bone metabolism are not clear yet. However, the relevance of periodicity and duration of PTH, as well as subsequent specific cell-cell communication, is highlighted for biological effects of PTHR signaling.

1.3.7. Parathyroid hormone receptors in pharmacological treatment

Osteoporosis is the most frequent bone disorder in the elderly. Primary osteoporosis is of unknown origin and constitutes 95 % of all osteoporosis diagnoses. Five percent of osteoporosis patients suffer from secondary osteoporosis which is induced by exogenic factors such as glucocorticoids. Thirty percent of postmenopausal women develop a clinically severe osteoporosis. The major risk of osteoporosis is the increased fracture risk in the elderly. The most frequent fractures are fractures of lumbar spine, femur and humerus, which lead to

disability and early mortality. Classical pharmacological treatment of osteoporosis includes administration of vitamin D3, calcium, bisphosphonates, calcitonin, estrogen or selective estrogen receptor modulators. These anti-resorptive treatments increase bone mineral density and reduce fracture risk. In contrast, anabolic compounds for treatment of osteoporosis directly stimulate bone formation. Anabolic agents include fluorides, growth hormones, insulin-like growth factor I, statins and PTH.

A double-blind randomized placebo-controlled study on 1637 postmenopausal women investigated the effects of 20 µg or 40 µg PTH 1-34 in once-daily injections [96]. The relative risks of vertebral fractures for the 20 µg or 40 µg PTH group were 0.35 and 0.31, respectively (CI_{95} 0.22 to 0.55 and 0.19 to 0.50). As well, relative risks of non-vertebral fractures were decreased. Additionally, an increase of bone mineral density in the lumbar spine of 9 % and 13 % and in femoral neck 3 % and 6 % for 20 µg or 40 µg PTH-treated groups, respectively, were observed. However, increased activity of PTH harbors an increased risk of osteosarcoma, thus teriparatide should not administered to patients who already are at increased risk of osteosarcoma [96]. In total, PTH stimulates bone formation, increases bone mineral density (BMD) and restores bone architecture and integrity [95]. PTH 1-34 (Teriparatide, Forteo™) and PTH 1-84 (PREOS®) represent new anabolic compounds for the treatment of osteoporosis [105, 106]. Teriparatide is available in Europe and the United States of America, whereas PREOS® is approved solely in Europe. These peptide hormones are subcutaneously administered once a day at a dose of 20 µg [107]. In sum, PTH represents an important anabolic compound in the treatment of osteoporosis and may also be useful for combination therapy with anti-resorptives.

1.3.8. Biased agonists and bone formation

As other GPCRs, the PTHR can activate multiple signaling pathways independently of each other. Consequently, PTH analogues were obtained which selectively activate G protein or β-arrestin pathways [103, 108]. The biased agonist for β-arrestin signaling, [D-W^{12}, Y^{34}] PTH 7-34, mediates bone formation in mice as the native agonist PTH 1-34 does [109]. The observation, that in β-arrestin2 knock-out mice the increase of bone density by PTH 1-34 was reduced and the increase of bone density by [D-W^{12}, Y^{34}] PTH 7-34 was diminished, led to the suggestion that β-arrestin-mediated signaling may play a role in bone formation [109]. Consequently, conformations of the PTHR may exist, which selectively activate signaling pathways. These conformations might be promoted by biased agonism to achieve a selective pharmacological benefit.

1.4. Sodium/hydrogen-exchanger regulatory factor (NHERF)

Sodium/hydrogen (Na^+/H^+)-exchanger regulatory factors are members of PDZ domain-containing proteins. PDZ proteins were named by sequence homologies to postsynaptic density proteins PSD-95/SAP90, septate-junction-protein discs-large and the epithelial tight-junction protein ZO-1 [110, 111]. The regulation of the Na^+/H^+ exchanger isoform 3 (NHE3) represents the function that was eponymous for NHERF proteins. NHE3 mediates NaCl and $NaHCO_3$ absorption in cooperation with the Cl^-/HCO_3^- exchanger or a Na^+/HCO_3^- cotransporter, respectively, in ileum, proximal colon, and proximal renal tubules [112, 113]. These functions of NHE3 are inhibited by the intracellular second messenger cAMP [114]. NHERFs are scaffolding proteins, thus they orchestrate the arrangement and function of protein complexes. NHERF proteins interact with membrane proteins (e.g. GPCRs or transporters) and cytosolic proteins, including other NHERF proteins, subsequently serving as multi-interaction scaffold proteins. Four subtypes of NHERF proteins exist **(Figure 4)**. NHERF1, also known as ezrin-binding protein 50 (EBP50), and NHERF2, also called E3KARP, both consist of two PDZ domains and one moesin-ezrin-radixin-merlin (MERM) domain. NHERF3 and NHERF4 also known as Na^+/Pi cotransporter C-terminal-associated protein 1 and 2, respectively, consist of four PDZ domains. This multi-domain structure of NHERF proteins allows interactions between plasma membrane proteins and cytoplasmic proteins and links these protein complexes to the actin cytoskeleton, thereby controlling their location and signaling abilities. Interestingly, NHERF subtypes are known to exhibit differential expression patterns [115, 116]. Their cell-type specific expression and their adaptor function allow NHERF proteins to affect cell signaling and protein trafficking.

NHERF2 was found to interact with the C-terminal tail of the PTHR [58]. Interestingly, there is significant evidence that NHERF2 affects PTHR signaling. NHERF2-PTHR complex propagated PTH-induced $G\alpha_q$/PLC activation and reduced AC activity by stimulating inhibitory $G\alpha_{i/o}$ proteins [58]. In contrast, cells expressing PTHR, but not NHERF2, activated AC rather than PLC upon PTH stimulation. The PDZ1 domain of NHERF2 binds to the last 4 amino acids “ETVM” of the PTHR constituting a PDZ consensus motive. The second PDZ domain of NHERF2 can bind to PLCβ1 simultaneously. Thereby, NHERF2 is thought to direct PTHR signaling towards PLC-mediated pathways. As mentioned above, NHERF proteins assemble protein complexes with the actin cytoskeleton by interaction with actin-binding MERM proteins, e.g. ezrin [117]. Consequently, the MERM binding domain of NHERF1 enables the formation of protein microdomains. For PTHR, within these microdomains the receptor and selected effectors are co-localized to direct receptor signaling.

In addition to regulation of PTHR signaling, NHERF2 was shown to co-localize with clathrin and is supposed to regulate PTHR trafficking by connecting PTHR to clathrin-coated pits and

subsequently to the actin cytoskeleton [118]. The PTHR-NHERF complex serves as a model, how receptor-adaptor interaction regulates signaling and trafficking events. Furthermore, cell-type specific expression patterns of adaptor subtypes may play a critical role for tissue selective receptor signaling.

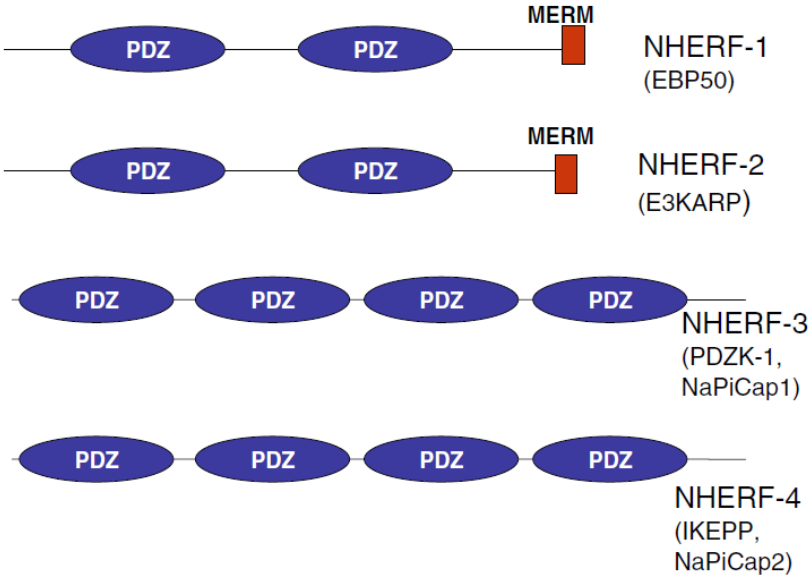

Figure 4. Family of NHERF proteins (Cunningham et al. 2010) [119]. Members of the NHERF family are NHERF1 (EBP50, ezrin-binding protein 50), NHERF2 (E3KARP, NHE3 kinase A regulatory protein), NHERF3 (NaPiCap1, Na^+/Pi cotransporter C-terminal-associated protein 1, encoded by the *PDZK-1* gene) and NHERF4 (IKEPP, Intestinal and kidney-enriched PDZ protein; or NaPiCap2, Na^+/Pi cotransporter C-terminal-associated protein 2). NHERF1 and NHERF2 consist of two PDZ domains, numbered as PDZ1 and PDZ2, as well as a moesin/ezrin/radixin/merlin binding domain. In contrast NHERF3 and NHERF4 contain four PDZ domains [119].

1.5. Rho family of small GTPases

Ras homolog (Rho) genes represent a large subdivision of the rat sarcoma (Ras) superfamily of small GTPases. GTPases are guanine nucleotide triphosphate (GTP) hydrolyzing proteins. Requiring GTP as a substrate, Rho GTPases control numerous cellular functions. The three most famous Rho family members are RhoA, Ras-related C3 botulinum toxin substrate 1 (Rac1) and cell division control protein 42 homolog (Cdc42). Altogether, 25 members of the RhoA family, encoded by 22 human genes, have been described [120]. Rho family proteins are fundamental regulators of numerous cellular processes including migration, secretion, neurite retraction, smooth muscle contraction and gene transcription [121]. In more detail, the major role of Rho

GTPases is defined as the regulation of cytoskeletal organization. RhoA and Rac1 signaling affect numerous downstream targets as myofilament proteins, ion channels, reactive oxygen species generation, NF-κB and other transcription factors [122]. Through these downstream targets Rho GTPases play an important role in the regulation of gene transcription, cell proliferation, survival, migration and differentiation [123]. Furthermore, Rho GTPases exhibit a significant impact on cellular morphology. Rho induces stress fibers, Rac regulates lamellipodia and membrane ruffle formation, whereas Cdc42 activity is fundamental for filopodium extension [124]. This variety of functions needs to be well regulated to orchestrate cellular function. Therefore, Rho GTPases are tightly regulated by GDP-GTP cycling. Cycling of GDP and GTP is controlled by three classes of proteins: (i) GTPase activating proteins (GAPs) which stimulate intrinsic GTPase activity, thus promoting inactive states; (ii) guanine nucleotide dissociation inhibitors (GDIs) retaining inactive conformations; (iii) and guanine nucleotide exchange factors (GEFs), activating GTPases by catalyzing GDP/GTP exchange [125].

1.6. Vav family of guanine-nucleotide exchange factors

Vav guanine-nucleotide exchange factors are multi-adaptor proteins which orchestrate various cellular functions. Named after the sixth letter of the Hebrew alphabet (waw or vav), three subtypes of vav are known in mammals. Vav1 is solely expressed in hematopoietic cells, whereas vav2 and vav3 are ubiquitously expressed. Vav proteins are critical adaptors for several signaling pathways, including adaption of cell surface receptor signals to effector functions and cytoskeleton reorganization. Vav proteins are GEFs for the Rho/Rac family of small GTPases, thereby catalyzing and regulating cytoskeleton reorganization **(Figure 5)**. Since vav proteins are evolutionarily preserved, vav analogues are expressed in many species. A multi-domain signature is characteristic for vav proteins, which enables their function as multi signal transducers. This signature includes a calponin-homology (CH) region, which enables binding of actin, an acidic-rich (Ac) region, a *dbl* homology (DH) region, which exhibits GEF activity, a pleckstrin homology (PH) domain, which mediates phosphoinositol interactions, a zinc finger domain (ZF), a prolin-rich region (PR), two Src-homology 3 (SH3) domains and one Src-Homology 2 (SH2) domain, which serve for protein-protein interactions **(Figure 6)** [125]. Interestingly, vav GEFs are unique in combining a DH/PH motif, a SH2 as well as a SH3 domain in one protein. Remarkably, vav proteins exhibit an intra-molecular mechanism for activity. In the unphosphorylated state, the Ac region inhibits GEF activity. Upon phosphorylation of specific tyrosine residues, for instance Y^{172} in human vav2 or Y^{174} in vav1, the conformation of the Ac region changes and the GEF function is restored. Tyrosine phosphorylation is tightly regulated

by the Src and Syk family of tyrosine kinases as well as by cell-surface receptors, such as EGFRs [126]. EGFR activation is capable to induce phosphorylation of three tyrosine residues in the Ac region of vav2: Y^{142}, Y^{159} and Y^{172} [126]. Mammalian vav proteins exhibit GEF function on both, Rho- and Rac-like members of GTPases, but GEF function on related Cdc42 proteins is under controversy [125, 127]. N-terminally truncated mutants of vav proteins, lacking the Ac domain, exhibit constitutively active GEF function, which is due to the absence of the auto-inhibitory domains. Because of increased GEF activity, these mutants over-activate Rho GTPases and, consequently, promote cell-proliferative effects of Rho GTPases as well as their apoptosis suppression. These Rho-mediated effects can lead to cancer. Consequently, constitutively active vav mutants are named oncoproteins, whereas vav2 wild-type is named as a proto-oncoprotein. Unlike for vav1 and vav3, both domains of vav2, the CH and Ac domain need to be deleted for constitutive activity [128]. This leads to the suggestion that for vav2 an additional structural auto-inhibitory mechanism exists which involves the CH domains. Mutations of the tyrosine residues at the Ac domain also diminish auto-inhibition and create oncoproteins. In addition to Ac domains and CH domains at vav2, the PH domain also impairs GEF function of vav proteins. PH domains in general are assumed to bind PI3K-generated lipid products, thus mediating membrane recruitment of proteins containing PH domains. PH domains of vav were proven to enhance GEF activity upon phosphatidylinositol-3,4,5-trisphosphate (PIP_3) binding, whereas binding to phosphatidylinositol-4,5-bisphosphate inhibits GEF activity (PIP_2) [129]. The fact that a PI3K-product, as PIP_3, enhances GEF activity and that a PI3K-substrate, as PIP_2, inhibits GEF activity suggests a feedback regulation between PI3K and vav proteins. Therefore, activated PI3K kinases act as vav stimulators by eliminating inhibitory phosphatidylinositol-4,5-bisphosphate and producing stimulatory phosphatidylinositol-3,4,5-trisphosphate [129].

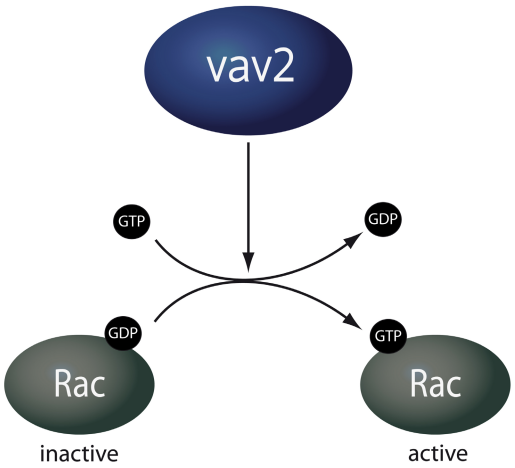

Figure 5. Guanine-nucleotide exchange for Rac GTPase by vav2. Vav proteins regulate activity of the Rho/Rac family of small GTPases by guanine-nucleotide exchange function. In detail, vav catalyzes the exchange of GDP on inactive Rac for GTP which activates Rho/Rac GTPases.

Figure 6. Multi-domain structure of vav proteins. The N-terminus consists of a calponin-homology (CH) region and an acidic-rich (Ac) region. The functional core of vav protein is composed of a *dbl* homology (GEF) region that exhibits GEF activity and a pleckstrin homology (PH) domain. The C-terminus consists of a zinc finger region (ZF), a prolin-rich region (PR) two Src-homology 3 (SH3) domains and one Src-Homology 2 (SH2) domain.

1.6.1. The guanine-nucleotide exchange factor vav2

Vav proteins represent the best-characterized family of mammalian guanine-nucleotide exchange factors (GEF) for Rho GTPases. Vav proteins were shown to mediate between the activation of Rho and several different signaling molecules as immune response receptors, protein tyrosine kinases and integrins. The gene for the guanine-nucleotide exchange factor vav2 is located at the human gene map locus 9q34 and shares 53 % identical amino acid residues with vav1, which is located at gene map locus 19p13.3-p13.2 [130]. Vav2 is ubiquitously expressed, however mRNA levels are elevated in testes, placenta and liver [128]. Vav2 was found to appear in two splice variants. Splice variants of proteins (e.g. alpha, beta variants) occur as a result of post-transcriptional modification of the RNA, where introns are removed and exons are linked. Alpha splice variants of vav2 are known to be expressed during development, while beta variants are specifically expressed in adults. Targets of vav2 are under intense discussion, especially the GEF activity on cell division control protein 42 homolog (Cdc42). Evidence is provided for the ability of vav2 to activate GEF function on RhoA, RhoG, Rac1 and Cdc42 GTPases of the Rho family [131, 132]. In addition, these studies found vav2 oncoprotein-mediated effects on phenotype transformation, including focus and colony formation, which requires RhoA, Rac1 and Cdc42 function. Taken together, it is clear that vav2 and vav1 share common downstream targets of the Rho family of GTPases. However, functional redundancy for RhoA regulation does not occur due to different expression patterns of vav proteins. By exerting influence on RhoA GTPases and subsequently on cytoskeleton reorganization, vav2 proteins exhibit effects on cell morphology and migration. For instance, oncoprotein and wild-type vav2 were shown to increase stress fibers, membrane ruffles as well as elevated Rac1 and Cdc42 mediated cell migration [132].

As mentioned above, known activation mechanisms for vav2 include phosphorylation by tyrosine-kinase receptors, as EGFR, and tyrosine kinases, as Src. The phosphorylation of vav2 by EGFRs happens by direct interaction with activated EGFRs [125, 133]. The interaction interface is believed to involve the SH2 domain at the C-terminus of vav2, whereas the N-terminus of vav2

represents the target of tyrosine kinase activity of EGFRs. Furthermore, it is suggested that membrane-targeting of vav2 via the SH2 domain is a key prerequisite for phosphorylation and activation of vav2 by EGF [134]. Remarkably, GEF function of vav2 in vivo requires kinase activity of Src indicating the second phosphorylation-dependent activation mechanism of vav2.

1.6.2. Regulation of RhoA guanine-nucleotide exchange factors by GPCRs

In addition to receptor tyrosine kinases, $G\alpha_{12/13}$-coupling GPCRs are known to regulate RhoA proteins via direct interactions with RhoA GEFs [135]. The number of identified RhoA GEFs exceeds 60, whereas three members were identified to directly interact with $G\alpha_{12/13}$-proteins; p115RhoGEF, PDZRhoGEF and leukemia-associated RhoGEF (LARG) [136-138]. These three Rho GEFs harbor a regulator of G protein signaling (RGS) homology domain which serves for the interaction with activated G proteins of the $G\alpha_{12}$ subfamily. Recent studies revealed a RhoA activation mechanism mediated by $G\alpha_{q/11}$-coupled receptors [139]. This mechanism was shown to be independent of PLCβ and downstream Ca^{2+} as well as PKA signaling [140]. LARG mediates RhoA activation induced by $G\alpha_q$ and $G\alpha_{12/13}$-coupled receptors, whereas it was demonstrated that a RhoA GEF named p63RhoGEF activates RhoA selectively by $G\alpha_{q/11}$ induction [141]. Furthermore, this study revealed p63RhoGEF as an inhibitor of PLCβ activity and IP_3 generation induced by constitutively active $G\alpha_q$ or activated M_3 muscarinic acetylcholine receptors. The effect of p63RhoGEF on M_3 muscarinic acetylcholine receptors-mediated IP_3 generation induced by carbachol was 70 % [141]. In contrast to p115RhoGEF and related, p63RhoGEF does not contain a RGS domain. Structural studies on the interaction with $G\alpha_q$ provide evidence that the GEF domain and PH domain of p63RhoGEF are involved [142]. The crystal structure of the p63RhoGEF and $G\alpha_q$ led to the suggestions that the auto inhibitory mechanism of the GEF and PH domains is diminished by $G\alpha_q$. The Interaction interface includes the effector binding site and C-terminal region of $G\alpha_q$. Further studies proved this mechanism to be independent of p63RhoGEF membrane translocation [143]. However, $G\alpha_q$ is thought to act allosterically on the linker region, which connects GEF and PH domains, thereby releasing autoinhibition.

Notably, one study reported vav proteins to transduce signals of GPCR to Rho GEFs [144]. This study revealed Rac2 activation in response to fMet-Leu-Phe receptor (fMLP receptor, also known as formyl-peptide receptor, FPR) stimulation, which is established by direct interactions of vav1 and Rac2 [144]. fMLP receptors belong to the GPCRs and are involved in chemotaxis and are responsible for neutrophil response. Deficiency in both P-Rex1 (IP_3-dependent Rac exchanger 1) and Vav1 diminished GPCR-dependent neutrophil responses and Rac activation,

thus P-Rex1 and Vav1 are believed to cooperate in controlling GPCR-dependent neutrophil responses [145].

1.7. Fluorescence ligand binding tools for PTHR

The use of PTHRs in pharmacological therapy is limited to the treatment of severe osteoporosis. Investigation of the PTHR as drug target for further diseases, e.g. osteosarcoma and other hormone-dependent cancer-types, requires suitable ligand binding tools.

Radioactively labeled ligands are commonly used for ligand-binding. Radiolabels usually provide high signal-noise ratios. Therefore, radiolabels are valuable, especially for peptide hormones which innately exhibit high unspecific binding. Moreover, the size of a radiolabel is usually smaller than most organic fluorophores. Thus, they often do not sterically interfere with binding of ligands. Consequently, for peptides exhibiting multi-step binding mechanisms, as PTH, the use of radiolabels is advisable **(ref. 1.3.3)**. However, peptide-radioligand generation is demanding and expensive. For example, high cost and potential harmfulness of I^{125}-PTH prohibited saturation binding for receptors. In sum, radioligand binding assays are well established tools, however, there is significant need for alternative methods.

In recent years, fluorescence ligand binding studies have been developed [146]. Especially time-resolved fluorescence (TRF) as a readout for ligand-binding experiments has gained relevance. However, ligand-binding assays utilizing fluorescent PTH have been missing. Fluorescent ligands are less harmful than radiolabels and enable protein-protein interaction-studies as well as imaging [147]. Unfortunately, fluorescent ligands typically provide (i) orientation bias (ii) insufficient signal intensities and (iii) are hampered by high auto-fluorescence of matrices. (i) Orientation bias of fluorescence emission, which occurs if fluorophores are inflexibly attached to the protein, can be disadvantageous when the position of fluorophores changes, e.g. upon conformational changes of ligands or receptors. (ii) Signal intensities are critical, as they represent the readout value. Low signals in combination with high noise by auto-fluorescence decrease signal to noise ratios. (iii) In general, biological matrices exhibit auto-fluorescence, which may interfere with fluorescent readouts.

In contrast to common fluorophores, lanthanides are lacking orientation bias and exhibit sustained fluorescence emissions. These sustained fluorescence emissions last much longer than auto-fluorescence of biological matrices. Lanthanides therefore can be used for time-resolved (TR) measurements of fluorescence, thus obtaining increased signal to noise ratios. Additionally, lanthanides exhibit acceptable fluorescence intensities and form very stable complexes, such as TrisBipyridine (Europium) Eu^{3+}-cryptate or more recently Terbium (Tb^{3+})-cryptate. These

coordination complexes improve the spectral properties of lanthanides and enable coupling reactions for labeling of peptides [148, 149]. Furthermore, lanthanides possess large stoke-shifts, which avoid bleed-through of donor emission into acceptor emission peaks. In addition, multiple emission peaks of the lanthanide Terbium (Tb^{3+}) allow direct measurement of fluorescence emission at 620 nm and energy transfer to acceptor fluorophores. This energy transfer called time-resolved (TR)-fluorescence resonance energy transfer (TR-FRET) then allows measurements of red or green acceptor emissions.

As an alternative to TR-FRET, fluorescence anisotropy or fluorescence polarization (FP) assays have become of interest. In FP measurements, the rotational speed of fluorophores, attached to ligands, changes upon binding to the receptor. The ability of fluorophores to depolarize polarized light is dependent on this rotational speed and thus can be measured [150]. Unfortunately, FP is limited in size of tagged ligands, up to 5 kDa, in the concentration of receptor, above 1 pmol/mg [151], and is very sensitive to unspecific binding as well as fluorescent background [150]. In contrast, TR-FRET assays overcame these limitations for several receptors, inter alia growth hormone secretagogue receptor type 1a, vasopressin V1a, oxytocin receptor and heterodimeric γ-aminobutyrate B receptor [152-154].

In these studies, time-resolved fluorescence was combined with a homogeneous assay procedure, which does not require washing. This is in contrast to classical radioligand or fluorescence ligand-binding assays, where ligands that did not bind to any receptor need to be eliminated by washing steps. Because of that, classical assays can be named as separation assays. Generally, washing procedures require low dissociation rates (k_{off}) compared to washing time. This is because during the time-consuming washing-procedure ligand dissociation may start and subsequently measurements of ligand-affinities get biased. Accelerated washing of cell suspensions or cell-membrane preparations can be achieved by using filter membranes. In contrast to use of filter membranes, adherent cells on 96-well plates need to be washed by addition of buffer and aspiration, which is time consuming. Since PTH exhibits low dissociation rates, this washing by aspiration from top is feasible. The advantage of a cell-based ligand-binding setup is represented by a more physiological environment for the ligand receptor binding mechanism than binding to receptors in cell-membrane-preparations. As mentioned above, the cellular environment, e.g. receptor G protein interactions, may have impact on the ligand receptor affinities, which are described in the extended ternary complex model of GPCRs **(ref. 2.2.1)** [16, 17].

In contrast to separation assay formats, washing-free homogenous assays use ratiometric fluorescent readouts which do not interfere with unbound ligands.

In sum, the development of time-resolved fluorescence ligand-binding assays on living cells may facilitate drug development for the PTHR.

1.8. Motivation

A key aspect of PTHR signaling, and GPCR signaling in general, is represented by functions of intracellular signaling complexes consisting of adaptor and effector proteins **(Figure 7)**. Adaptor proteins are capable of transducing signals of transmembrane proteins to the intracellular compartment, thereby mediating between receptor conformation and signal pathway activation. Frequently, these adaptor proteins are expressed in a cell type-specific manner. Consequently, expression and binding patterns of adaptor proteins can determine the direction of receptor signaling depending on the cellular context. Thus, this key aspect of PTHR signaling is under intense research. The focus of this work is on the identification of novel adaptor proteins of the PTHR, their influence on functions of the PTHR and the determination of their physiological role.

Ligand binding assays represent fundamental tools for pharmacological research. To be suitable for drug screenings as well as fundamental research, ligand binding tools need to be time-saving, nonhazardous, robust, reproducible, precise and cost-effective. Usually, radioligands are used to perform robust ligand binding assays. Nevertheless, there is significant interest to substitute expensive and harmful radioligand binding assays. A promising substitution is represented by fluorescence-based ligand-binding assays. The second aim of this work is to provide time-resolved fluorescence ligand binding tools for the PTHR.

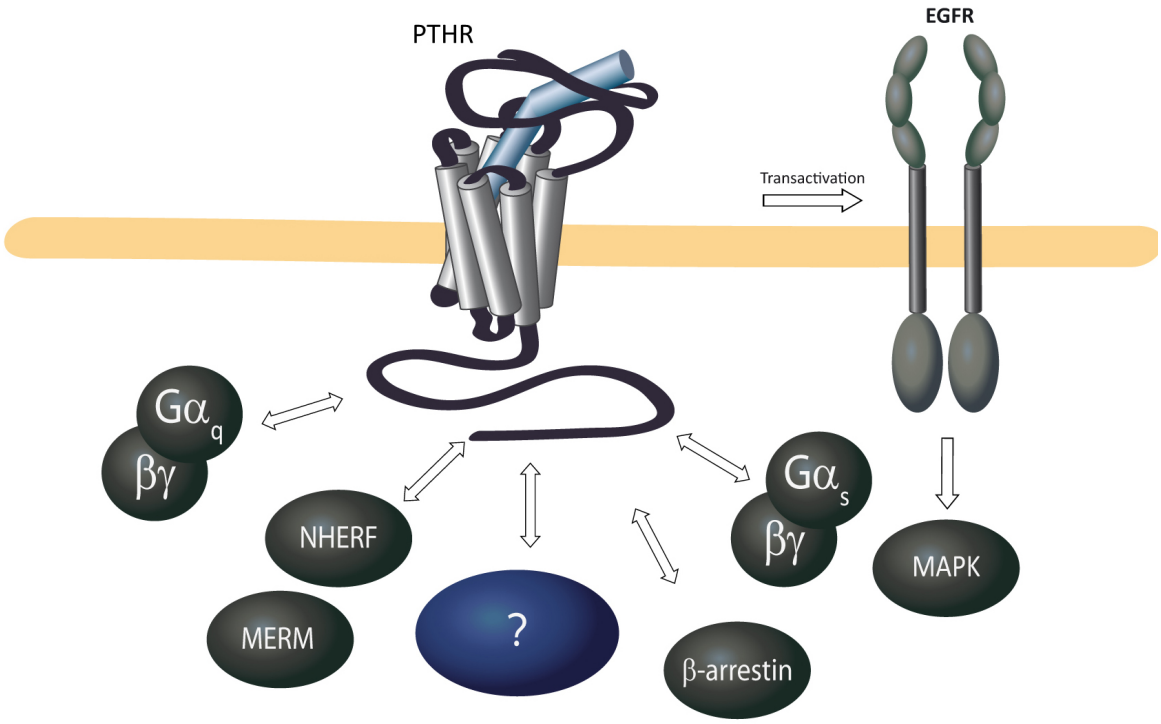

Figure 7. PTHR represent the core of signaling complexes. The PTHR is embedded in protein complexes which direct exogenous stimuli towards intracellular signaling by differential signal transduction. Ligand-dependent conformational changes of the PTHR can lead to selective activation of distinct pathways. In addition, the interaction pattern of adaptor proteins directs selective PTHR signaling. For PTHR, signaling complexes include inter alia heterotrimeric G protein (Gα-subunits $G\alpha_q$ or $G\alpha_s$), β-arrestin, Na^+/H^+ exchanger regulatory factor (NHERF) and moesin-ezrin-radixin-merlin (MERM) proteins, epidermal growth factor receptors (EGFR) which activate mitogen-activated protein kinase (MAPK). An unknown adaptor protein for PTHR signaling, which may direct effector activation towards selective signaling events, is illustrated by dark blue globe, whereas a signaling pathway-selective ligand is illustrated as a light-blue rod.

2. Materials

2.1. Eukaryotic cell culture

2.1.1. Cell Lines

Cell type	Description
HEK 293 ad	Human embryonic kidney 293 cells with improved adherence and plaque formation properties
HEK 293T	human embryonic kidney cells 293 transformed with the SV40 large T antigen
ROS 17 / 2.8	Osteosarcoma cell line from rat origin
COS-7 cells	Cell line derived from *African green monkey* kidney fibroblasts (CV-1). CV-1 (simian) in Origin, and carrying the SV40 genetic material.

2.1.2. Medium

Dulbecco‘s modified Eagle‘s medium (DMEM) 4.5 g/l glucose, Phenol red-free DMEM 4.5 g/l glucose and Dulbecco’s modified Eagle’s medium/Ham’s F12 (1:1, DMEM/F12) were obtained from Pan Biotech, Aidenbach. For passaging, medium was supplemented with 10 % (v/v) fetal calf serum (FCS) (Biochrome AG, Berlin), 2 mM glutamine, 100 units / ml penicillin and 0.1 mg / ml streptomycin (Pan Biotech, Aidenbach). Inositol-free medium was obtained from MP Biochemicals LLC (Solon).

2.1.3. Transfection reagents

Calcium phosphate transfections were conducted using 2.5 M $CaCl_2$, sterile double-distilled water and 2x BES buffered saline (BBS) containing 280 mM NaCl, 1.5 mM Na_2HPO_4 and 50 mM N,N-bis[2-hydroxyethyl]-2-aminoethanesulfonic acid (BES). Final concentrations of reagents for calcium phosphate transfection were 125 mM $CaCl_2$, 140 mM NaCl, 0.75 mM Na_2HPO_4 and 25 mM BES at pH of pH 6.95. Transfections using Lipofectamine™ were performed using supplied Lipofectamine™ and Opti-MEM® (Invitrogen™). Transfections by Effectene® were conducted according to manufacturer’s protocol (QIAGEN©) using supplied reagents.

2.2. Bacterial cell culture

2.2.1. Bacteria strains

Strain	Genotype
E.coli XL1 blue (Stratagene)	endA1, hsdR17 (rK- mK+), supE44, lambda-, recA1, gyrA1, gyrA96, relA1, (lac-), (F', proAB, lacqZΔM15, Tn10[tetR])
E.coli BL21(DE3)-pLysS (Stratagene)	F-, ompT, gal, dcm, lon, $hsdS_B(r_B- m_B-)$, λ(DE3), pLysS(cm^R)
E.coli BL21 Star™-pLysS	F-, ompT, $hsdS_B(r_b- m_B-)$, gal, dcm, rne131, (DE3) Bl21 Star™
E.coli BL21 (DE3) CodonPlus-RIL	B, F–, ompT, $hsdS_B(r_B- m_B-)$, dcm+, Tetr, gal, endA, Hte, [argU ileY leuW Camr]
E.coli BRP (codon-plus RP)	B, F–, ompT, $hsdS_B(r_B- m_B-)$, dcm+, Tetr, gal, endA, Hte, [argU proL Camr]
E.coli BL21 Rosetta™	F-, ompT, $hsdS_B(r_B- m_B-)$, gal, dcm, pRARE, (Cam^R)

2.2.2. Media for bacteria

Lysogeny broth (LB) medium for bacteria contained 1 % peptone from casein, 0.5 % yeast extract, 1 % NaCl at pH 7.2. Agar plates were produced with LB-medium plus 1.5 % (w/v) Agar.

2.3. Buffer and solutions

2.3.1. Buffer for molecular biology

10x DNA-loading buffer	
	100 mM EDTA 30 % (v/v) Glycerol 0.05 % (w/v) Bromphenol blue 0.05 % (w/v) Xylenecyanol in distilled water
10x TAE	
	400 mM Tris-HCl, pH 8.0 50 mM Sodium acetate 10 mM EDTA in distilled water

2.3.2. Buffer for biochemistry

5x SDS-Laemmli-buffer	
	250 mM Tris-HCl, pH 6.8 5 % (w/v) SDS 1 % (w/v) DTT 40 % (w/v) Glycerol 0.005 % Bromphenol blue in distilled water
PBS	
	137 mM NaCl 2.7 mM KCl 4.3 mM Na_2HPO_4 1.4 mM KH_2PO_4 in distilled water pH 7.4
PBS plus Tween	
	PBS 0.1 % (v/v) Tween 20 in distilled water
RIPA buffer (radio immuno precipitation assay buffer)	
	150 mM NaCl 50 mM Tris, pH 7.5 5 mM EDTA 1 % (v/v) Nonidet P40 0.5 % (w/v) Na-Deoxycholate 0.1 % (w/v) SDS in distilled water pH 7.5
10x SDS Electrophoresis buffer	
	248 mM Tris-HCl, pH 8.2 1.92 M Glycine 1 % (w/v) SDS in distilled water
Transfer buffer	
	20 mM Tris-HCl, pH 8.3 150 mM Glycine 20 % (v/v) Methanol in distilled water
Blocking buffer	
	5 % (w/v) Non-fat milk powder 100 mM NaCl 10 mM Tris-HCl, pH 7.4 0.1 % (v/v) Tween 20 in distilled water
Phospho-block buffer	
	10 mM HEPES, pH 7.5 500 mM NaCl 1 % BSA 0.2 % Tween-20 0.02 % NaN_3 in distilled water

Stripping-buffer	
	25 mM Glycine-HCl 0.1 % (w/v) SDS pH 2.5
KCM solution	
	100 mM KCl 30 mM $CaCl_2$ 50 mM $MgCl_2$ in distilled water
Wash buffer	
	20 mM HEPES 200 mM NaCl 1 mM EDTA pH 7.5
NP40 buffer	
	5 mM HEPES 150 mM NaCl 1 mM EDTA 10 % Glycerol 0.5 % NP40 Optional: 0.1 % Dodecylmaltoside (DDM) in distilled water pH 7.5
NP40 phosphate buffer	
	5 mM Phosphate 150 mM NaCl 1 mM EDTA 10 % Glycerol 0.5 % NP40 Optional: 0.1 % Dodecylmaltoside (DDM) in distilled water pH 7.5
Binding buffer	
	20 mM HEPES 100 mM NaCl 3 mM $MgCl_2$ pH 7.5
Inositol buffer	
	137 mM NaCl 5 mM KCl 1 mM $MgCl_2$ 1 mM $CaCl_2$ 15 mM HEPES pH 7.3
Tyrode buffer	
	137 mM NaCl 5.4 mM KCl 2 mM $CaCl_2$ 1 mM $MgCl_2$ 10 mM HEPES pH 7.3

2.3.3. Staining solutions

Fixing Solution	
	50 % (v/v) Ethanol 12 % (v/v) Acetic acid in distilled water
Silver-Staining Solution	
	0.3 % (v/v) NH_4OH 0.06 % (m/v) NaOH 0.6 % (m/v) $AgNO_3$ (adjusted by titration to light-brown color) in distilled water
Silver-Development Solution	
	0.005 % citric acid 0.0001 % formalin in distilled water
Silver-Stop-Solution	
	50 % (v/v) MeOH 12 % (v/v) Acetic acid in distilled water
Coomassie-Washing Solution	
	50 % (v/v) MeOH 10 % (v/v) Acetic acid in distilled water
Coomassie-Staining-Solution	
	45 % (v/v) MeOH 10 % (v/v) Acetic acid 0.25 % (m/v) Coomassie Brilliant Blue in distilled water
Coomassie-Destain-Solution	
	45 % (v/v) MeOH 10 % (v/v) Acetic acid in distilled water

2.4. Antibodies

Epitope	Species	Properties	Source
anti-mouse	Goat	Monoclonal, Cy2™-conjugated	Jackson Immuno R. Inc.
Flag	Mouse	D2-Labeled, monoclonal	Cisbio
$G\alpha_{q/11}$ (C-19)	Rabbit	Polyclonal	Santa Cruz
HA.11 (16B12)	Mouse	Monoclonal	Covance
HA	Mouse	Monoclonal, Agarose-conjugated	Sigma
His_6-tag	Mouse	Monoclonal	Cell Signaling
Myc	Mouse	Monoclonal	Cell Signaling
c-Myc	Rabbit	Polyclonal, Agarose-conjugated	Sigma
NHERF1 (EBP50)	Rabbit	Polyclonal	Covance
PTHR CT (1781)	Rabbit	Polyclonal	Klenk et al.
P-Tyr (4G10)	Mouse	Monoclonal	Millipore
P^{172}-vav2	Rabbit	Polyclonal	Santa Cruz
Vav2 [EP1067Y]	Rabbit	Monoclonal	Abcam

2.5. Plasmids

Name	Sequence	Vektor	Origin
$G\alpha_q$	human $G\alpha_q$ 1-359	pcDNA3	Department stock
$G\alpha_s$-His_6	bovine $G\alpha_s$1-73[HHHHHH]74-394	NpT7-5	Taylor et al.
HA-PTHR1	hPTHR1 1-92[YPYDVPDYA]102-593	pcDNA3	Ulrike Zabel
HA-PTHR1 T480	hPTHR1 1-92[YPYDVPDYA]102-480	pcDNA3	Frank Dicker
HA-PTHR1 T470	hPTHR1 1-92[YPYDVPDYA]102-470	pcDNA3	Alexander Emami
HA-PTHR1 T459	hPTHR1 1-92[YPYDVPDYA]102-459	pcDNA3	Alexander Emami
MBP	MBP 1-397-[DDDDK]	pMal-c3E	New Eng. Biolabs
MBP-PTHR CT	MBP-[DDDDK]-hPTHR1 463-593	pMal-c3E	Alexander Emami
Myc-vav2	[EQKLISEEDL]-linker-vav2 1-879	pRK5	Elisabeth Jeanclos
Myc-vav2$^{188-512}$	[EQKLISEEDL]-linker-vav2 188-512	pRK5	Elisabeth Jeanclos
HA-NHERF1	[YPYDVPDYA]-NHERF1	pcDNA3	Christoph Klenk
dnNHERF1$^{1-326}$	NHERF11-326	pcDNA3	Peter A. Friedman
SNAP®-hPTHR1	SNAP®-hPTHR1 1-593	pcDNA3	Cisbio
Flag-PTHR	hPTHR1 1-93[DYKDDDDA]102-593	pcDNA3	Alexander Emami
S2-PTHR	ssHA-[DYKDDDDA]-TEV-hPTHR1 1-593	pcDNA3	Alexander Emami
S3-PTHR	hPTHR1 1-60[DYKDDDDA]AR-106-593	pcDNA3	Alexander Emami

TEV: cleavage site for cysteine protease of *Tobacco Etch Virus*.

ssHA: modified signal peptide from influenza hemaglutinin [155, 156].

SNAP®: SNAP-tag® represents a mutant of the DNA repair protein O^6-alkylguanine-DNA alkyltransferase that reacts with benzylguanine (BG). Thereby an irreversible (covalent) bond between the SNAP-tag and BG is formed. By fusing fluorophores to BG, this technique allows fluorescent labeling of proteins.

2.6. Small interfering RNA

Name	Target Sequence	Target Gene (Gene Id)
si vav2 RNA	GGAUGGAGCAGUUCGAGAU	Knock-down of human vav2 oncogene
si Ctrl RNA	UGGUUUACAUGUCGACUAA	Non-targeting siRNA #1

ON-TARGETplus siRNAs were obtained from Thermo Scientific (Dharmacon).

2.7. Enzymes

Name	Origin
Thermus aquaticus DNA polymerase (Taq)	Eppendorf
Thermococcus litoralis DNA polymerase (Vent)	New England Biolabs
T4 DNA ligase	New England Biolabs
Restriction enzymes	New England Biolabs
Enterokinase	New England Biolabs
DNAase	Sigma Aldrich

2.8. Columns and resin for chromatography

Name	Origin
Amylose resin	New England Biolabs
Mono Q	GE Healthcare
Protein G Sepharose Fast flow	GE Healthcare
Dowex 1x8-Anion Exchanger (100-200 mesh)	Applichem

2.9. Parathyroid hormone analogues and polypeptides

Name	Origin
[$Nle^{8,18}$, Y^{34}] human PTH 1-34	Peptide Specialty Laboratories GmbH (Heidelberg)
[$Nle^{8,18}$, C^{13}, Y^{34}] human PTH 1-34	Peptide Specialty Laboratories GmbH (Heidelberg)
[$Nle^{8,18}$, Y^{34}, C^{35}] human PTH 1-34	Peptide Specialty Laboratories GmbH (Heidelberg)
[$Nle^{8,18}$, Y^{34}] bovine PTH 3-34 amide	Polypeptide Laboratories (Strasbourg, France)
PTHrP 7-34 amide	Polypeptide Laboratories (Strasbourg, France)
human PTH 1-34 wild-type	Tocris Bioscience (Ellisville, USA)
Epidermal Growth Factor (human)	Sigma Aldrich (St. Louis, USA)

Peptides obtained from Peptide Specialty Laboratories GmbH (www.peptid.de) were generated by solid phase peptide synthesis and HPLC purification. PTH analogue [$Nle^{8,18}$, Y^{34}] human PTH 1-34 in latter named as PTH 1-34.

2.10. Fluorescent PTH analogues

Name	tag	Sequence
[C^{13}-Tb^{3+}-cryptate] PTH 1-34	Terbium^{3+}-cryptate	[$Nle^{8,18}$, C^{13}-Tb^{3+}-cryptate, Y^{34}] PTH 1-34
[C^{35}-Tb^{3+}-cryptate] PTH 1-34	Terbium^{3+}-cryptate	[$Nle^{8,18}$, Y^{34}, C^{35}-Tb^{3+}-cryptate] PTH 1-34
[C^{13}- d2] PTH 1-34	d2	[$Nle^{8,18}$, C^{13}-d2, Y^{34}] PTH 1-34
[C^{35}- d2] PTH 1-34	d2	[$Nle^{8,18}$, Y^{34}, C^{35}-d2] PTH 1-34

Labeling of cysteine mutants [C^{13} or C^{35}] PTH 1-34 with Tb^{3+}-cryptate (Lumi4®-Terbium) or d2 was done by Cis bio (Marcoule, France) using maleimide-based conjugation.

2.11. Chemicals

Chemical	Origin
Acetic Acid	Roth
Agar	Applichem
Agarose	Peqlab Biotechnology
$AgNO_3$	Applichem
$AlCl_3$	Sigma Aldrich
Ammonium persulfate	Sigma Aldrich
Bromphenol Blue	Sigma Aldrich
$CaCl_2$	Sigma
Citric Acid	Applichem
Coomassie Brilliant Blue	Applichem
Desoxycholate	Applichem
Dodecylmaltoside	Applichem
DTT	Applichem
EDTA	Applichem
Ethanol	Sigma Aldrich
Formalin	Merck
Geneticine	Gibco
Glycine	Applichem
HEPES	Applichem
IBMX, 3-isobutyl-1-methylxanthine	Applichem
KCl	Applichem
Methanol	Sigma Aldrich
$MgCl_2$	Applichem
myo-[2-^{3}H (N)] inositol, 1 mCi / ml, in EtOH:H_2O 9:1	Perkin Elmer
Na_2HPO_4	Merck
NaCl	Applichem
NaF	Sigma Aldrich
NaH_2OP_4	Merck
NaN_3	Merck
NaOH	Merck
NH_4OH	Applichem
Non-fat milk	Applichem
Nonidet	Applichem
O^6-benzylguanine-Tb^{3+}-cryptate	Cis bio

Peptone from casein	Applichem
RIA cAMP assay kit	Beckman Coulter
Scintillation liquid, IRGA Safe plus	Perkin Elmer
SDS	Applichem
TEMED	Applichem
TRIS	Applichem
Tween-20	Applichem
Yeast extract	Applichem

3. Methods

3.1. Genetic engineering

3.1.1. DNA isolation and preparation

DNA isolation and preparation was achieved using the "Plasmid Maxi kit" from Qiagen (Hilden).

3.1.2. Polymerase chain reaction

Polymerase chain reactions were used for amplification and mutation of cDNA. PCRs for site-directed mutagenesis and gene amplification for subcloning were done using Vent-Polymerase (*Thermococcus litoralis*) with 3'-5' exonuclease activity. Control amplifications were done with Taq-Polymerase (*Therophilus aquaticus*) without exonuclease activity. For a final volume of 50 µl the PCR samples were mixed as follows:

200 µM Deoxyribonucleic acid triphosphates (dNTP)
0.5 µM 5' Primer
0.5 µM 3' Primer
10 µl Polymerase buffer (10-fold)
2.5 U DNA-Polymerase
Ad 50 µl ddH_2O

Thermocycling was induced by a 95 °C phase for 30 sec followed by primer annealing phase for 30 sec. The annealing temperature was adjusted 8 °C lower than the calculated melting point of the annealing region. The elongation phase was performed at 75 °C for 60 sec for 1,000 base pairs. This cycle was repeated 20-30 times as an agreement between yield and specificity. A final denaturation step and an elongation phase for 10 min assured completeness of the amplified DNA fragments.

3.1.3. DNA gel electrophoresis

DNA gel electrophoresis was performed for identification and purification of amplified or restricted DNA fragments. 0.8 % to 1.5 % (m/V) agarose was solved in TAE buffer (with 0.1 % Ethidium bromide) by heating. A constant voltage between 80 V and 140 V was used for

electrophoretic separation up to 60 min. Target bands were identified with UV-light (λ=365 nm) and extracted with the QIAQuick Gel Extraction Kit (Qiagen) according to the manufacturer's manual.

3.1.4. Restriction of DNA

Restrictions of plasmid DNA or PCR DNA fragments were carried out with enzymes provided by New England Biolabs and the corresponding buffers. The enzyme amount varied between 2 and 20 units per µg DNA depending on the restriction site quality and samples were incubated at 37 °C for 2 h. Restricted DNA was purified with agarose gel electrophoresis or QIAQuick PCR Purification Kit (Qiagen).

3.1.5. Ligation of DNA

Ligation of sticky DNA fragments was performed with T4-DNA ligase according to the manufacturer's protocol, and samples with different ratios between insert and backbone DNA increased probability of a successful ligation.

3.1.6. Transformation of *E.coli* strains

For heat-shock transformation, 100 µl competent bacteria aliquots were gently thawed and mixed with 0.1 µg DNA and chilled on ice for 2 min. The mixture was incubated for 30 sec at 43 °C and chilled on ice for 5 min. The bacterial suspension was diluted to 1 ml with LB medium and incubated at 37 °C for 1 h. 100 µl of bacterial suspension was spread on an Agar-plate containing an appropriate antibiotic for selection.

For chemical transformation with KCM solution, 0.1 µg DNA was dissolved in 10 µl H_2O and 90 µl KCM, and 100 µl of bacterial suspension was added and chilled on ice for 20 min. Afterwards, the mixture was warmed 10 min at room temperature, diluted with LB medium to 1 ml and incubated for 1 h at 37 °C. The transformed bacterial suspension was centrifuged at 2,700 g for 3 min, and the pellet was resuspended in 100 µl LB medium and spread on an agar-plate containing an appropriate antibiotic for selection.

3.2. Cell Culture

3.2.1. Bacterial cell culture

Bacterial strains were cultured in LB-Medium at 37 °C. As a selection marker, ampicillin was used at 100 mg / ml. For rotation, a shaker (Adolf-Kühner AG, Birsfelden) was used. Two hundred ml bacterial cultures were rotated in 1 liter flasks and 1 liter cultures in 2 liter flasks. Agar plates were incubated at 37 °C.

3.2.2. Eukaryotic cell culture

Human embryonic kidney 293 cells (HEK) and the cell line derived from *African green monkey* kidney fibroblasts (COS7) cells were cultured at 37 °C and 7 % CO_2 in DMEM **(ref. 2.1.1)**. The osteosarcoma cell line from rat origin was cultured in DMEM/F12 at 5 % CO_2 **(ref. 2.1.1)**. For stable cell lines 0.2 mg/ml G418 (Geneticine) was added to the medium.

3.2.3. Transfections

Calcium phosphate transfection

Calcium phosphate transfections were performed according to Chen et al. [157]. To do so, cells were split 3 to 5 h before transfection onto culture plates in dilution ratios of 1:2 to 1:3. The transfection solution was prepared as follows: For one 10 cm culture plate, plasmid cDNA was mixed with 50 µl of 2.5 M calcium chloride and 450 µl of double-distilled sterile water were added. This solution was mixed and finally 500 µl of 2x BBS were added. The transfection solution was mixed vigorously for at least 10 sec and incubated for 10 to 15 min at room temperature. Afterwards, this transfection solution was added to cell culture plates containing cells in 10 ml medium and panned to mix transfection solution with medium. Culture plates were incubated at 37 °C, saturated humidity and 5 % CO_2 atmosphere for 16 to 24 h. Afterwards medium was discarded and cells were fed with fresh medium and grown at 7 % CO_2 atmosphere. Amounts of transfection solution for culture-plates of smaller areas were calculated according to area ratios to 10 cm plates. For transfections of siRNA with calcium phosphate, final concentrations of 10 nM siRNA and double amounts of calcium phosphate reagent were used.

Lipofectamine transfection

For immunoprecipitation and detection of phospho-proteins in COS7 cells, lipofectamine was used for transfection **(ref. 3.5.3)**. For this purpose, cells were split 18 h before transfection in antibiotic free-medium. 6 µg of plasmid cDNA coding for HA-PTHR and myc-vav2 were used with 20 µl Lipofectamine for one 10 cm culture plate. Transfection mix was generated according to manufacturer's protocol (Invitrogen®). Afterwards, the transfection mix was incubated for 5-6 h and medium was exchanged.

Transfections for tag-lite based HTRF **(ref. 3.6.2)** were prepared using 200 ng of SNAP-PTHR1 plasmid, 0.8 µl of Lipofectamine 2000, and 50 µl optiMEM culture medium per well of a 96-well plate. Transfection mixtures were incubated for 20 min at room temperature. Prior to plating of 50,000 HEK293T cells per well, 96-well plates were coated with poly-L-ornithine (50 µl of 10 mg/ml) for 30 min at 37 °C. Then cells and transfection mix were added to 96-well plates and incubated at 37 °C, 5 % CO_2 for 24 h. For Lipofectamine transfections of COS7 cells consider **(ref. 3.5.3)**.

Effectene transfection

For TRFS and antibody-based HTRF **(ref. 3.6.1** and **ref. 3.6.3)** 500,000 HEK293 ad cells were transfected with 0.5 µg HA-PTHR cDNA (pcDNA3), using 5 µl Effectene, 4 µl Enhancer and 150 µl EC buffer per well of a 6-well plate. Before splitting to 96-well plates, black bottom 96-well culture plates (PerkinElmer) were coated with poly-D-lysine at 37 °C for 30 min. Then, transfected cells growing on 6-well plates were plated 18 h post-transfection to black bottom 96-well plates at a ratio of 1 to 2.

3.2.4. Generation of stably expressing cell lines

After transfection polyclonal cells were cultured in medium without antibiotic selection. Cells were selected with 0.5 mg / ml G418 (Geneticine) after 48 h post-transfection. The medium was changed every 48 h until cell growth started after 2-3 weeks. The polyclonal culture was split and seeded at a cell density of 1 cell per well in a 96-well plate. The resulting monoclonal cell lines were tested for homogenous receptor expression by immunofluorescence and Western Blots.

3.3. Basic biochemical techniques

3.3.1. Sodium dodecyl sulfate polyacrylamide gel electrophoresis

Sodium dodecyl sulfate polyacrylamide gel electrophoresis (SDS-PAGE) was performed according to Laemmli [158] using a Protean 4 Mini electrophoresis system, dimension 10 cm x 8 cm (Bio-Rad). Prior to electrophoresis, SDS-Laemmli-buffer was added to all protein samples and incubated for 5 min at 95 °C. Samples containing GPCRs were incubated at 20 °C for 20 min instead. Gels were assembled into Protean 4 Mini apparatuses containing electrophoresis buffer. Samples and pre-stained or non-stained molecular-weight marker for protein staining or Western-blotting, respectively, were loaded to pockets of SDS-gels. Proteins were separated at 200 V.
SDS-gels were generated as follows:

Stacking gel (4 %):

250 µl	0.5 M Tris-HCl, pH 6.8
20 µl	10 % (w/v) SDS
125 µl	Rotiphorese 30®, Acrylamide / Bisacrylamide (30 % / 0.8 % (w/v))
1.25 ml	double-distilled water
2 µl	N, N, N', N'-tetramethylethylendiamine (TEMED)
10 µl	Ammonium persulfate solution (10 %) (APS)

Resolving Gel (10 %):

2.0 ml	1.5 M Tris-HCl, pH 8.8
80 µl	10 % (w/v) SDS
2.7 ml	Rotiphorese 30®, Bisacrylamide 30 % / 0.8 % (w/v)
3.3 ml	double-distilled water
4 µl	N, N, N', N'-tetramethylethylendiamine (TEMED)
40 µl	Ammonium persulfate solution (10 %) (APS)

SDS-PAGE for sample preparation prior to mass spectrometry was conducted according to **(ref. 3.4.4)**.

3.3.2. Silver-staining

SDS-Gels were fixed for 20 min in fixing solution. Prior to staining, gels were washed two times with distilled water containing 10 % (v/v) Ethanol for 10 min, followed by washing steps with pure distilled water for a total of 20 min. Staining solution was mixed directly before staining; to do so, up to 3.5 ml of silver nitrate was titrated to 17 ml of sodium hydroxide and 1.2 ml ammonium hydroxide until the solution had a light-brown color. Afterwards, 80 ml of water were added and the staining solution was incubated on gels for 10 min. After incubation, gels were washed at least 5 times with distilled water for over-all 30 min. Silver-stained gels were incubated in development solution until protein bands were visible, washed with water and stopped by stop-solution for 20 min. Afterwards gels were washed with aqueous solutions containing 50 % Methanol for 20 min, 30 % Methanol for 20 min and 3 % Glycerol for 30 min. Gels were stored in saran paper and scanned for documentation.

3.3.3. Coomassie staining

SDS-gels were incubated for at least 1 h with fixing solution, washed for 1 h with Coomassie-Washing-Solution. Afterwards, gels were incubated with Coomassie-Staining-Solution for 15 min and destained for at least 2 h with Coomassie-Destain-Solution. Gels were stored in saran wrap and scanned for documentation.

3.3.4. Western-blots and immunoblotting

SDS-PAGE-separated proteins were transferred to polyvinylidene fluoride (PVDF) membranes by electrophoresis. To do so, filter paper (Schleicher & Schuell, Dassel) equilibrated in transfer buffer and fiber-pads were packed with SDS-gels and PVDF membranes into the Western-blot sandwich chamber (Biorad). A constant current of 350 mA was applied for 70 min. After electrophoresis, unspecific binding-sites of membranes were saturated in block buffer for at least 1 h. Afterwards membranes were incubated for 1 h with appropriate primary antibody dilutions (1:200 to 1:20,000) in block buffer or phospho-block buffer for phospho-proteins. For phospho-proteins, membranes were washed with phospho-block buffer prior incubation with primary antibodies. For depletion of unbound antibodies, membranes were washed three times with PBS + Tween for 10 min and were incubated in horseradish peroxidase (HRP)-coupled

secondary antibodies diluted (1:10,000) for 1 h. Afterwards, for depletion of unbound antibodies membranes were washed three times with PBS + Tween for 10 min. Chemiluminescence of secondary antibodies was activated using ECL Plus™ solution (GE Healthcare, München) according to the manufacturer's protocols and recorded on radiographic films (Fujifilm, Düsseldorf). For documentation, films were scanned with an Epson Perfection V700 Scanner (Epson, Meerbusch). Detection of different epitopes on the same membrane was achieved by depletion ('stripping') of antibodies with stripping buffer, prior to a second immunodetection. Membranes were incubated in stripping buffer for at least 1 h, washed intensively with distilled water, and a second immunodetection starting with a blocking step was performed.

3.4. Proteomic approach

3.4.1. Recombinant expression and purification of the PTHR C-terminus

Human PTHR1 C-terminus (residues 463-593) was cloned into the vector pMal-c3E using *BamHI* and *SalI* restriction sites. *E.coli* BL21 cells were transformed by heat-shock with PTHR CT pMal-c3E plasmid or pMal-c3E plasmid as a control. After 16-20 h one bacterial colony of each construct was picked and grown in LB-medium supplemented with 2 g / l glucose and ampicillin 100 mg / ml for 24 h, shaking with 180 rpm at 37 °C. These pre-cultures were diluted 1 to 50 in LB-medium, supplemented with 2 g / l glucose as well as ampicillin 100 mg / ml, and shaken with 180 rpm at 37 °C until optical density (OD) values of 0.6 OD were measured at a wavelength of 600 nm with a double beam photometer. Afterwards, expression was induced by 200 µM isopropyl β-D-1-thiogalactopyranoside (IPTG) for 3 h. Bacteria were centrifuged at 7,000 g, 4 °C for 10 min and resuspended with wash buffer containing Complete™ protease inhibitor cocktail (Roche). Bacteria were disrupted using 2,000 bar pressure in a French press (SLM Instruments, Rochester, NY, USA) at 4 °C. Bacterial lysate was centrifuged at 20,000 g and 4 °C for 60 min. The resulting supernatant was supplemented with 10 µg / ml DNAase and diluted with wash buffer to 2.5 mg / ml. Protein concentrations were measured by Biuret assay kit (Thermo Scientific). In the biuret assay peptide bonds of proteins form a complex with Cu^{2+}. These complexes are magenta-colored, and by measuring the specific absorption at 540 nm wavelength the protein concentration can be quantified according to the Beer-Lambert law. Supernatants were applied to 10 ml columns (Biorad) containing amylose resin. Bacterial lysate obtained from 1 l expression culture was applied to 4 ml amylose resin (New England Biolabs) and circulated for 16-20 h at 4 °C. Afterwards, the lysate was discarded and the resin was washed using 10 column volumes wash buffer. Specific elution was achieved by 10 mM maltose

and the total elution volume of 15 ml was collected in fractions of 3 ml. Eluted proteins were analyzed by SDS-PAGE with Coomassie staining, and yields were quantified by Biuret assay. Elutions fractions showing high proteins yields and sufficient purity were pooled, diluted to salt concentrations of 20 mM and subjected to ion-exchange chromatography using MonoQ columns on an ÄKTApurifier™ setup (GE Healthcare). Proteins were eluted by a NaCl gradient of 20 mM to 500 mM at flow-rates of 2 ml / min and 1.5 MPa column pressure.

3.4.2. Preparation of kidney and osteosarcoma cell lysates

Fresh kidney of a juvenile *bos taurus* was used for generation of cytosolic lysates. For that, the renal pelvis was removed and renal cortex was placed in 500 ml buffer containing 20 mM TRIS, 100 mM NaCl, 2 mM EDTA, 1 mM DTT, 1 mM phenylmethanesulfonylfluoride (PMSF), 10 µg trypsin inhibitor (soybean) and 30 µg / ml benzamidine at pH 7.6. The kidney was mechanically homogenized by a blender for 3 min and an Ultra-Turrax® for 5 min. Crude lysates were centrifuged at 4 °C for 20 min at 5,000 g, 20 min at 20,000 g and two times for 60 min at 400,000 g. After each centrifugation step, the lipid phase was discarded and the supernatant subjected to the next centrifugation step. The final supernatant was re-supplied with protease inhibitor cocktail Complete™ (Roche). Supernatants were frozen in liquid nitrogen and stored at -80 °C. For interaction screenings, bovine kidney lysate was diluted to a protein concentration of 10 mg / ml, as measured by Biuret assay.

Rat osteosarcoma cells were grown on 15 cm plates to confluence. Cells were washed with PBS and resuspended in ice-cold buffer containing 20 mM Tris, 300 mM NaCl, 2 mM EDTA, 1 mM DTT and protease inhibitors at pH 7.6. Afterwards, cells were disrupted by six strokes of an Ultra-turrax®, 15 sec each on ice, and centrifuged at 400,000 g for 30 min at 4 °C. Supernatants were pooled and protein concentration was measured by Biuret assay. For interaction screenings, osteosarcoma lysates were diluted to 2.5 mg / ml.

3.4.3. Interaction screening with tissue and cell lysates

Two mg of the MBP-PTHR CT or MBP construct were applied to 1 ml amylose resin on separate columns and incubated for at least 2 h at 4 °C. Each resin-containing column was washed using 10 ml wash buffer, and 10 mg of kidney lysate or 16 mg osteosarcoma lysate were applied. For that, lysates were diluted with wash buffer to a total volume of 10 ml and were applied to each column containing 1 ml amylose resin. Columns were rotated for 14-16 h and subsequently,

lysates were depleted by gravity flow. Columns incubated with kidney lysate were washed with 100 ml wash buffer containing 1 % Triton X-100 without protease inhibitors. Columns incubated with osteosarcoma cell lysate were washed with 25 ml wash buffer without Triton X-100. Afterwards, all columns were washed with 10 ml enterokinase buffer, containing 50 mM NaCl, 20 mM Tris, and 2 mM $CaCl_2$ at pH 8. Amylose resin was resuspended once during washing with enterokinase buffer, and washed with another 10 ml enterokinase buffer to remove remaining protease inhibitors. On each column 16 ng (10 units) of enterokinase (New England Biolabs) were applied and incubated in enterokinase buffer in a total volume of 2 ml for 18 h at room temperature. After enterokinase cleavage, three elution steps were performed for each column and the flow-through of each step was collected. First, the incubation solution of the enterokinase cleavage was collected. Second, 2 ml of enterokinase buffer were added to the resin and eluted. Third, 5 ml enterokinase buffer containing 10 mM maltose were added to the resin and flow-through was collected. The elutions of the first and second step were pooled and concentrated to volumes of 100 µl using a Microcon® centrifugal filter device (Ultracell YM-3, 0.5 ml, MWCO 3,000 kDa) at 20,000 g. Before further analysis by mass spectrometry, the quality of derived samples was verified by two experiments. First, samples were applied to SDS-PAGE and gels were silver-stained. Experiments that obtained samples which displayed appropriate protein intensities were used for analysis by mass spectrometry. Moreover, the protein concentration of each sample was determined before analysis by mass spectrometry. Samples with >1 mg / ml protein were subjected to analysis by mass spectrometry.

3.4.4. Mass spectrometry and data analysis

Protein samples were separated by 1D PAGE (NuPAGE® Novex Bis-Tris Gels system (Invitrogen Corporation, Carlsbad, CA, USA)) and stained with colloidal Commassie blue. Entire lanes were cut into 23 slices and proteins within each slice were digested in-gel with trypsin according to Shevchenko et al. [159]. Peptides were extracted and analyzed by LC-MSMS on an Orbitrap XL mass spectrometer (ThermoFisherScientific) under standard conditions. Briefly, tryptic peptides were injected into a C_{18} precolumn (1.5 cm, 360 µm o.d., 150 µm i.d., Reprosil-Pur 120 Å, 5 µm, C18-AQ, Dr. Maisch GmbH) at a flow rate of 10 µL / min. Bound peptides were eluted and separated on a C_{18} capillary column (15 cm, 360 µm o.d., 75 µm i.d., Reprosil-Pur 120Å, 5 µm, C_{18}-AQ, Dr. Maisch GmbH) at a flow rate of 300 nL / min, with a gradient from 7.5 to 37.5 % ACN in 0.1 % formic acid for 60 min using an Agilent 1100 nano-flow LC system (Agilent Technologies) coupled to the LTQ-Orbitrap XL hybrid mass spectrometer. MS conditions were as followed: spray voltage, 1.8 kV; heated capillary temperature, 150 °C; normalized collision-

induced dissociation (CID) collision energy 37.5 % for MS/MS in LTQ. An activation q = 0.25 and activation time of 30 ms were used. The mass spectrometer was operated in the data-dependent mode to automatically switch between MS and MS/MS acquisition. Survey MS spectra were acquired in the Orbitrap (m/z 350–1600) with the resolution set to 30,000 at m/z 400 and automatic gain control target at 5x105. The five most intense ions were sequentially isolated for CID MS/MS fragmentation and detection in the linear ion trap. Ions with single and unrecognized charge states were excluded.

Raw data were searched against NCBInr database using Mascot, a search engine with the following criteria: MS/MS peak lists were filtered to contain at most 6 peaks per 100 Da intervals and searched with Mascot server. The MS mass tolerance was set to 7 ppm and MS/MS mass tolerance was set to 0.8 Da. Up to 3 missed cleavages of trypsin were allowed. Oxidized methionine and cysteine carbamidomethylation were searched as variable modifications. The false positive rate was set to 1 % at the peptide level, the false discovery rate was set to 1 % at the protein level and the minimum required peptide length was set to 6 amino acids. Evaluation and annotation of obtained search results was performed with software Scaffold.
Signal intensity for each protein was expressed in the value *number of unique peptides*. Protein specificity ratios were calculated as follows. The *number of unique peptides* found in samples of MBP-PTHR CT was divided by the *number of unique peptides* found in MBP control constructs. Ratios from individual experiments were added. Values with a numerator of zero were subtracted from the total value.
The mass spectrometry analysis and data processing by Mascot search engine were performed by the Bioanalytical Mass Spectrometry Group of Dr. Henning Urlaub at the Max Planck Institute for Biophysical Chemistry in Göttingen.

3.5. Protein biochemistry

3.5.1. Immunoprecipitation of vav2 and PTHR

A 10-cm dish of HEK 293 ad cells were transfected with 5 µg plasmid cDNA coding for HA-tagged human PTHR1 full-length or T480 (pcDNA3) together with 1 µg plasmid cDNA coding for human myc-vav2 (pRK5) or truncated vav2 using calcium phosphate method. After 40 h, cells were incubated with 5 µM latrunculin A at 37 °C for 30 min and afterwards stimulated with 500 nM PTH 1-34. Cells were lysed in 1 ml ice-cold NP40 lysis buffer shaking for 20 min on ice. Lysates were resuspended once by pipetting within these 20 min. Afterwards lysates were centrifuged in 1.5 ml Eppendorf® tubes for at least 20 min at 20,000 g and 4 °C. Fifty µl of the supernatant were mixed with Laemmli buffer, boiled and saved for immunoblotting of total lysate. The remaining 950 µl were pipetted into 1 ml Micro Bio-spin® columns (Biorad). Twenty-five µl slurry of Agarose-conjugated monoclonal anti-HA antibodies were added to the lysate, and columns were head-over rotated for least 2 h at 4 °C. Subsequently, the lysate was removed by gravity flow and the resin was washed three times with ice-cold NP40 buffer without DDM. Bound proteins were eluted by addition of 100 µl 1x Laemmli buffer at 95 °C. Afterwards, total lysates and eluted proteins were separated by SDS-page and immunoblotted. For immunoprecipitation of myc-vav2, 25 µl slurry of agarose-conjugated c-Myc antibodies was applied instead of conjugated anti-HA antibodies. For co-immunoprecipitation of endogenous vav2, no myc-vav2 plasmid was transfected. Chemiluminescence of immunoblots was measured on Fujifilm luminescence-camera LAS-1000 or radiographic films. For co-immunoprecipitations of wild-type vav2 with increased GEF activity, 25 µl slurry of agarose-conjugated monoclonal anti-HA antibodies were incubated for 2 h while rotating over-head at 4 °C. Then, columns were washed with 1 ml NP40 buffer and two times 1 ml PBS. Afterwards 100 µM phosphatidylinositol-3,4,5-trisphosphate, dioctanoyl (C_8-PIP_3) was added in a volume of 1 ml and columns were over-head rotated at 4 °C for 16 h. Then, columns were washed two times with 1 ml NP40 buffer. SDS-PAGE and immunoblotting was performed according to vav2-PTHR co-immunoprecipitation experiments.

3.5.2. Immunofluorescence

Transfected HEK 293 ad cells were seeded on poly-*D*-lysine-coated clear-bottom 96-well culture plates (Perkin Elmer) for at least 24 h. Cells were washed with PBS and fixed for 40 min with Zamboni solution containing 0.2 % (m/v) picric acid, 4 % (m/v) *para*-formaldehyde and 100 mM sodium phosphate at pH 7.5. Afterwards cells were washed with PBS 3 to 5 times, until

Zamboni was visually depleted and permeablized by an ice-cold aqueous 50 % (v/v) methanol solution. Next, cells were washed with PBS supplemented with 0.25 % (m/v) BSA (PBS plus BSA) three times for 5 min. Then, anti-HA antibodies were diluted in PBS (plus BSA) 1 to 1,000 and incubated on cells for 1 h. Next, cells were washed three times with PBS (plus BSA) and incubated with a 1 to 200 dilution of secondary Cy2-labeled anti-mouse IgG antibodies (in PBS plus BSA) for 1 h. Afterwards, cells were washed three times with PBS (plus BSA) and cells were covered with Fluoromount™ (Sigma Aldrich). Plates were stored and dried at least 24 h at 4 °C before microscopic analysis.

3.5.3. Immunoprecipitation and detection of phospho-proteins

HEK 293 ad cells

HEK 293 ad cells were transfected with 5 µg plasmid cDNA coding for HA-tagged human PTHR1 full-length and 5 µg plasmid cDNA coding for human myc-vav2 (pRK5) for one 10 cm culture plate using calcium phosphate method. Cells were resuspended 16 h after transfection, pooled and reseeded on 10 cm plates. After 8 h, cells were starved for 20 h with phenol red-free medium and 0.1 % FCS. For stimulation, 5 ml conditioned medium were aspirated carefully and supplemented with PTH 1-34 and EGF at final concentrations of 500 nM and 100 ng / ml, respectively. Controls were treated with conditioned medium only. Cells were stimulated for 2 min at 37 °C and 7 % CO_2. Cells were protected from mechanical stress and kept at 37 °C through-out the stimulation until lysis. Thereafter, the medium was aspirated and 1 ml per 10 cm plate of ice-cold NP40 phosphate buffer supplemented with 0.1 % DDM, 50 mM NaF and 200 µM Na_3VO_4 was added immediately. Lysates were prepared according to **(ref. 3.5.1)**. Afterwards, 25 µl slurry of agarose-conjugated monoclonal anti-myc antibodies were added to the lysate and columns were head-over rotated for 2 h at 4 °C. Then columns were washed three times with 1 ml ice-cold NP40 buffer supplemented with 50 mM NaF and 200 µM Na_3VO_4. Proteins were eluted by 100 µl 1x Laemmli buffer at 80 °C and were not boiled for immunoblotting analysis. Chemiluminescence of immunoblots was measured on Fujifilm luminescence-camera LAS-1000 and radiographic films. Immunoprecipitation experiments of endogenous vav2 were conducted utilizing anti-vav2 antibodies and no myc-vav2 was transfected.

COS7 cells

Lipofectamine transfection was used for COS7 cells. Transfected cells were grown for 16 h on 10 cm plates, and then splitted, pooled and reseeded on 10 cm plates. After 8 h, cells were starved

for 20 h with phenol red-free medium and 0.1 % FCS. Assay procedure was accomplished according to assays with HEK 293 ad cells.

3.5.4. Co-immunoprecipitation of G-alpha subunits

HEK 293 ad cells were transfected by the calcium phosphate method on 10 cm culture plates. 1 µg plasmid cDNA coding for myc-vav2, 10 nM si RNA, 5 µg plasmid cDNA HA-PTHR and G-alpha subunit His_6-$G\alpha_s$ (NpT7-5) or $G\alpha_q$ (pcDNA3) were used per 10 cm culture plate. Total amounts of plasmid were adjusted equally with empty pcDNA3 or pRK5 vectors. After 40 h, cells were stimulated with 500 nM PTH 1-34 for 20 min as indicated. Afterwards, cells were lysed with NP40 phosphate buffer supplemented with 0.1 % DDM, 5 mM $MgCl_2$, 10 µM GDP, 200 µM Na_3VO_4, 10 µg trypsin inhibitor and 30 µg / ml Benzamidine for 20 min on ice. To activate Gα subunits, 30 µM $AlCl_3$ and 5 mM NaF were added to the lysis buffer. Lysates were prepared according to **(ref. 3.5.1)**. For immunoprecipitation of HA-PTHR, 25 µl slurry of Agarose-conjugated monoclonal anti-HA antibodies were added to the lysate. For immunoprecipitations of myc-vav2, 2 µl anti-myc monoclonal antibodies and 25 µl slurry of Protein G Sepharose (GE Healthcare) were incubated with cell lysates. For this purpose, columns were over-head rotated for at least 3 h at 4 °C. After removal of cell lysates, columns were washed using ice-cold NP40 phosphate buffer supplemented with 5 mM $MgCl_2$, 10 µM GDP, 200 µM Na_3VO_4. For samples, indicated with AlF_4^-, NP40 phosphate buffer was additionally supplemented with 30 µM $AlCl_3$ and 5 mM NaF. Proteins were eluted by addition of 100 µl 1x Laemmli buffer at 95 °C and analyzed according to **(ref. 3.5.1)**.

3.5.5. Accumulation of IP or cAMP in living cells

Measurement of inositol phosphates

HEK 293 ad cells stably expressing HA-PTHR on 10 cm culture plates were transfected with 0.1 nmol (10 nM in 10 ml) si vav2 RNA or si Ctrl RNA using calcium phosphate. For experiments involving dominant-negative NHERF1 or NHERF1 1 µg plasmid DNA was added to siRNAs. Cells were detached 16 h after transfection, pooled and seeded on coated 6-well plates. All wells were washed once with 2 ml PBS 48 h after transfection, and 2 ml inositol-free DMEM supplemented with 0.2 % FCS, and 1 µCi / ml myo-[2-^{3}H] inositol was added to each well. Cells were labeled for 16 h. Plates for immunoblotting were incubated with the same media lacking myo-[2-^{3}H] inositol. Afterwards, medium was aspirated and wells were washed with 2 ml inositol buffer.

Then 1 ml of inositol buffer supplemented with 10 mM LiCl to inhibit inositol phospholipid hydrolysis was added to each well. Serial dilutions of PTH 1-34 were generated in LiCl-containing inositol buffer. Then, 110 µl of the indicated PTH 1-34 dilution was added to each well of a 6-well culture plate. After 60 min incubation at 37 °C, stimulation was stopped by addition of 120 µl ice-cold 20 % (v/v) $HClO_4$, and plates were shaken for 20 min on ice. Lysates were neutralized by 1 M KOH and centrifuged for 20 min at 20,000 g. Amounts of KOH necessary for neutralization of $HClO_4$ were determined by titration (e.g. 460 µl 1 M KOH). One ml supernatant of each sample was added to 2 ml 5 mM Tris pH 7.4 and mixed. Solutions were applied to columns containing water-equilibrated Dowex Ion-exchange resin. Samples passed through resin by gravity-flow and columns were washed twice with 4 ml distilled water. Myo-[2-^{3}H] inositol phosphates were eluted by addition of 3 ml 1 M HCl, and eluates were mixed with 15 ml of scintillation cocktail. Subsequently, beta-emission of tritium was measured in a liquid scintillation counter (Beckman). To confirm equal PTHR expression and vav2 knockdown, lysates from 3 wells of a 6-well culture plate were prepared and proteins were assessed in Western blots.

Generation of 3'-5'-cyclic adenosine monophosphate

HEK 293 ad cells stably expressing HA-PTHR were prepared according to inositol assays but not starved or fed with myo-[2-^{3}H] inositol. The medium was aspirated 60 h after transfection and 1 ml inositol buffer supplemented with 100 µM IBMX, a competitive nonselective phosphodiesterase inhibitor, was added to each well. Serial dilutions of PTH 1-34 were generated in inositol buffer containing IBMX. Then, 110 µl of the indicated PTH 1-34 dilution was added to each well of a 6-well culture plate. After 20 min incubation, at 37 °C, stimulation was stopped by addition of 120 µl ice-cold 20 % (v/v) $HClO_4$ and plates were shaken for 20 min on ice. Lysates were neutralized by 1 M KOH and centrifuged for 20 min at 20,000 g. Fifty µl supernatant of each sample were mixed with diluent solution from RIA cAMP assay kit (Beckman Coulter) kit. One hundred µl of the sample-diluent mix were added to anti-cAMP antibody-coated tubes (RIA tubes). In addition, 100 µl standard dilutions, of 0 nM to 50 nM cAMP, were added to RIA tubes. Five hundred µl tracer (^{125}I-cAMP) (2 Bq/µl) were added to each RIA tube and mixed for 2 sec. Two RIA tubes were filled with 500 µl pure tracer for determination of total activity. RIA tubes were incubated for 18 h at 4 °C, and solutions were aspirated. Measurements of γ-emissions were done on a gamma counter (Wallac 1480 automatic gamma counter, Finnland).

3.6. Time-resolved fluorescence ligand binding assays

3.6.1. Time-resolved fluorescence separation assay (TRFS)

TRFS saturation experiments on HA-PTHR

HEK 293 ad cells transiently expressing HA-hPTHR1 were utilized for saturation binding assays. For that, the Effectene protocol was used for transfection **(ref. 3.2.3)**. Transfected cells were plated on black bottom 96-well plates and were used for ligand binding experiments 48 h later. For this purpose, dilution series of [C^{13}-Tb^{3+}-cryptate] PTH 1-34 or [C^{35}-Tb^{3+}-cryptate] PTH 1-34 in binding buffer containing 0.2 % NFM were generated. Medium of 96-well plates was removed by inverting the plate and 50 µl of binding buffer (0.2 % NFM) were added to each well. Then, 50 µl of indicated dilutions of [C^{13}-Tb^{3+}-cryptate] PTH 1-34 or [C^{35}-Tb^{3+}-cryptate] PTH 1-34 were added to each well. To determine unspecific binding, 10 µM PTH 1-34 was added to every second well to block specific interactions. Plates were gently shaken at 20 °C for 4 h. Then, wells were washed three times with 100 µl binding buffer without NFM. Finally, 50 µl RIPA buffer was added to each well and incubated for 10 min at 20 °C. TRFS was measured on a flash light Envision multilabel reader (PerkinElmer) equipped with an excitation filter UV2 (TRF) 340 nm, emission filter Terbium 545 nm and mirror module D400 (PerkinElmer) using scan mode 6x6 points per well with 0.8 mm point distance. Measurement parameters were set to 1.9 mm height, 500 µs delay and 1400 µs integration time. One hundred flashes were used at 100 % excitation light.

TRFS competition experiments on HA-hPTHR1

For competition experiments, 5 nM [C^{35}-Tb^{3+}-cryptate] PTH 1-34 was used as tracer. Cells were pre-incubated with 100 µl Tag-lite labeling medium for 1 h at 37 °C. Competition ligands were diluted in Tag-lite labeling medium at the indicated concentrations. Experimental procedures were carried out according to saturation binding assays.

TRFS kinetic experiments

TRFS kinetic experiments were conducted according to TRFS competition experiments. Cells were incubated with 5 nM [C^{13}-Tb^{3+}-cryptate] PTH 1-34 for the indicated time intervals. Unspecific binding was determined by addition of 10 µM PTH 1-34.

3.6.2. Homogeneous time-resolved fluorescence using SNAP-PTHRs

SNAP-tag labeling of adherent cells

After 24 h post-transfection, cell culture medium was removed from 96-well plates, and 100 µl Tag-lite labeling medium containing 100 nM of SNAP-Tb^{3+}-cryptate per well was added and incubated for 1 h at 37 °C, 5 % CO_2. Removal of excess SNAP-Tb^{3+}-cryptate was achieved by washing each well four times with 100 µl of Tag-lite labeling medium.

HTRF tag-lite saturation binding assay

HEK293T cells were incubated with indicated concentrations of [C^{13}-d2] PTH 1-34 or [C^{35}-d2] PTH 1-34 diluted in Tag-lite labeling medium. Nonspecific binding was determined by adding 10 µM unlabeled [$Nle^{8,18}$, Y^{34}] bovine PTH 3-34 amide diluted in the same buffer. Fifty µl of Tag-lite labeling medium, 25 µl of unlabeled [$Nle^{8,18}$, Y^{34}] bovine PTH 3-34 amide, or Tag-lite labeling medium was added to plates containing labeled cells followed by the addition of 25 µl [C^{13}-d2] PTH 1-34 or [C^{35}-d2] PTH 1-34. Plates were incubated for 4 h at 20 °C. Signals were detected using an Envision multilabel reader (PerkinElmer) equipped with a HTRF optic module allowing a donor excitation at 337 nm and a signal collection at 665 nm and 620 nm. A laser was used for excitation with 20 flashes per well. One point measurement mode was utilized with the following time-resolved settings: delay 50 µs, integration time 400 µs. HTRF ratios were obtained from dividing the acceptor signal (665 nm) by the donor signal (620 nm) and multiplying this value by 10,000.

HTRF tag-lite competition binding assay

HEK293 ad cells were incubated with 5 nM [C^{35}-d2] PTH 1-34 diluted in Tag-lite labeling medium in the presence of competitor at indicated concentrations. Assay preparation and signal detection was performed according to HTRF tag-lite saturation binding. Plates were incubated at 20 °C for 4 h before signal detection.

Tag-lite-based homogeneous time-resolved fluorescence (HTRF) saturation ligand-binding studies were performed by Cis bio (Marcoule, France).

3.6.3. Homogeneous time-resolved fluorescence with antibodies

HTRF antibody experiments

Assay preparation was performed according to TRFS experiments using Flag-PTHR, S2-PTHR or S3-PTHR for transfections of HEK 293 ad cells. The Effectene protocol was used for transfection of HEK 293 ad cells **(ref. 3.2.3)**. Transfected cells were plated on black bottom 96-well plates and were used for ligand binding experiments 24 h later. For detection of ligand-binding, 4 nM d2-labeled anti-Flag antibodies and 5 nM [C^{13}-Tb^{3+}-cryptate] PTH 1-34 or 5 nM [C^{35}-Tb^{3+}-cryptate] PTH 1-34 were mixed in assay buffer containing 0.2 % NFM. [$Nle^{8,18}$, Y^{34}] human PTH 1-34 was utilized for competition on Flag-PTHR at 20 °C. Signals were detected using an Envision multilabel reader (PerkinElmer) allowing a donor excitation at 340 nm and a signal collection at 665 nm and 620 nm. A frequency of 100 flashes per well was selected for the xenon flash lamp excitation. One point measurement mode was utilized with the following time-resolved settings: delay 50 µs, integration time 400 µs. HTRF ratios were obtained from dividing the acceptor signal (665 nm) by the donor signal (620 nm) and multiplying this value by 10,000.

Kinetic HTRF antibody experiments

Experimental procedures were conducted according to antibody HTRF experiments using scan mode 3x3 points per well with 0.8 mm point distance. Cells were incubated with 5 nM [C^{13}-Tb^{3+}-cryptate] PTH 1-34 or 5 nM [C^{35}-Tb^{3+}-cryptate] PTH 1-34 for the indicated time intervals.

3.7. Microscopy

3.7.1. Wide-field microscopy

Cells were prepared for the detection of HA-tagged PTHR by immunofluorescence and wide-field microscopy as described in **(3.5.2)**. Monoclonal HEK 293 ad cells, stably expressing the PTHR, were incubated with anti-HA antibodies, stained by Cy2-labeled secondary antibodies and visualized on a wide-field microscope (BD Pathway™). The fluorescent dye Cy2 was excited with light of 488 nm wavelength, bandwidth 10 nm, and fluorescence was recorded using a band-pass filter of 500 - 560 nm.

3.7.2. Confocal microscopy

Transfection of HEK293 ad cells with HA-PTHR was performed as described in the Effectene protocol **(ref. 3.2.3)**. Cells were plated 24 h post-transfection to 24 mm coverslips and grown for 48 h. [C^{13}-d2] PTH 1-34 was diluted in binding buffer containing 0.2 % NFM to a concentration of 100 nM. Cells were incubated with ligand dilution containing 100 nM [C^{13}-d2] PTH 1-34, and confocal images were taken on a Leica SP5 laser scanning confocal microscope. Pictures were taken using a 63 x 1.4 objective with immersion oil with 2048 x 2048 pixel resolution at a laser scanning frequency of 200 Hz. Images were recorded by LAS AF software (Leica). For the fluorescent dye d2 a Helium/Neon laser line with 633 nm wavelength was utilized for excitation and the spectral range for emission was 650 nm to 750 nm.

3.8. Data analysis and software

Cloning strategies and analysis by alignments were accomplished using Vector NTI Advanced 11.0 (Invitrogen) and Geneious Pro 5.0.4 (Biomatters Ltd., New Zealand). Predictions of isoelectric points were done using ExPASy Bioinformatics Resource Portal (http://web.expasy.org/protparam/).

Graph-Pad Prism software (GraphPad Software, Inc., San Diego, CA) was utilized for non-linear regression curves, statistical analysis and illustration of graphs. Signal-to-noise calculations were done by dividing the mean of highest signal by the mean of lowest signal. Envision reader results of scan mode measurements were averaged per well and used as one point values. Visual Molecular Dynamics (VMD) software (University of Illinois, Urbana, IL) was utilized for the illustration of the crystal structure **(Figure 3)**. Scaffold 2 Viewer, Proteome Software (Proteom Software Inc., Portland, USA) was used for processing of data derived by LC-MSMS.

4. Results

4.1. PTHR interacting proteins - a proteomic approach

GPCRs are embedded in protein complexes, consisting of signaling effectors and adaptor proteins. Intracellular domains of GPCRs presumably represent the binding interface for proteins complexes. This interface includes the carboxy-terminal tail (C-terminal; CT) and intracellular loops of GPCRs. The PTHR exhibits a large C-terminal domain (CT) consisting of about 130 amino acids. The carboxy-terminal domain is believed to be mainly unstructured, thereby flexible for interactions with several adaptor and effector proteins. The PTHR CT serves for binding to adaptor proteins, as NHERF, β-arrestin and heterotrimeric G proteins [58, 77, 160]. Furthermore, G protein-coupled receptor kinases (GRK) phosphorylate serine residues at the PTHR CT, thereby marking the receptor for the following stable β-arrestin interaction and receptor internalization [160, 161]. As mentioned in **(1.3.3)**, PTHR signaling from early endosomes is suggested to represent a different quality of PTHR signaling. It seems evident that the internalization process and the following signaling are enabled by adaptor proteins within signaling complexes. Consequently, as adaptor proteins of the PTHR are known to regulate receptor signaling and trafficking, there is a significant interest to reveal the identity of unknown adaptor proteins and to gain a better understanding of their interaction pattern in different cell types that enables cell-type specific signaling.

To identify novel adaptor proteins of the PTHR and their biological relevance, at first, a proteomic approach was chosen. Using the C-terminal domain of the PTHR as bait, a mass spectrometry interaction screening was established to identify adaptor proteins. For this purpose, the PTHR CT, including residues N463 to M593, was fused to the maltose-binding protein linked by an enterokinase cleavage site **(Figure 8a)**. To this end, the cDNA coding for PTHR C-terminal domain was cloned into the pMal bacterial expression plasmid. As a control, MBP without fusion partner was expressed separately. The MBP control protein and the MBP-PTHR CT fusion protein were expressed in *Escherichia coli* (*E. coli*), purified by affinity purification and ion-exchange chromatography **(Figure 8b)**. At a final step, a pull-down approach was performed that utilizes cell lysates to screen for novel PTHR interaction proteins. For this purpose, both proteins were immobilized on affinity-resin, incubated with cell lysate, washed and finally a enterokinase cleavage site allowed specific elution by release of PTHR-CT and bound proteins from the affinity matrix **(ref. 4.1.2) (Figure 8b)**. The eluted samples were analyzed by mass spectrometry to identify the proteins that were bound to the PTHR CT.

In general, this proteomic approach allows screenings for cytosolic adaptor proteins in any cell types and tissues from which a cytosolic fraction can be prepared. Consequently, this method is

not limited to cDNA libraries, which is in contrast to yeast-to-hybrid screenings. The final identification of interacting proteins was accomplished by mass spectrometry. In recent years, the progress of mass spectrometry technology increased in sensitivity and robustness. Thus, for this kind of proteomic approach, analysis by mass spectrometry is the method of choice, because interacting proteins may exhibit low intensities, and proteins which interact non-specifically with component of the experiment may generate high background. To reduce background as much as possible, this approach was differentially conducted by performing the experiments with PTHR fusion-protein and a control protein in parallel.

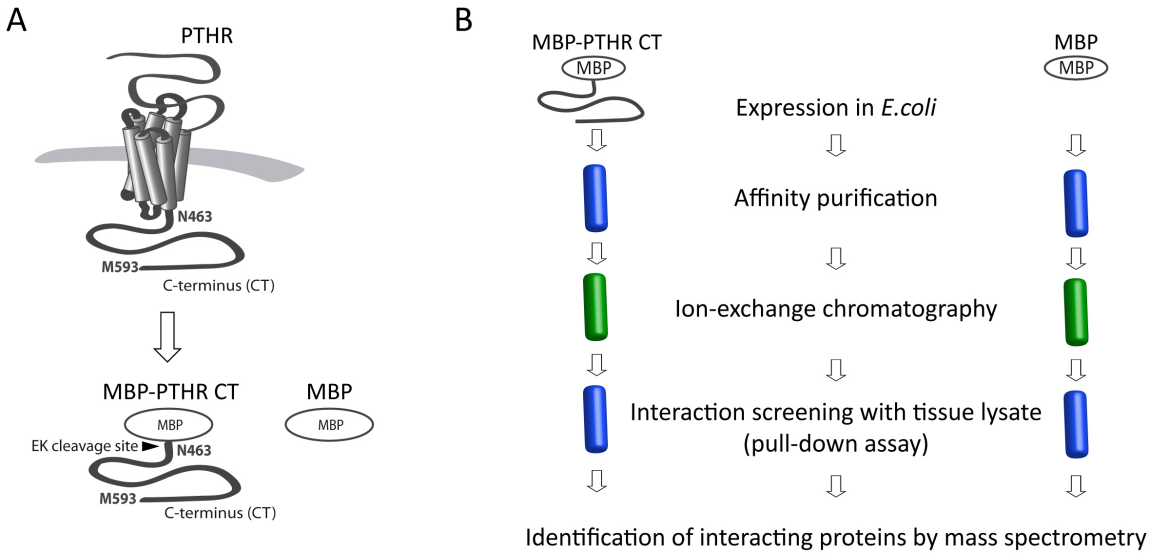

Figure 8. Proteomic approach to identify PTHR interacting proteins. (a) The C-terminal domain of the PTHR (N463 to M593) was fused to maltose-binding protein (MBP). The PTHR CT and MBP were linked by an enterokinase cleavage site. **(b)** Each experiment was performed using the MBP-PTHR CT and MBP as a control. MBP-PTHR CT and MBP were expressed in *E.coli BL21*, purified by affinity (illustrated as blue columns) and ion-exchange chromatography (green columns). Afterwards, the proteins were immobilized on affinity-resin (blue columns) and a pull-down assay using cell lysates was performed. The PTHR CT and bond proteins were eluted by an enterokinase cleavage and analyzed by mass spectrometry.

4.1.1. Expression and purification of the PTHR C-terminal domain

A recombinant bacterial expression system was chosen to generate a bait protein of the PTHR C-terminal tail for the following interaction screening. For that, a MBP-PTHR CT fusion protein was generated. Fusion to maltose-binding protein (MBP) was used for two reasons: first, MBP serves as an affinity tag for subsequent immobilization of the bait protein; second, it remarkably increased the solubility and expression level of the PTHR C-terminus (PTHR CT) in (*E.coli*) (data not shown).

The expression of the MBP-PTHR-CT fusion protein was optimized using several bacterial strains. These include the *Escherichia coli* strains BL21 (DE3)-pLysS, BL21 Star™-pLysS, BL21 (DE3) CodonPlus-RIL (for high adenine/thymine content), BRP (codon-plus RP) and rosetta™ (codon supplements for high guanine/cytosine contents) **(Figure 9a)**. Expression levels of MBP-PTHR-CT in the individual bacterial strains were analyzed by pull-down with amylose-resin, followed by SDS-PAGE and Coomassie staining. Expression tests revealed the strain BL21 (DE3)-pLysS as the most efficient strain in terms of producing the MBP-PTHR CT fusion protein and thus BL21 (DE3)-pLysS were used in all further experiments **(Figure 9a)**. Expressions in BL21 (DE3)-pLysS bacteria were scaled-up to 1 to 4 liters of bacterial culture. The expression conditions were optimized for temperature, time and IPTG concentration (data not shown). The expression was induced at an optical density (OD) at a wavelength of 600 nm of 0.6 of the bacterial cultures at 37 °C with 200 µM isopropyl β-D-1-thiogalactopyranoside (IPTG). Bacterial cultures were shaken for 3 h at 180 rpm. To stop expression, bacterial cultures were centrifuged at 7,000 g, 4 °C for 10 min and resuspended with wash buffer containing protease inhibitors. Afterwards, bacteria were disrupted using a French press. To clear these crude extracts, the bacterial lysate was centrifuged at 20,000 g for 60 min. The following purification was conducted with the cleared supernatants.

The purification protocol was optimized by testing different types of chromatography. For that, single and tandem affinity purification, combined with dialysis; size-exclusion chromatography and ion-exchange chromatography were tested (data not shown). The final and most efficient purification protocol consisted of two steps. First, affinity purification using amylose-resin was performed. Second, samples were further purified using MonoQ ion-exchange column **(Figure 9b)**. Both steps were optimized for washing and elution conditions (data not shown). Further purification by size-exclusion or additional affinity-purification did not significantly increase protein purity (data not shown). Using this expression and purification protocol, 1 liter bacterial culture was sufficient to produce more than 10 mg MBP-PTHR CT fusion protein at purity of about 90 % **(Figure 9b)**. Yields of the MBP construct were about 15 mg per 1 liter bacterial

culture. These yields of pure and stable proteins were sufficient to use both constructs for the following interaction screenings.

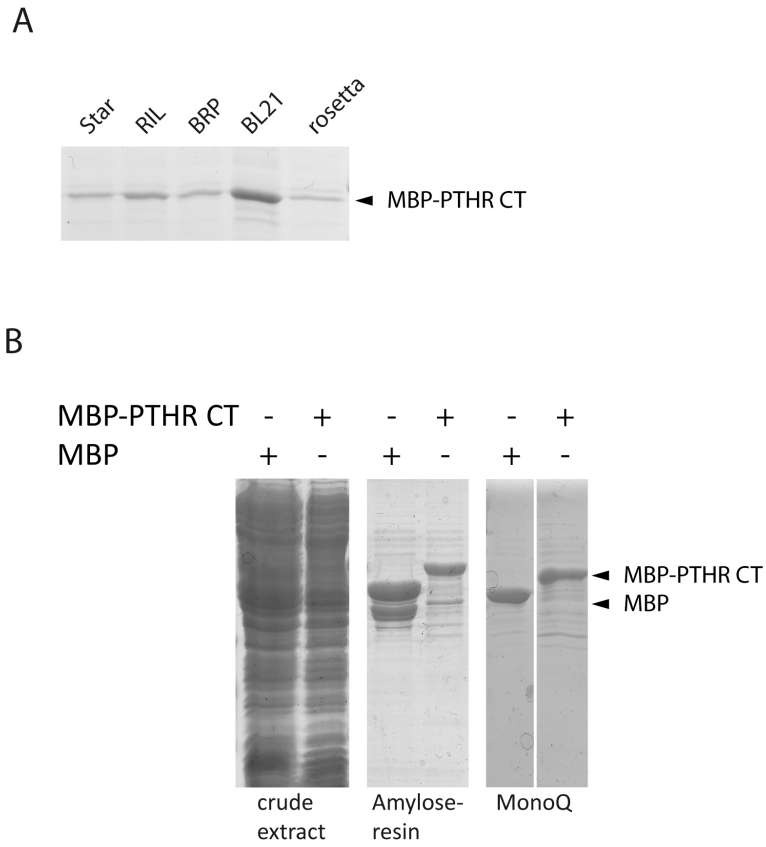

Figure 9. Expression and purification of MBP-PTHR CT construct and MBP. (a) The MBP-PTHR-CT fusion protein was expressed in the *Escherichia coli* strains BL21 (DE3)-pLysS, BL21 Star™-pLysS, BL21 (DE3) CodonPlus-RIL, BRP and rosetta™. The amount of recombinantly expressed MBP-PTHR-CT in 5 ml bacterial culture of individual bacterial strains was assessed by pull-down with 30 µl amylose-resin. The resin was washed twice with 500 µl wash buffer, and MBP-PTHR-CT was eluted by addition of 200 µl Laemmli buffer at 95 °C. Twenty µl of each sample were separated by SDS-PAGE and stained with Coomassie. **(b)** The MBP-PTHR-CT fusion protein and the MBP control protein was expressed in the *Escherichia coli* BL21 (DE3)-pLysS. An aliquot of the crude bacterial extract was saved for SDS-PAGE. The crude extract of 1 liter bacterial culture was applied to 4 ml amylose resin and incubated for at least 16 h at 4 °C. The resin was washed with 40 ml wash buffer, and the proteins were eluted using 10 mM maltose. The eluates were collected in 5 fractions of 3 ml and the fractions showing highest protein yields and sufficient purity were pooled. Elution fractions were diluted to salt concentrations of 20 mM or lower and subjected to MonoQ ion-exchange chromatography. Proteins were eluted by a NaCl gradient of 20 mM to 500 mM. Finally, the crude bacterial extract and purified fractions of both constructs from affinity and ion-exchange chromatography were analyzed using Coomassie staining of SDS-PAGE Gels.

4.1.2. Interaction screenings with tissue lysates

Purified MBP-PTHR CT and MBP proteins enabled a pull-down-based interaction screening with proteins derived from different cell-types. As mentioned above, PTHR are predominantly expressed in cells of bone and kidney. Thus, two cells-types, which are related to these human organs, were utilized for the interaction screening in this study. The interaction screening was performed using cytosolic fraction of bovine kidney tissue lysate and osteosarcoma cell lysate as described in **(ref. 3.4.3)**. Two milligrams of MBP-PTHR CT or MBP protein was immobilized on columns containing 1 ml amylose-resin. The resin was washed with 10 column-volumes wash buffer to further deplete unbound fusion protein or control protein and other impurities. At first instance, the fusion and control protein were incubated with 10 mg protein of cytosolic fractions from bovine kidney lysates or 16 mg from osteosarcoma lysates. Higher amounts of osteosarcoma lysates were used, because osteosarcoma lysates exhibited less intensive interactions with the PTHR-CT than bovine kidney lysates in previous experiments (data not shown). This procedure was done at 4 °C and in the presence of protease inhibitors to increase protein stability. After incubation, the resins were washed with 100 column-volumes of wash buffer containing 1 % Triton X-100 for kidney tissue lysate, or with wash buffer without Triton for rat osteosarcoma lysate. Immobilized MBP-PTHR-CT, which was incubated with osteosarcoma lysates, was washed at more gentle conditions omitting Triton X-100. This modification was necessary, as a significant proportion of bound proteins were lost when washing with Triton X-100-containing buffer (data not shown). In sum, the excess of cytosolic lysate and unspecifically bound interacting proteins of the PTHR were removed by indicated washing procedures. To specifically elute PTHR CT-interacting proteins, the resin was incubated with 16 ng (10 units) enterokinase in 2 ml of enterokinase buffer at room temperature for 18 h, thereby cleaving the PTHR CT from MBP. The supernatant after the enterokinase incubation represented the first elution fraction. After collecting the first elution fraction, the amylose resin was washed with 2 ml washing buffer to obtain the second elution fraction. These two elution fractions should ideally contain solely PTHR CT interacting proteins. In a third step, the resin was incubated with 5 ml washing buffer containing 10 mM maltose to elute MBP and remaining MBP-PTHR CT and to recover the columns. This third elution fraction contained proteins interacting with MBP or PTHR CT suggesting unspecific binding. Thus, only the first and the second elution fraction were pooled and subjected to SDS-PAGE. Afterwards proteins were visualized by silver staining **(Figure 10a) (ref. 3.3.2)**. The same protocol was performed with lysates from rat osteosarcoma (ROS) cells **(Figure 10b)**. In both cases, specific and intense protein bands were visible in the MBP-PTHR CT sample, showing that the first and second elution fraction obtained appropriate protein amounts.

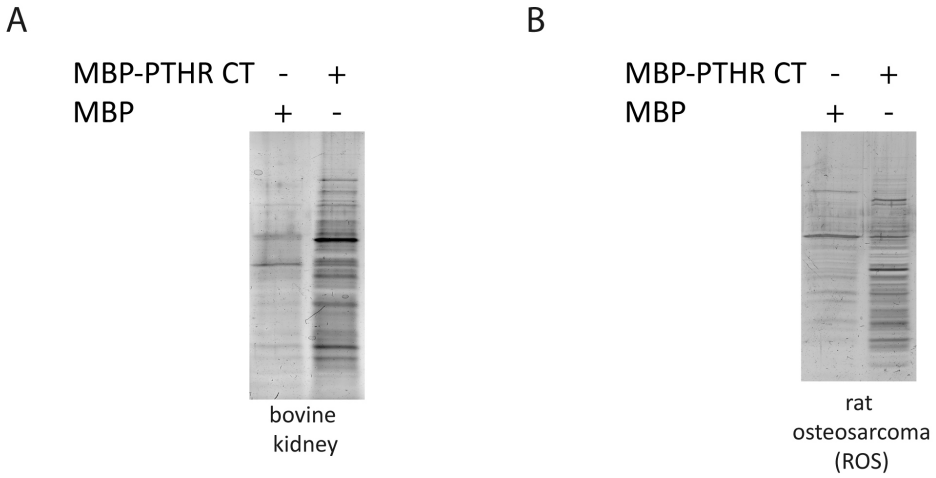

Figure 10. Enterokinase elution fraction of interaction screening with tissue or cell lysates. (a) Two mg of purified MBP or MBP-PTHR CT was immobilized on 1 ml amylose resin and incubated with 10 mg cytosolic fractions of bovine kidney tissue lysate. **(b)** Two mg of immobilized MBP or MBP-PTHR CT was incubated with 16 mg cytosolic fractions of lysates derived from rat osteosarcoma cells. PTHR C-terminus and bound proteins were eluted by enterokinase cleavage and were visualized by SDS-PAGE and silver staining.

4.1.3. Validation of construct integrity after incubation with tissue lysates

The integrity of the MBP-PTHR CT construct was verified prior to the analysis of elution fractions. Often the inability of bacteria to achieve post-translational modifications, like glycosylation, disulfide-bridges and phosphorylation, disrupts the integrity of recombinantly expressed mammalian proteins. Especially, a risk of incorrect folding, i.e. the tertiary structure, of mammalian proteins is present in bacteria. Thus, experiments to confirm the integrity of the MBP-PTHR CT construct, in terms of binding interacting proteins, were mandatory. In addition to correct protein folding, proteolysis during incubation with cell lysates and during the elution with enterokinases may have affected the stability of the PTHR CT. To confirm the construct integrity, enterokinase elution fractions and maltose-elution fractions were assessed by immunoblotting **(Figure 11a)**. For this purpose, an antibody directed to the last 20 amino acids of the PTHR C-terminus (PTHR CT 1781) was used. Cleavage of MBP-PTHR CT by enterokinase, SDS-PAGE and immunoblotting resulted in a band of approximately 14 kDa, whereas probes of the MBP control revealed no band with PTHR CT 1781 antibodies **(Figure 11a)**. This indicates that enterokinase successfully cleaved the MBP-PTHR CT construct. After enterokinase cleavage, residual proteins were eluted with maltose. The maltose elution fraction contained proteins detected by anti-PTHR CT antibodies at 58 kDa, presumably representing non-cleaved MBP-

PTHR CT construct **(Figure 11a)**. Furthermore, several bands at lower molecular weight occurred, which may represent potential degradation fragments of MBP-PTHR CT. Also a 14 kDa band was visible which represents residual cleaved PTHR CT that had not been completely eluted from the column after the enterokinase cleavage step.

As mentioned above, the integrity of the MBP-PTHR CT needs to be verified. For that, the binding capability to known PTHR interacting proteins represents a key ability. NHERF is a well-known adaptor protein and was shown to bind to the very C-terminal part of the PTHR CT. Moreover, NHERF1 is expressed in bovine kidney and can be detected by an anti-EBP50 (ezrin-binding protein 50) antibody **(ref. Figure 11b, lane 3)**. To verify whether the MBP-PTHR CT fusion protein was capable of binding NHERF1, a pull-down assay was performed. Purified MBP-PTHR CT was incubated with kidney lysate, precipitated using amylose resin, washed with wash buffer containing 1 % Triton X-100 and eluted by enterokinase cleavage. The elution fraction was examined by immunoblotting. Approximately 1.5 % of the total elution fractions and 0.15% of the amount of kidney lysate that was used for the interaction screening were separated by SDS-PAGE. Immunoblotting of NHERF1 using the enterokinase elution fraction revealed a specific band around 40 kDa. This 40 kDa band represents NHERF1 of kidney lysate, as it is verified by the control lane where kidney lysate was directly applied **(Figure 11b)**. Consequently, the integrity of the MBP-PTHR CT construct after the incubation with tissue lysates was confirmed in terms of NHERF1 binding. Furthermore, these data show that the procedure for the incubation with tissue lysate is suitable and that the MBP-PTHR CT fusion protein exhibits functional domains for interaction with other PTHR interacting proteins.

In sum, NHERF1 from kidney lysates interacted to a high proportion with the PTHR CT in the pull-down experiments. Consequently, it can be assumed that the recombinantly expressed PTHR CT has sufficient capacities to bind NHERF1, and it may be suggested that other unknown PTHR CT interacting proteins bind to the MBP-PTHR CT and would be present in the enterokinase elution fraction.

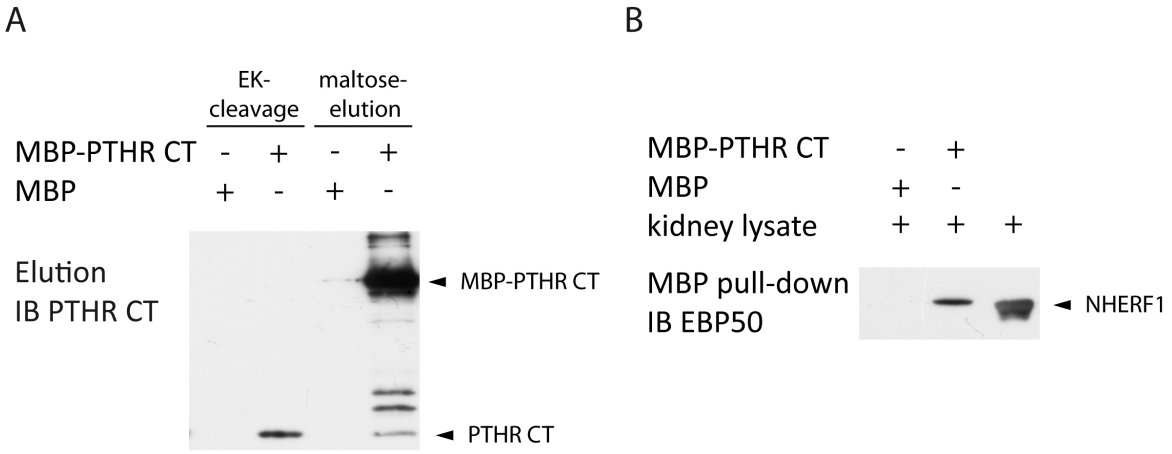

Figure 11. Validation of the integrity of the MBP-PTHR CT construct. (a) Thirty µl of the second or third elution fraction (1.5 % of the sample volume) derived from interaction screenings **(ref. 4.1.2)** were analyzed by SDS-PAGE and immunoblotting. For this purpose, antibodies directed against the PTHR C-terminus (CT) were utilized. First two lanes represent samples derived from elution via enterokinase cleavage, whereas lane three and four were derived from maltose elution. **(b)** For pull-down assay of MBP, MBP-PTHR CT or MBP was immobilized on amylose resin, incubated with kidney lysate, washed with wash buffer containing 1 % Triton X-100. Finally, elution via enterokinase cleavage was conducted. Thirty µl of the second elution fraction (1.5 % of the sample volume) was applied to SDS-PAGE. Thereafter, NHERF1 was detected by immunoblotting using anti-EBP50 antibodies. The third lane represents 0.15 % (15 µg) of the bovine kidney lysate that was applied to one sample of the interaction screening.

4.1.4. Mass spectrometry analysis

The first and second elution fraction derived from enterokinase cleavage **(ref. 4.1.2, 3.4.3)** was pooled and concentrated by utilizing Microcon® centrifugal filter devices. The quality of derived proteins samples was assessed by silver-staining of SDS-PAGE and by the determination of the protein concentration of each sample **(Figure 10)**. Protein samples which obtained sufficient intensities by silver staining and protein concentrations above 1 mg / ml were subjected to analysis by mass spectrometry (LC-MSMS) **(ref. 3.4.4)**. Evaluation and annotation of the results obtained by liquid chromatography and tandem mass spectrometry (LC-MSMS) was performed with the Scaffold software. Intensity of found protein fragments was expressed as *number of unique peptides*. The *number of unique peptides* expresses the quantity of the individual peptides that were assigned to a protein. For each identified protein, the *number of unique peptides* that were found in samples of the PTHR CT was divided by the *number of unique peptides* that were found in the control sample. This ratio, in latter named as specificity ratio, reflects the specific appearance of each protein in one experiment. The proteins were ranked by the resulting specificity ratio. The specificity ratios from individual experiments were added up to the total

specificity ratio. About 350 proteins were identified with a total specificity ratio greater than 2. The identified proteins exhibit various known biological functions. However, proteins of the keratin, myosin or albumin family were not considered for further data analysis as they represent unavoidable unspecific interacting proteins for this assay. Among the 350 proteins with specificity ratios above 2, 10 proteins were selected which appeared feasible as PTHR interacting proteins. Those 10 proteins included vav2, a guanine nucleotide exchange factor (GEF) for Rho GTPases, which appeared to be a reasonable PTHR interacting protein since other Rho GEFs have been described as adaptors for GPCR signaling [136-138, 140, 141, 162, 163].
Peptide fragments of vav2 were found in two of two experiments using bovine kidney lysates **(Figure 12) (Table 1)**. In detail, four unique peptides of vav2 were found in samples generated by incubation with the PTHR C-terminus, whereas no peptides of vav2 were found in samples generated by incubation with MBP **(Table 1)**. In addition, the mass spectrometry analysis obtained several known PTHR interacting proteins, such as NHERF1, NHERF3 and 14-3-3 protein gamma **(Table 1)**. Original raw data of mascot search are attached in the annex chapter. In experiments using cytosolic fractions of rat osteosarcoma cells, 50 proteins were identified with a specificity ratio above 2. Compared to 350 proteins from experiments conducted with kidney lysates, this might indicate a lower overall intensity of all proteins in the samples of those experiments. In line with the low representation of proteins, the mass spectrometry analysis of rat osteosarcoma cells also failed to identify the PTHR CT. Neither was vav2 identified in those samples. This data and direct immunoblotting of vav2 in rat osteosarcoma lysates suggested an absence of vav2 in this cell line (data not shown), which was unexpected since vav2 is known as a widely expressed protein. Nonetheless, the interaction of vav2 to the PTHR CT found in kidney lysates was examined in further experiments.

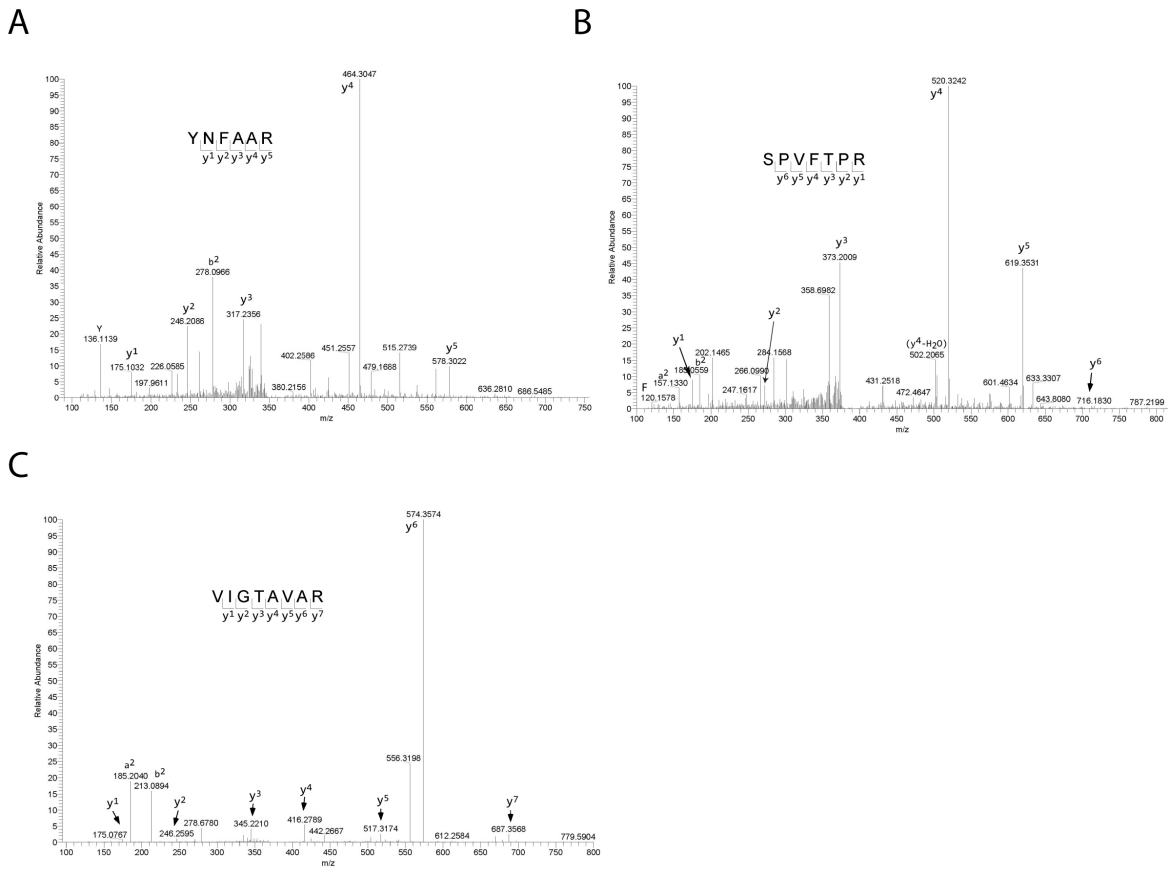

Figure 12. Fragment spectra (MSMS) of unique peptides that were obtained from kidney lysate and assigned to vav2. MSMS raw data were searched against NCBInr database using Mascot search engine. Relative intensities (abundance) of detected ions were assigned to mass to charge ratios. Y-type ion series for unique peptides were annotated. **(a)** YNAFAAR was assigned to vav2 with 90 % probability. **(b)** SPVFTPR was assigned to vav2 with a probability of 91 %. **(c)** VIGTAVAR was assigned to vav2 with 95 % probability. The mass spectrometry analysis and data processing by Mascot search engine were performed by the Bioanalytical Mass Spectrometry Group of Dr. Henning Urlaub at the Max Planck Institute for Biophysical Chemistry in Göttingen.

Protein	Kidney1 ratio	Kidney2 ratio	ROS ratio	total specificity ratio
NHERF1	6 : 0	2 : 1	0 : 0	8
NHERF3	15 : 0	0 : 2	0 : 0	15
14-3-3 protein gamma subtype	8 : 1	7 : 2	1 : 0	12.5
Parathyroid hormone receptor	3 : 0	3 : 0	0 : 0	6
vav 2 oncogene isoform 3	3 : 0	1 : 0	0 : 0	4

Table 1. Protein fragment identified by LC-MSMS. Specificity ratios (ratio) were calculated by *number of unique peptides* that were obtained from MBP-PTHR CT pull-down divided by the *number of unique peptides* derived from MBP pull-down. Specificity ratios are listed for each experiment using bovine kidney or rat osteosarcoma lysates. Total specificity ratios were obtained by addition of ratios from each individual experiment.

4.2. Vav2 directs PTHR signaling

Vav2 is a regulator of small Rho GTPases involved in cytoskeleton reorganization. To elucidate the relevance of the interaction of vav2 to PTHR, further experiments on the interaction to PTHR were conducted and the effect on PTHR-related signaling events was investigated.

4.2.1. Vav2 interacts with intracellular domains of PTHR

The interaction of vav2 with the PTHR-CT was identified by the interaction screening using recombinantly expressed MBP-PTHR CT and cytosolic lysates of bovine kidney. Results derived from mass spectrometry indicated this interaction to be specific to the PTHR CT. However, the environment of this interaction was rather artificial.

Further experiments were required to verify the interaction of vav2 to the PTHR. Therefore, a context similar to a physiological setting would be advisable. To confirm the PTHR vav2 interaction, co-immunoprecipitations were conducted in HEK 293 ad cells. HEK 293 ad cells are derived from embryonic kidney cells and serve as a simple model for cell biological and biochemical studies. At first instance, co-immunoprecipitations were performed by overexpressing myc-tagged human vav2 (myc-vav2) and HA-tagged human PTHR1 (HA-PTHR) or a C-terminally truncated HA-PTHR (T480). Prior to stimulation with 500 nM PTH 1-34 for 20 min at 37 °C, HEK 293 ad cells were incubated with latrunculin A. As an actin-pertubing compound, latrunculin A inhibits unspecific protein-interactions with the actin-cytoskeleton by reduction of F-actin. HA-PTHR was precipitated with agarose-gel-conjugated anti-HA antibodies (Sigma) and co-immunoprecipitation of myc-vav2 was detected with anti-myc antibodies. For better visualization, all samples were diluted at a ratio of 1 to 10 in Laemmli buffer before SDS-PAGE. Myc-vav2 did not precipitate with components of cells lacking PTHR or the affinity matrix itself **(Figure 13a)**. Thus, myc-vav2 did specifically interact with samples of co-transfected full-length HA-PTHR or truncated HA-PTHR T480. The interaction of vav2 with HA-PTHR was significantly stronger compared to HA-PTHR T480. Since the interaction of vav2 with the HA-PTHR T480 was still detectable, it can be assumed that part of the interaction relies on components of the PTHR CT from residue 481 to 593 or on intracellular loops of the receptor. Interestingly, the activation of PTHR with PTH 1-34 did not affect the interaction of vav2 **(Figure 13a)**. To confirm that equal amounts of myc-vav2 were expressed and that equal amounts of HA-PTHR were immunoprecipitated in all samples, control immunoblots using anti-vav2 and anti-HA antibodies were performed **(Figure 13a)**. The interaction between vav2 and PTHR, which appeared in co-immunoprecipitation experiments, was further elucidated by experiments

precipitating myc-vav2 and immunodetection of HA-PTHR **(Figure 13b)**. Here, HA-PTHR specifically interacted with samples derived from cells expressing myc-vav2. The immunoprecipitation experiments confirmed that the PTHR CT interacts with vav2.

Vav2 consists of multiple domains that serve as protein adaptors and displays a molecular weight of about 120 kDa. Thus, vav2 has a more than two-fold higher molecular weight compared to non-glycosylated PTHR. Hence it appears likely that the interface of vav2 that is required for the interaction to PTHR does not consist of the full protein but may be determined by certain domains. To further investigate which domains of vav2 serve for the interaction to the PTHR, a truncated vav2 mutant lacking N-terminal and C-terminal domains was utilized. N-terminal residues 1-187 and C-terminal residues 513-879 were deleted in this vav2 mutant. Hence, solely the GEF and the PH domain of vav2 were present **(Figure 6)**. HEK 293 ad cells transiently expressing the HA-PTHR and myc-vav2$^{188-512}$ were utilized for co-immunoprecipitation experiments. In detail, HA-PTHR was immunoprecipitated by anti-HA antibodies and co-precipitated myc-vav2$^{188-512}$ was detected by anti-myc antibodies. Interestingly, the truncated vav2 mutant, myc-vav2$^{188-512}$, was still capable of co-immunoprecipitating with HA-PTHR **(Figure 13c)**. Since HEK 293 ad cells endogenously express vav2 at high levels, the interaction of PTHR with endogenous vav2 could be elucidated in a more physiological setting. Subsequently, HEK 293 ad cells transiently expressing HA-PTHR were utilized for co-immunoprecipitations. For that, HA-PTHR was immunoprecipitated with anti-HA antibodies. Endogenously expressed and co-precipitated vav2 was detected by anti-vav2 antibodies **(Figure 13d)**. Remarkably, a strong band corresponding to the molecular size of vav2 appeared in the co-immunoprecipitated samples **(Figure 13d)**. Similarly to the overexpression experiments, endogenous vav2 co-precipitated in higher amounts with full-length HA-PTHR than with truncated HA-PTHR T480. To quantify the reduced interaction of vav2 upon deletion of the PTHR CT in the truncated PTHR construct, densitometry experiments of five co-immunoprecipitations were performed **(Figure 13e)**. For this quantification, intensities were plotted relative to the intensity of HA-PTHR. This analysis showed that levels of vav2 that co-precipitated with HA-PTHR T480 construct were about 50 percent lower compared to full-length HA-PTHR **(Figure 13e)**. A statistical analysis by performing non-parametric one-way analysis of variance was done between conditions HA-PTHR and HA-PTHR T480 resulting in significant differences for vav2-interactions ($P<0.001$, CI_{95} 0.4535 to 0.6169). In sum, myc-vav2 as well as endogenous vav2 interacts with PTHR in HEK 293 ad cells, and about half of the interaction is established by the PTHR C-terminal domain.

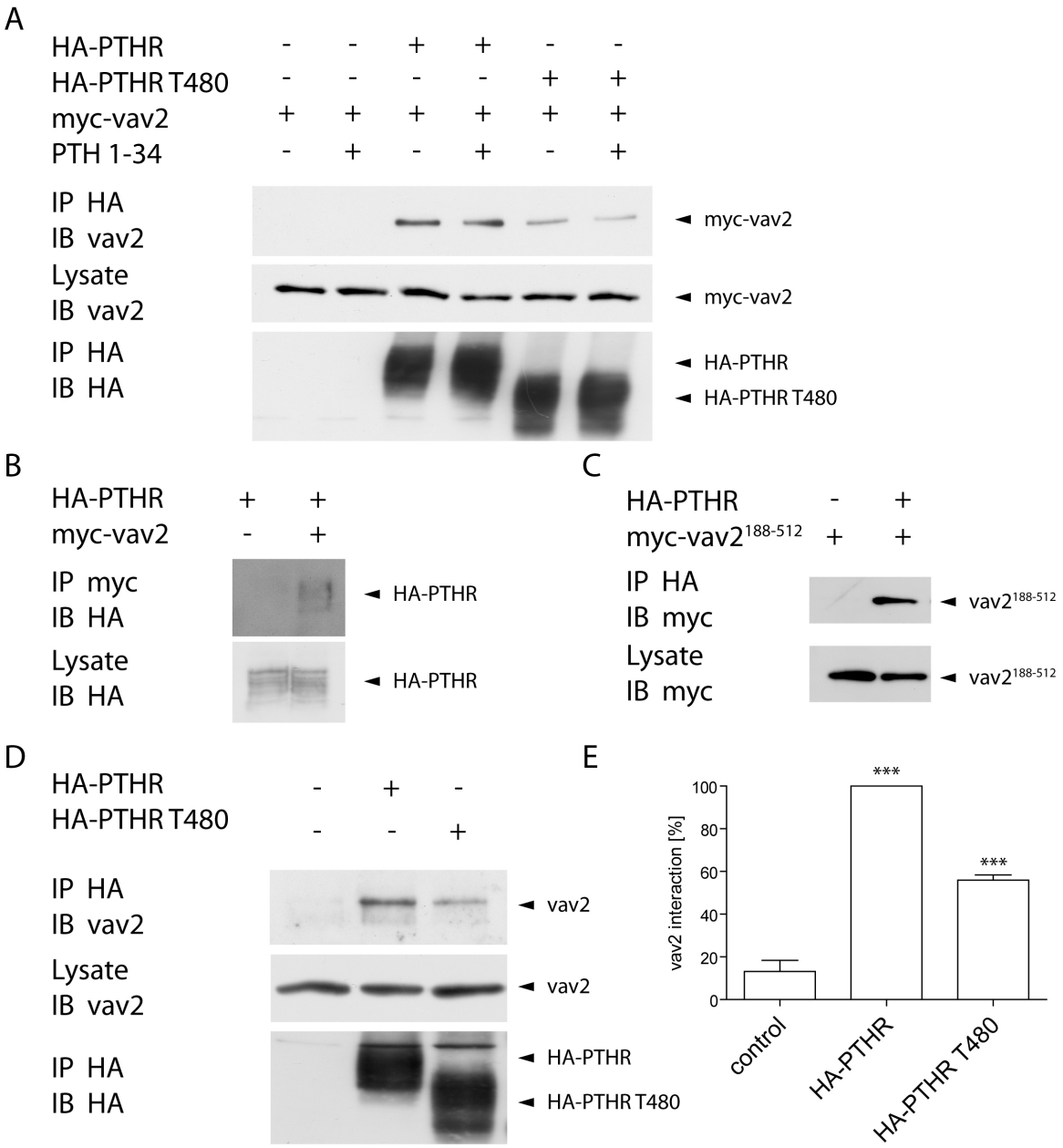

Figure 13. Vav2 interacts with PTHR independent of receptor activation. (a) Myc-vav2 and HA-PTHR or C-terminal truncated HA-PTHR (T480) were transiently expressed in HEK293 ad cells. Cells were stimulated with 1 µM PTH 1-34 or medium for 20 min, and HA-PTHR or HA-PTHR T480 was immunoprecipitated (IP) with anti HA-antibodies. Immunoblotting (IB) of myc-vav2 was accomplished using anti-myc-antibodies. Expression levels of HA-PTHR and myc-vav2 in the lysate were assessed using anti-HA and anti-myc antibodies. **(b)** Myc-vav2 was immunoprecipitated and PTHR was detected by immunoblotting with anti-HA-antibodies. **(c)** Myc-vav2$^{188-512}$ and HA-PTHR were transiently expressed in HEK293 ad cells. HA-PTHR was immunoprecipitated with anti-HA affinity beads and Western blots of immunoprecipitates were probed for myc. **(d)** Immunoprecipitation of HA-PTHR with anti-HA antibodies was conducted by using HEK 293 ad cells transiently expressing the PTHR. Endogenous vav2 in lysates and precipitates was detected by immunoblotting (IB) with anti-vav2 antibodies. **(e)** Luminescence intensities obtained from antibodies bound to co-precipitated vav2 **(d)** were measured, normalized and are shown relative to vav2 and receptor expression. n = 5, error bars: SEM. Statistical significance was determined by one-way ANOVA (***, $p < 0.001$, mean difference 44.05 %, CI_{95}: 31.92 to 56.18).

Similar to full-length vav2, constitutively active vav2$^{188-512}$ interacted with the PTHR suggesting that GEF activity does not alter PTHR interaction of vav2. Nevertheless, the quantity of interaction between full-length or truncated vav2 to PTHR was hard to compare, since transfection efficiency of two different constructs dramatically affects experimental outcome. To further elucidate whether GEF activity had an influence on the interaction, an additional approach was applied. In previous studies, it was shown for vav that GEF activity was enhanced upon phosphatidylinositol-3,4,5-trisphosphate binding, whereas binding to phosphatidylinositol-4,5-bisphosphate inhibits GEF activity **(ref. 1.6)** [129]. This enhancement of GEF activity probably relies on conformational changes between auto-inhibitory domains and the GEF domain. By addition of phosphatidylinositol-3,4,5-triphosphate dioctanoyl (C_8-PIP_3) to cell lysates of HA-PTHR expressing HEK 293 ad cells, the effect of GEF activity on the PTHR-vav2 interaction was examined. Remarkably, the incubation with C_8-PIP_3 did not affect the amount of co-immunoprecipitated vav2 compared to untreated cell lysates (lane 2 and 3) **(Figure 14)**. This indicates that the GEF activity of vav2 does not impair the binding of vav2 to PTHR. Notably, this result supports the data on constitutively active vav2$^{188-512}$, which interacts with PTHR likewise full-length vav2 **(Figure 13c)**.

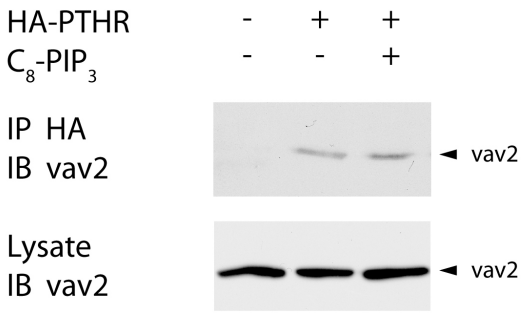

Figure 14. Influence of C_8-PIP_3 on the interaction between vav2 and PTHR. HA-PTHR was transiently expressed in HEK 293 ad cells, as indicated. HA-PTHR was immunoprecipitated in absence and presence of 100 µM L-α-phosphatidyl-D-myo-inositol-(3,4,5)-trisphosphate, dioctanoyl (C8-PIP3). Co-precipitated vav2 was detected by anti-vav2 antibodies in Western blots.

Full-length PTHR exhibited approximately double the interaction capacity for vav2 proteins than truncated PTHR T480 mutants. To elucidate whether additional residues located between positions 460 to 480 of the C-terminal domain are required for the interaction with vav2, two truncation mutants of the PTHR at position 470 and 459 were generated. To test receptor integrity of the truncation mutants HA-PTHR T459 or HA-PTHR T470 were stably expressed in HEK 293 ad cells. Prior to immunodetection, cells were permeablized to detect HA-tagged

receptor at the cell surface as well as at intracellular compartments. Afterwards, the PTHR mutants were detected by anti-HA antibodies and Cy2-tagged anti-mouse antibodies. Immunofluorescence was visualized by a wide-field fluorescence microscope. For the PTHR WT and PTHR T480, a clear membrane-staining appeared in the immunofluorescence experiments **(Figure 15a-b)**. In contrast to PTHR WT and PTHR T480 weak surface expression for PTHR T470 and PTHR T459 was observable. Rather, these mutants appeared to be trapped in intracellular compartments **(Figure 15c-d)**. Consequently, PTHR T470 and PTHR T459 were not employed for further experiments.

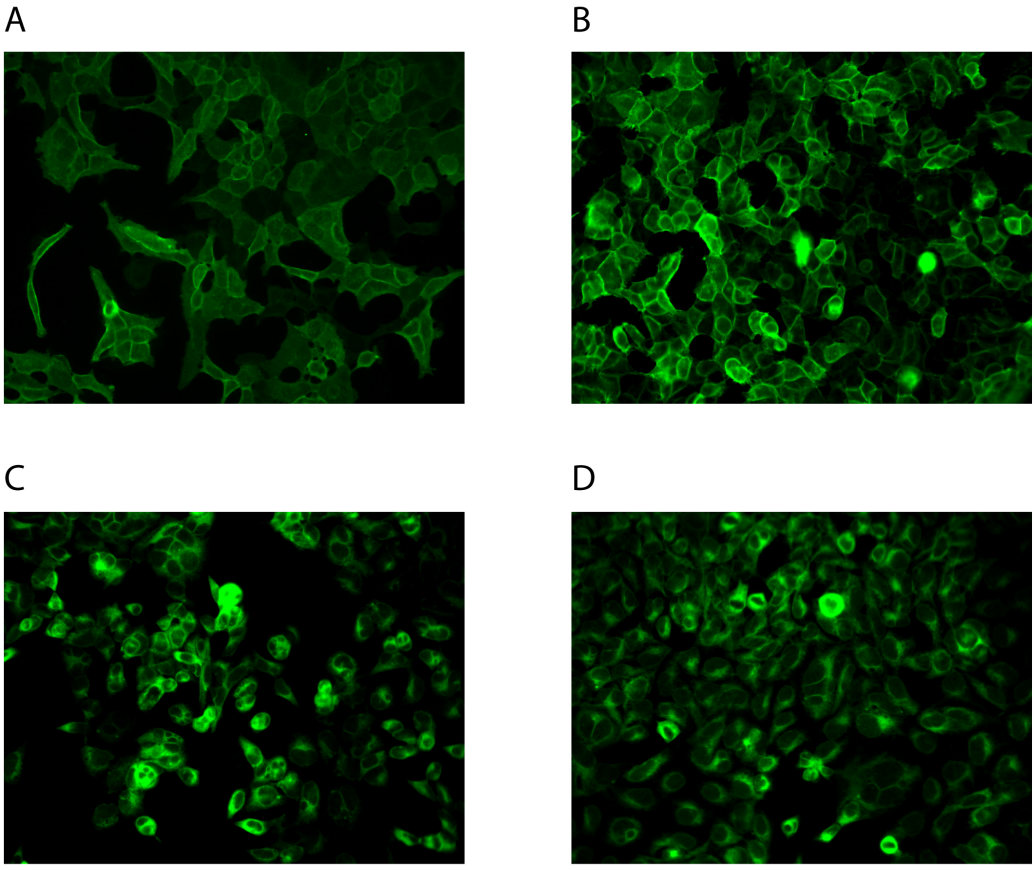

Figure 15. Wide-field microscopy for detection of HA-PTHR mutants by immunofluorescence. Monoclonal HEK 293 ad cells, stably expressing HA-PTHR mutants, were fixed on 96-well plates and visualized by Cy2-tagged anti-HA antibodies on a wide-field microscope (BD Pathway™). Full-length HA-PTHR **(a)** and HA-PTHR T480 **(b)** can be observed as mostly plasma membrane localized fluorescence staining. Whereas, for HA-PTHR T470 **(c)** and HA-PTHR T459 **(d)** predominant fluorescence staining in intracellular compartments was observed.

4.2.2. PTH induces phosphorylation of vav2

As shown above, vav2 was identified as a novel interaction partner for intracellular domains of the PTHR. Thus, the question arose whether this interaction has an impact on the activity of either or both interaction partners. Vav2 tightly regulates cytoskeleton reorganization by GEF function for Rho GTPases, thereby controlling intracellular compartmentalization, cellular morphology and movement **(ref. 1.6)**. The GEF function of vav2 itself, is controlled by auto-inhibitory function of N-terminal domains on the GEF domain **(ref. 1.6.1)**. Tyrosine phosphorylation at N-terminal residues, especially Y^{172} in human vav2, abrogates auto-inhibition, thus triggering the release of the vav2 GEF function. To investigate how PTHR and vav2 are mechanistically linked, tyrosine phosphorylation of vav2 was examined in dependence of PTHR activation. Myc-vav2 and HA-PTHR were overexpressed in HEK 293 ad cells or COS-7 cells. The COS-7 cell model was often used for phosphorylation studies on vav2 proteins, therefore serving as prove of principle for the parallel experiments using HEK 293 ad cells. Both cell lines were starved before stimulation with PTH 1-34 or EGF. Basal phosphorylation was measured by addition of medium without stimulation compounds. Post-stimulation, myc-vav2 was immunoprecipitated and phospho-tyrosine (P-Y) or phospho-tyrosine^{172} (P-Y^{172}) was detected by immunoblotting with corresponding phospho-antibodies. Stimulation with EGF was used as a positive control for vav2 phosphorylation. Since, EGFR are endogenously expressed in HEK 293 ad and COS-7 cells stimulation by EGF should lead to activation of the EGFR and subsequently to vav2 phosphorylation via the receptor tyrosine kinase activity of the EGFR. This mechanism was confirmed as a strong signal was obtained with P-Y and P-Y^{172} antibodies after EGF stimulation **(Figure 16a-b)**. Interestingly, upon stimulation of HEK 293 ad and COS7 cells with PTH 1-34, immunoblotting with P-Y and P-Y^{172} antibodies revealed strong signals at the molecular weight of vav2 **(Figure 16a-b)**.

Furthermore, vav2 phosphorylation was quantified by densitometric measurements of signals obtained by anti-P-Y antibodies **(Figure 16a-b)**. EGF-mediated and PTH 1-34-mediated phosphorylation of vav2 were significantly higher than basal phosphorylation ($P<0.01$) **(Table 2)**. However, vav2 phosphorylation, induced by PTH 1-34, seems to be less intense than the vav2 phosphorylation which was induced by EGF. Immunoblotting of precipitated myc-vav2 verified equal expression levels for each stimulation probe. It should be mentioned that some vav2 phosphorylation was detected even under basal conditions. Overexpression of vav2 in HEK 293 ad or COS7 cells dramatically increased the amount of vav2. Since vav2 regulates proliferation and apoptosis, increased amounts of vav2 affect cellular homeostasis for several physiological processes. Consequently, experiments conducted by overexpression of myc-vav2 may generate artifacts regarding vav2 phosphorylation. To elucidate whether PTH-induced vav2

phosphorylation is present in HEK 293 ad cells at physiological vav2 expression levels, phosphorylation experiments detecting endogenous vav2-phosphorylation were performed. For that, after 2 min of stimulation with EGF or PTH 1-34, vav2 proteins were precipitated with anti-vav2 antibodies and phosphorylation of P-Y^{172} was detected with corresponding antibodies in Western blots **(Figure 16c)**. Similar to overexpressed vav2, the phosphorylation state of endogenously expressed vav2 was increased after stimulation with PTH 1-34 **(Figure 16c)**. Immunoblotting of precipitated vav2 verified equal expression levels for each stimulation probe. In sum, these results suggest that the activation of the PTHR affects the phosphorylation state of key tyrosine residues for GEF activity and therefore dynamically regulates vav2 activity.

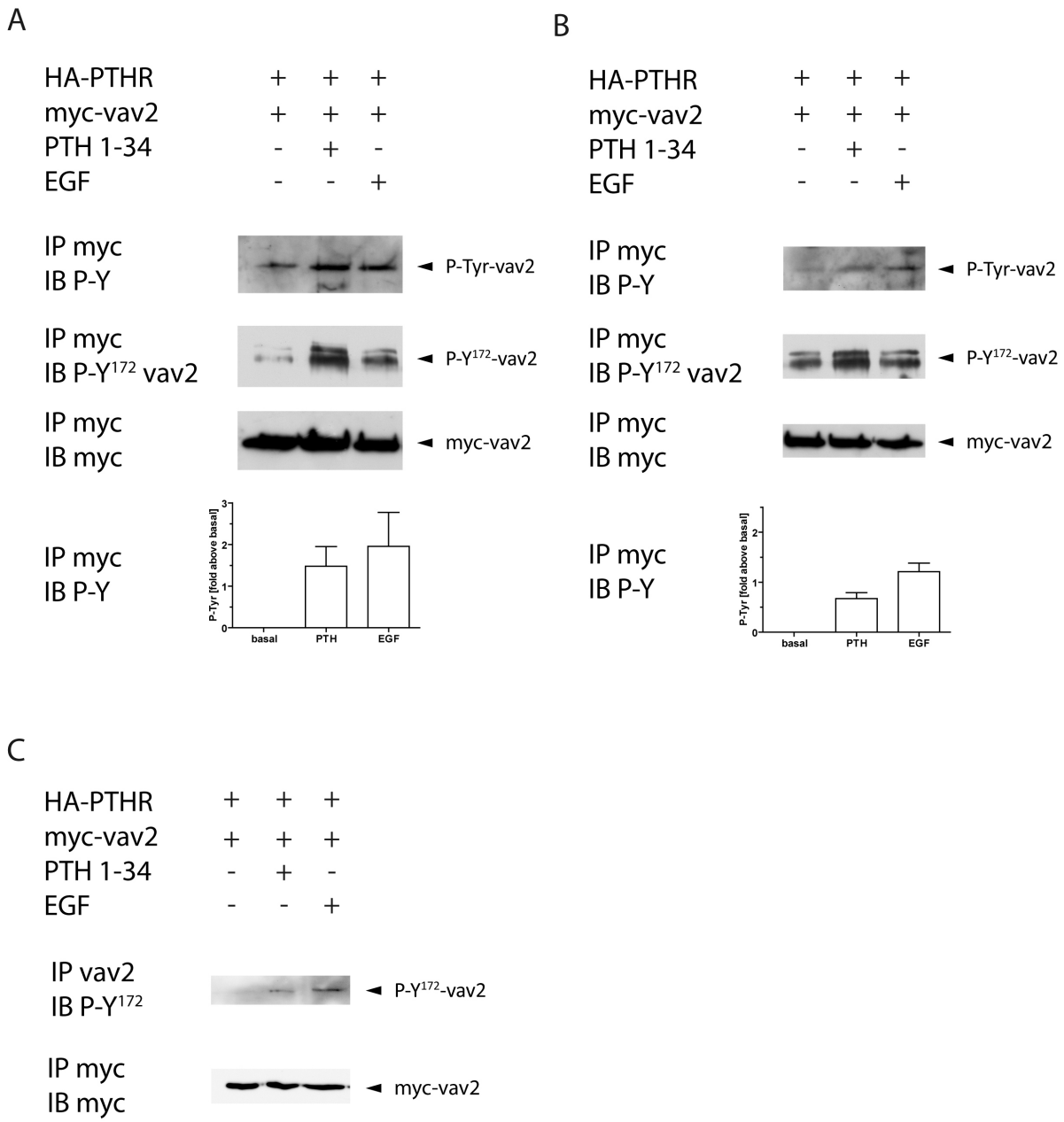

Figure 16. PTH-induced tyrosine-phosphorylation of vav2. COS7 cells **(a)** or HEK 293 ad cells **(b)** were transfected with cDNA coding for HA-PTHR and myc-vav2. Cells were stimulated for 2 min with 500 nM PTH 1-34, 100 ng / ml EGF or pure medium. Directly after stimulation, cells were lysed and myc-vav2 was immunoprecipitated using anti-myc antibodies. Myc-vav2 phosphorylation was detected utilizing anti-phospho-tyrosine or anti-phospho-Y^{172}-vav2 antibodies. Luminescence was quantified, normalized to basal phosphorylation and shown relative to vav2 expression. n = 5, error bars represent SEM. **(c)** Phosphorylation of Y^{172} of endogenously expressed vav2 in HEK 293 ad cells was detected with anti-phospho-Y^{172}-vav2 antibodies. Experiments were performed according to **(b)**.

Dunnett's Multiple Comparison Test	Mean Diff.	q ratio	P-value	CI_{95}
basal vs. PTH	-0.6731	3.802	P < 0.01	-1.121 to -0.2252
basal vs. EGF	-1.211	7.253	P < 0.01	-1.633 to -0.7883

Table 2. Statistics on vav2 tyrosine-phosphorylation (P-Tyr) in HEK 293 ad cells (Figure 16b). Luminescence obtained from Western blotting against P-Y in HEK 293 ad cells was quantified and statistically analyzed. For this purpose, analysis of variance and a post-test (Dunnett's Multiple Comparison Test) was performed to compare luminescence intensities. Samples stimulated with PTH 1-34 or EGF and non-stimulated (basal) cells were compared. Q ratio was calculated as the difference of the mean divided by standard error of difference (SED). n=5, (P<0.01). CI_{95} represents the 95 % confidence interval.

4.2.3. Vav2 specifically couples to $G\alpha_q$- but not to $G\alpha_s$-G protein subunits

To this point, it was shown that activation of the PTHR by PTH 1-34 affects the phosphorylation state of tyrosine residues that directly regulate GEF activity of vav2. Next, it was investigated whether vav2, vice versa, impaired the signaling activity of PTHR. Since the predominant PTHR signaling is represented by G protein-mediated pathways, investigation was initially focused on a link between vav2 and subunits of heterotrimeric G proteins. Vav2 as well as heterotrimeric G proteins are abundantly expressed in many tissues and cell-types. Consequently, the question arises, whether vav2 interacts with subunits of heterotrimeric G proteins in those cell-types. As a multi-adaptor protein, vav2 may exhibit the ability to scaffold G protein subunits and PTHRs. At first, co-immunoprecipitation experiments were conducted using differential overexpression of $G\alpha_q$, or $G\alpha_s$, myc-vav2 and PTHR. As PTHR signaling affected the activity of vav2, in the following precipitation experiment, G proteins were driven into and kept in an active state by stimulation of HEK 293 ad cells with PTH 1-34 and the addition of aluminum fluoride. The complex aluminum fluoride (AlF_4^-) represents a high affinity analogue of phosphate, thus mimicking the phosphate of GTP at the GTP-binding pocket of the G protein. This mimic is possible due to similar steric orientation and charge. Myc-vav2 was immunoprecipitated and antibodies specific for $G\alpha_q$ or His_6-$G\alpha_s$ were used to detect co-immunoprecipitation **(Figure 17a-b)**. Interestingly, activated $G\alpha_q$ subunits were specifically co-immunoprecipitated in presence of myc-vav2 **(Figure 17a)**. The amount of co-immunoprecipitated $G\alpha_q$ decreased when PTHR was co-expressed, suggesting a competition between PTHR and myc-vav2 for $G\alpha_q$ binding **(Figure 17a)**. Remarkably, myc-vav2 did not co-precipitate with the $G\alpha_s$ subunits in presence or absence of PTHR **(Figure 17b)**. This strikingly demonstrates that vav2 specifically interacts with $G\alpha_q$. As a control, equal expression levels for Gα subtypes and precipitated myc-vav2 amounts were monitored by immunoblotting with corresponding antibodies. In sum, vav2 bound to activated $G\alpha_q$, but not to $G\alpha_s$, in a competitive manner with activated PTHR.

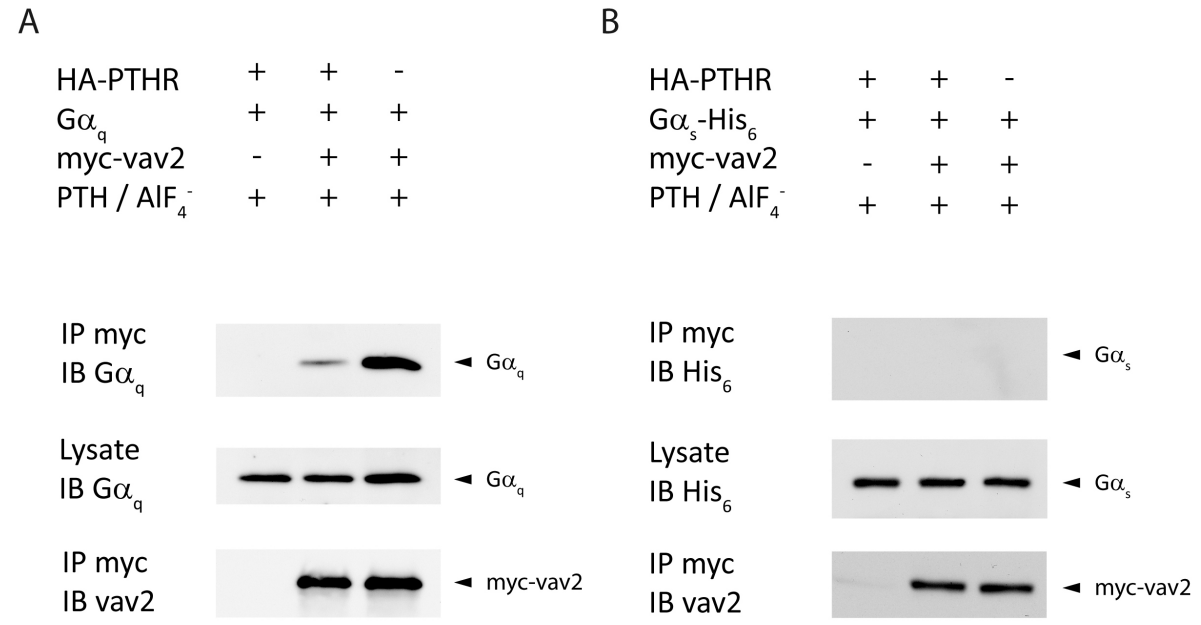

Figure 17. Vav2 and PTHR compete for activated Gαq, but not Gαs G protein subtypes. HEK 293 ad cells were transfected with HA-PTHR, myc-vav2 and Gαq **(a)** or Gαs **(b)**, as indicated. Myc-vav2 was immunoprecipitated and co-immunoprecipitated Gαq or Gαs was detected by immunoblotting. Amounts of precipitated myc-vav2 and expression levels Gαq or Gαs subunits were assessed using anti-myc and anti-G-alpha antibodies, respectively.

4.2.4. Vav2 and activated G-alpha$_q$ compete for PTHR

So far, it was shown that myc-vav2 binds to Gαq subunits of heterotrimeric G proteins **(4.2.3)**. This interaction may interfere with coupling of Gαq to the PTHR. Thus, these interactions were assessed further using immunoprecipitations of PTHRs and detection of co-immunoprecipitated Gαq in dependence of vav2 expression levels. For this purpose, vav2 expression levels were reduced by small-interfering RNA (siRNA) directed to endogenous vav2 or increased by overexpression of myc-vav2 **(Figure 18a)**. HA-PTHR was overexpressed in HEK 293 ad cells and stimulated with PTH 1-34. In addition, Gαq subunits were activated with aluminum fluoride during co-immunoprecipitation experiments. PTHR was precipitated by anti-HA antibodies and co-immunoprecipitated Gαq was detected by immunoblotting. Gαq specifically interacted with PTHR and co-immunoprecipitated in detectable amounts. Interestingly, overexpression of myc-vav2 led to a decreased PTHR-Gαq interaction **(Figure 18a)**. Precipitations of equal amounts of HA-PTHR were verified by immunoblotting for the HA-epitope. Expression levels of Gαq and vav2 were monitored by immunoblotting using anti-Gαq and anti-vav2 antibodies, respectively. Overexpression of myc-vav2 significantly increased the overall vav2 expression levels, whereas

knockdown of endogenous vav2 by siRNA had minor effects on vav2 expression in this experiment.

These results suggest that vav2 and PTHR compete for $G\alpha_q$-binding. PTHR-$G\alpha_q$ binding is assumed to be dependent on the activation state of the G protein subunit, according to the ternary complex and precoupling models **(ref. 1.2.1)**. To address the question whether myc-vav2 binds to $G\alpha_q$ in an activation dependent manner, co-immunoprecipitation experiments were performed **(Figure 18b)**. For that, $G\alpha_q$ was differentially activated by PTH-mediated PTHR activation or the GTP-mimicking salt aluminum fluoride. Myc-vav2 was immunoprecipitated and co-immunoprecipitated $G\alpha_q$ was detected with anti-$G\alpha_q$ antibodies. Activated $G\alpha_q$ did not interact in an unspecific manner with compounds or material of the co-immunoprecipitation experiment in absence of myc-vav2. Furthermore, non-activated $G\alpha_q$ displayed a weak interaction with myc-vav2. Interestingly, the addition of aluminum fluoride led to a small increase of the vav2-$G\alpha_q$ interaction, whereas PTH-mediated activation of the PTHR strongly increased vav2-$G\alpha_q$ interaction **(Figure 18b)**. Expression levels of $G\alpha_q$ and amounts of precipitated myc-vav2 were monitored by immunoblotting using anti-$G\alpha_q$ and anti-vav2 antibodies, respectively **(Figure 18b)**. Hence, additional evidence is provided that vav2 and PTHR compete for interactions with $G\alpha_q$. Furthermore, interactions of vav2 and $G\alpha_q$ were increased upon PTH-induced activation of $G\alpha_q$.

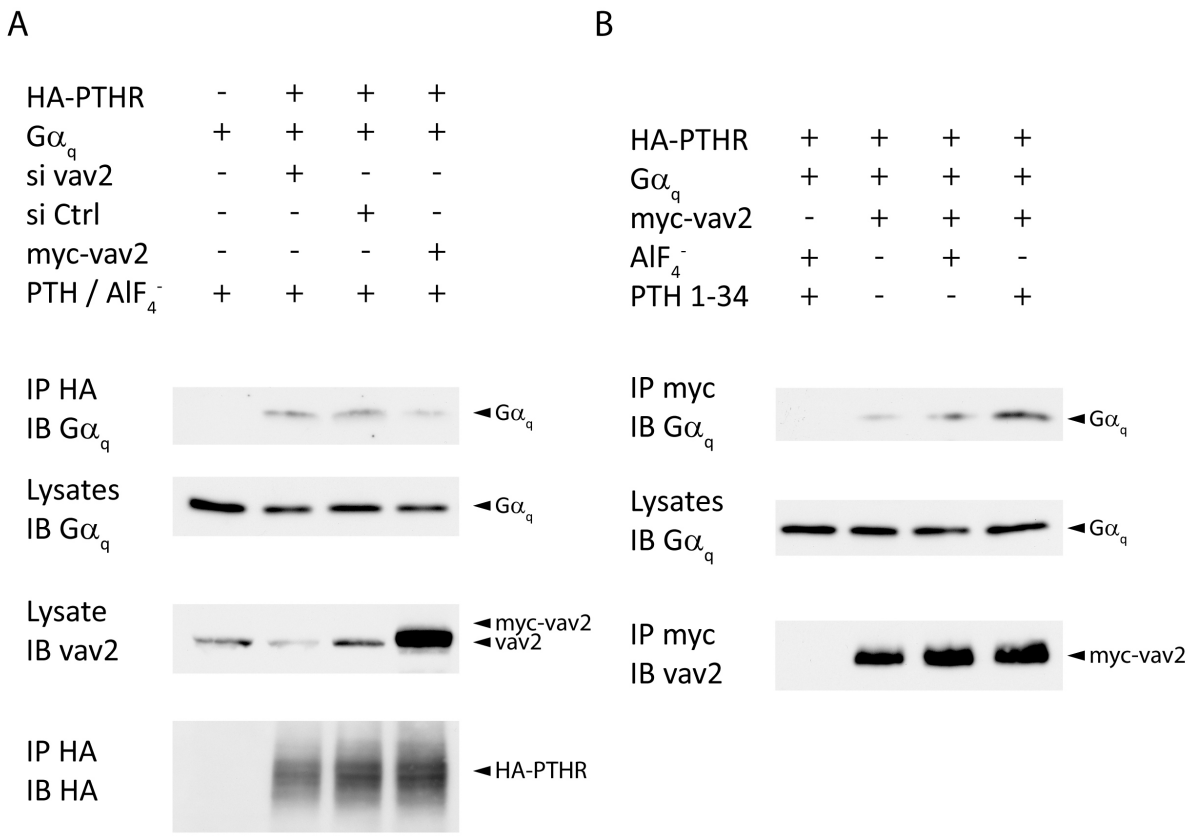

Figure 18. Vav2 interferes with coupling of $G\alpha_q$ to PTHR in an activation-dependent manner. (a) HEK 293 ad cells were transiently transfected with HA-PTHR and $G\alpha_q$. In addition, si vav2 RNA, non-targeting siRNA (si Ctrl) or myc-vav2 were co-transfected as indicated. Cells were stimulated with 1 µM PTH 1-34 for 20 min and lysed. HA-PTHR was immunoprecipitated (IP) using anti-HA antibodies and $G\alpha_q$ was detected with anti-$G\alpha_q$-antibodies (IB). Expression levels of vav2 and HA-PTHR in cell lysates were assessed by immunoblotting using anti-vav2 and anti-$G\alpha_q$ antibodies, respectively. Lysis, incubation and washing were performed in presence of aluminum fluoride. **(b)** HEK 293 cells were transfected with HA-PTHR, $G\alpha_q$ and myc-vav2, stimulated with PTH, according to (a), and myc-vav2 was immunoprecipitated in the presence or absence of aluminum fluoride. Co-immunoprecipitated $G\alpha_q$ was detected with anti-$G\alpha_q$-antibodies. Precipitated amounts of myc-vav2 and expression levels of $G\alpha_q$ were assessed according to (a).

4.2.5. PTH-induced PLC signaling is impaired by vav2

It was becoming clear, that vav2 displays interaction with $G\alpha_q$ subunits of heterotrimeric G proteins. Thus, the question arose whether vav2 is involved in $G\alpha_q$-mediated PTHR signaling. Consequently, the relevance of vav2 for the PTHR signaling-pathway, which is mediated by $G\alpha_q$ subunits and leads to PLCβ-activation towards generation of inositol trisphosphate (IP_3), was examined. To further confirm that vav2 has specific effects on $G\alpha_q$ subunits, but not $G\alpha_s$ subunits, signaling experiments on AC activation and subsequent generation cyclic AMP (cAMP) were also performed. For this purpose, a monoclonal HEK 293 ad cell line was generated that stably expresses HA-PTHR. Monoclonal cell lines allowed more accurate investigation of PTHR-mediated signaling events than cells transiently overexpressing PTHR. Furthermore, PTHR expression levels are more constant in stable cell lines. Previous co-immunoprecipitation experiments were performed using overexpression of vav2 and $G\alpha_q$. To achieve a more native environment for cell signaling, effects of vav2 were elucidated without overexpression but by silencing endogenous vav2 expression. For that, si vav2 RNA was used to reduce endogenous amounts of vav2. Signaling events were compared to cells transfected with non-targeting si control RNA (si Ctrl). The monoclonal HA-PTHR expressing cell line was transfected with si vav2 RNA or si Ctrl RNA, incubated with myo-[2-^{3}H] inositol, and 60 h post-transfection cells were stimulated with PTH 1-34, and inositol phosphate generation was measured **(Figure 19a)**. Strikingly, PTH-induced generation of myo-[2-^{3}H] inositol phosphate ([^{3}H]-IP) was significantly increased upon down-regulation of vav2 **(Figure 19a) (Table 3)**. Interestingly, the basal level of [^{3}H]-IP_3 and EC_{50} values for PTH 1-34 did not change **(Table 4.)**. In contrast, co-immunoprecipitation experiments suggested that vav2 does not interfere with PTHR signaling to $G\alpha_s$ **(4.2.3)**, and therefore it seems reasonable that vav2 does not affect PTH-induced cAMP generation. To confirm this hypothesis, cAMP generation was examined in cells where vav2 expression was silenced and in cells with native vav2 expression levels, similar to the IP_3 measurements **(Figure 19b) (Table 3)**. In line with the above mentioned hypothesis, down-regulation of vav2 had no impact on PTH-induced cAMP generation. Simultaneously to signaling experiments, immunoblotting of vav2 and HA-PTHR in cell lysates were performed to confirm knockdown of vav2 by siRNA and amounts of stably expressing HA-PTHR **(Figure 19c)**. Thus, the data provides evidence that vav2 selectively impairs PTH-induced PTHR signaling via $G\alpha_q$ and PLCβ, resulting in impaired IP_3 generation.

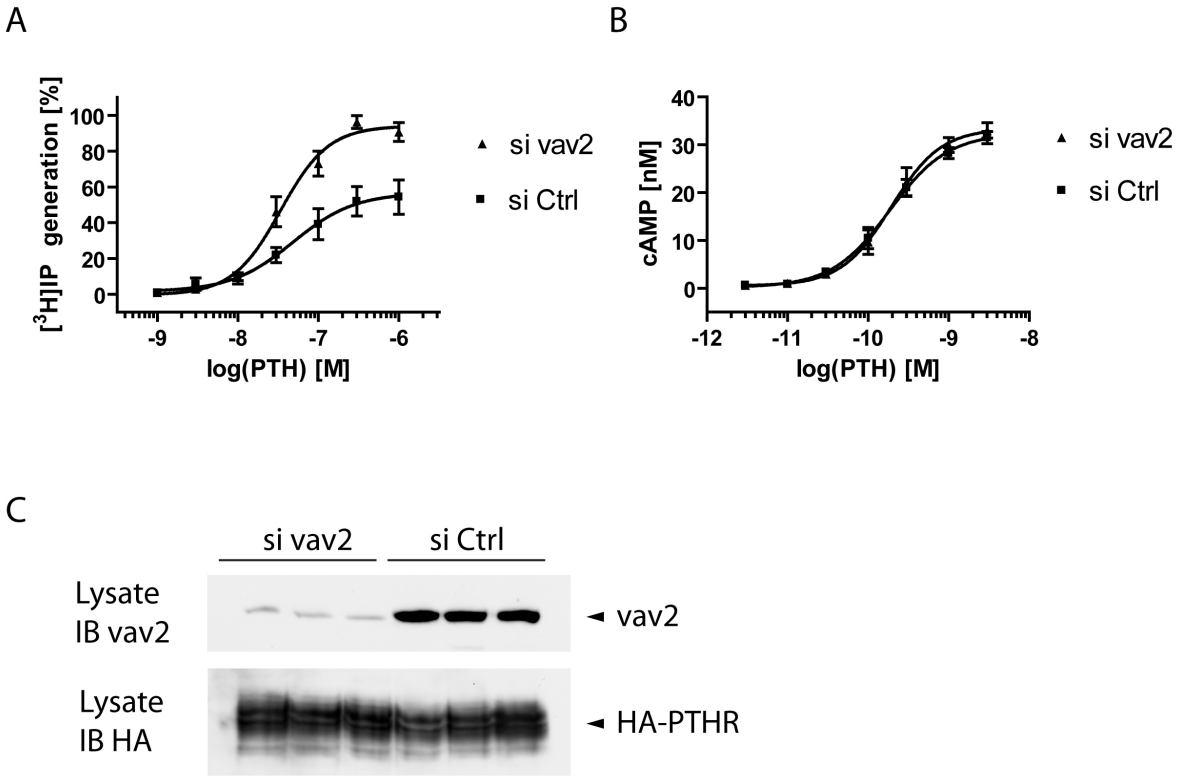

Figure 19. Vav2 impairs PTH-induced PLCβ signaling, but not AC signaling. HEK 293 ad cells stably expressing HA-PTHR were transfected with si vav2 RNA or non-targeting siRNA (si Ctrl). **(a)** Cells were incubated with myo-[2-^{3}H] inositol and 0.2 % FCS for 16 h prior to stimulation. Cells were stimulated for 60 min with PTH 1-34 at the indicated concentrations, and [^{3}H]-inositol phosphate was quantified in a Beckmann counter after chromatographic separation. Error bars represent SEM of five independent experiments. **(b)** HEK 293 ad cells were stimulated for 20 min with PTH 1-34 at indicated concentrations and cAMP levels were determined in a radioimmunoassay. Error bars represent SEM of five independent experiments. **(c)** The extent of vav2 knockdown by si vav2 RNA and HA-PTHR expression levels was assessed by immunoblotting using anti-vav2 and anti-HA antibodies, respectively.

Student t-test (unpaired)	**Mean Diff. ± SEM**	**P-value (two-tailed)**	**CI_{95}**
[^{3}H]-IP generation: si Ctrl vs. si vav2 [%]	44.3 ± 7.7	0.0012	25.4 to 63.1
cAMP generation: si Ctrl vs. si vav2 [nM]	1.5 ± 2.1	0.49	-3.3 to 6.2

Table 3. Effects of vav2 knockdown on PTH-induced [^{3}H]-IP and cAMP generation. The mean difference of [^{3}H]-IP generation, induced by 300 nM PTH 1-34, was compared for vav2 knockdown and endogenous vav2 expression in HEK 293 ad cells by an unpaired t-test. According to [^{3}H]-IP generation, the mean difference of cAMP generation was compared between vav2 knockdown and endogenous vav2 expression by an unpaired t-test. Data summarizes results of five independent experiments.

[^{3}H]-IP generation	PTH 1-34 EC_{50} (CI_{95}) [nM]	Basal (CI_{95}) [%]
si vav2	34.0 (24.3 to 47.2)	-0.4 (-9.0 to 8.2)
si Ctrl	48.2 (19.9 to 117.2)	1.5 (-9.3 to 12.3)

Table 4. Effect of vav2 knockdown on basal [^{3}H]-IP levels or EC_{50} values for PTH 1-34. EC_{50} values for PTH 1-34 on PTHR expressing cells having decreased vav2 expression level were 34.0 nM (CI_{95} 24.3 to 47.2 nM) and for cells expressing native amounts of vav2 48.2 nM (CI_{95} 19.9 to 117.2 nM). In accordance, basal [^{3}H]-IP levels for cells exhibiting decreased vav2 levels are not significantly different compared to cells having native vav2 expression levels -0.4 % (CI_{95} -9.0 to 8.2 %) and 1.5 % (CI_{95} -9.3 to 12.3 %), respectively. Data summarizes results of five independent experiments.

4.2.6. PLC-pathway inhibition by vav2 requires MERM domain of NHERF

So far, the data provided evidence that direct or indirect interaction of vav2 with PTHR and $G\alpha_q$ leads to inhibition of PLC-mediated signaling. This effect was demonstrated in vav2-knockdown cells by si vav2 RNA and was significant compared to si Ctrl RNA. The vav2-PTHR interaction was independent of PTH, but affected the balance of AC- and PLC-mediated pathways. This vav2-PTHR interplay displays similarities to the NHERF-PTHR relation since NHERF likewise interacts with PTHR in a stimulation-independent manner but propagates PLC-signaling [58, 164]. It is hypothesized that the scaffold function of NHERF with two PDZ and one MERM binding domain leads to propagation of the PLC-pathway. PTHR and PLCβ are brought into close proximity by binding to each of the PDZ domains of NHERF. In addition, the whole complex is linked to the actin cytoskeleton through the MERM binding domain of NHERF and MERM binding proteins which seems to be crucial for selective signaling to $G\alpha_q$ [117]. As such a complex formation might likely interfere with other PTHR-interacting proteins, it should be investigated whether the scaffold function of NHERF1 - in detail the linkage to actin cytoskeleton and the subsequent assembly of microdomains - would interfere with the effects of vav2 on PTH-induced PLC-activation. For this purpose, a dominant-negative NHERF mutant ($NHERF1^{1-326}$, dnNHERF) was co-transfected to compete for effects of endogenous NHERF in HEK 293 ad cells. In addition, cells were transfected with si vav2 RNA or si Ctrl RNA, according to **(4.2.5)**. Cells which were not transfected with $NHERF1^{1-326}$ were transfected with equal amounts of NHERF1 wild-type (NHERF wt). As expected, the transfection of NHERF wt and si vav2 RNA increased IP generation in HEK 293 ad cells, compared to si Ctrl RNA **(Figure 20a)**. This result is in accordance to **(Figure 19a)**. Overexpression of NHERF1 did not alter the IP levels compared to endogenous NHERF expression. Co-transfected dnNHERF is thought to retain the scaffolding function via both PDZ domains but is unable to tether the signaling complexes to the cytoskeleton.

Remarkably, dnNHERF completely blunted the effect of vav2 knockdown, thereby retaining IP generation at equal levels compared to cells without vav2 knockdown **(Figure 20a)**. Equal expression levels of HA-PTHR, vav2 and NHERF1 species were confirmed by immunoblotting **(Figure 20b)**. One-way analysis of variance was performed for all transfection-conditions, and significant differences were obtained between NHERF wt with si vav2 and si Ctrl ($P<0.01$) as well as between si vav2 with NHERF wt or dnNHERF **(Table 5)**. In sum, knockdown of vav2 leads to increased PTH-induced IP generation in presence of wild-type NHERF, whereas the vav2 knockdown did not affect the IP generation in absence of the MERM domain of NHERF. This data strongly suggests that the MERM domain of NHERF represents a prerequisite for the increase of IP in absence of vav2. Furthermore, it may be assumed that NHERF and vav2 assemble in PTHR-related signaling complex to differentially regulate PTHR signaling.

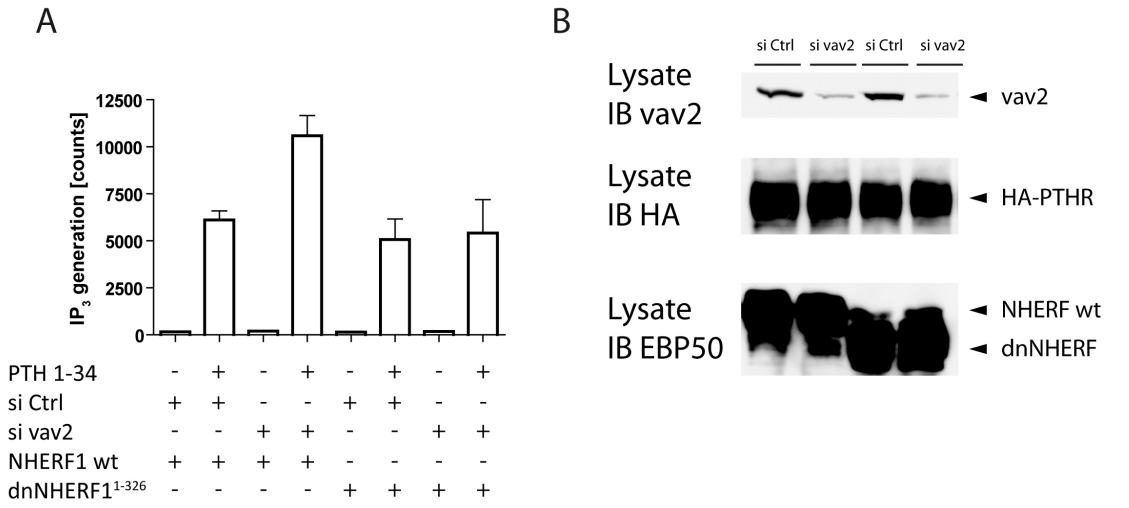

Figure 20. NHERF1 MERM domain is required for increased IP generation upon vav2 knockdown. HEK 293 ad cells stably expressing HA-PTHR were transfected with si vav2 RNA or si Ctrl RNA and NHERF1 wild-type (NHERF wt) or dominant-negative NHERF1$^{1-326}$ (dnNHERF), respectively. **(a)** Cells were incubated with myo-[2-^{3}H] inositol and 0.2 % FCS for 16 h prior to stimulation. Cells were stimulated with 300 nM PTH 1-34 for 60 min and [^{3}H]-inositol phosphates were quantified. Error bars represent SEM of four independent experiments. **(b)** Vav2 knockdown, expression levels of HA-PTHR and NHERF1 wild-type or dominant-negative NHERF1 was assessed by immunoblotting using anti-vav2, anti-HA or anti-EBP50 antibodies, respectively.

Bonferroni's Multiple Comparison (one-way ANOVA)	**Mean Diff. [counts]**	**t**	**P-value**	**CI_{95} [counts]**
si Ctrl (NHERFwt, +PTH) **vs. si vav2**(NHERFwt, +PTH)	-4479	2.645	P < 0.05	-8815 to -143.3
NHERFwt (si vav2, +PTH) **vs. dnNHERF** (si vav2, +PTH)	5183	3.060	P < 0.05	847.0 to 9518

Table 5. Statistics on PTH-induced IP generation in dependence of NHERF and vav2. Statistical analysis of IP levels, which were generated in cells transfected with si vav2 RNA or si Ctrl RNA. IP generations in cells transfected with NHERF wild-type or dominant-negative NHERF1 were statistically compared.

4.3. Ligand binding assays for parathyroid hormone receptors

4.3.1. Time-resolved fluorescence PTH binding assays

For scopes of academic and commercial research, labeled PTH was utilized to set up three different time-resolved fluorescence assay formats. (i) Time-resolved fluorescence separation assay (TRFS), a classical binding assay designed for native receptors **(Figure 21a)**. (ii) Homogeneous time-resolved fluorescence resonance energy transfer (HTRF), based on tag-lite technology for high through-put screenings **(Figure 21b)**. (iii) Antibody-based HTRF, a synergistic approach using HTRF with minimized receptor modification **(Figure 21c)**. In this work, for the first time PTH-binding assays are described which are based on time-resolved fluorescence.

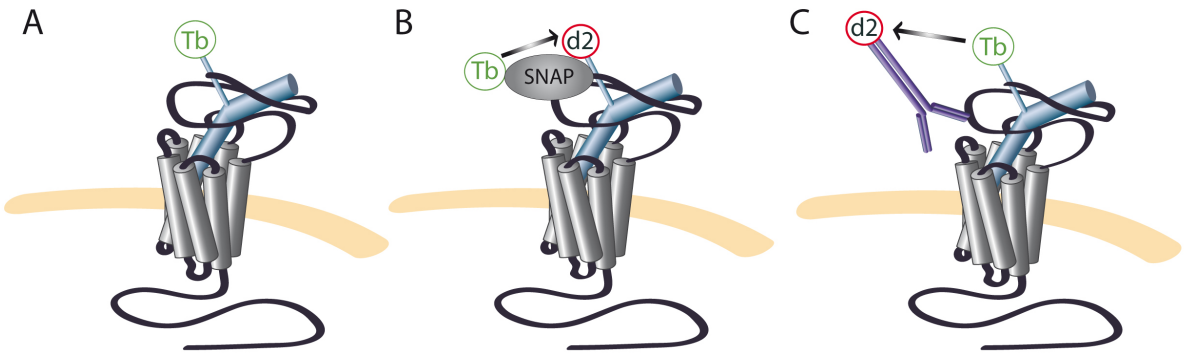

Figure 21. Illustration of time-resolved ligand-binding assays for the PTHR. (a) Time-resolved fluorescence separation assay (TRFS) is accomplished by measuring Terbium-cryptate (Tb^{3+}-cryptate)-labeled PTH (green/blue) bound to the PTHR (gray). **(b)** Homogeneous time-resolved fluorescence (HTRF), based on tag-lite technology, requires Tb^{3+}-cryptate-labeled SNAP-hPTHR1 (green/gray) and d2-labeled PTH (red/blue). Thereby, Tb^{3+}-cryptate represents the donor fluorophore and d2 the acceptor fluorophore for fluorescence energy transfer (FRET). Fluorescence resonance energy transfer is represented by arrowheads (black/gray). **(c)** In homogeneous time-resolved fluorescence (HTRF), based on antibodies, Tb^{3+}-cryptate-labeled PTH (green/blue) and d2-labeled antibodies (red/magenta) provide the donor and acceptor fluorophore, respectively.

4.3.2. Generation of fluorescent PTH analogues

Crystal structures of PTH 1-34 alone and the extracellular domain of the PTHR bound to a PTH fragment [42, 165]. These studies and enormous investigation of structure-function relationships of PTH and PTHR suggested adequate labeling positions for PTH [59, 74]. At first instance, fluorescent PTH analogues had to be generated, which exhibit properties of native PTH in terms of affinity, activity and internalization. For that, PTH was site-specifically labeled at position 13 or 35 by introduction of cysteine residues. Selective labeling was achieved because native PTH 1-34 represents a cysteine-free hormone. The PTH analog [$Nle^{8,18}$, Y^{34}] human PTH 1-34, in the following termed PTH 1-34, displays increased potency as well as oxidative resistance and served as a template for fluorescent PTH derivative [64, 166]. In sum, four variants of fluorescent PTH were designed in this work, labeled with d2 or Terbium-cryptate (Tb^{3+}-cryptate) on position 13 or 35 of PTH.

4.3.3. Evaluation of the integrity of fluorescent PTH analogues

Fluorescent PTH analogues may have impaired biological properties compared to native PTH. Consequently, the testing of the integrity of PTH analogues in terms of binding to PTHR, inducing PTHR activation and internalization, was obligatory. To do so, a radioimmunoassay (RIA) was performed to monitor PTH-induced cAMP generation **(Figure 22a)**. Results derived by RIA indicated that, compared to PTH 1-34, [C^{13}-Tb^{3+}-cryptate] PTH 1-34 did not exhibit decreased potency in terms of cAMP-signaling. However, an exact determination of the potency of PTH analogues would require concentration-response curves. [C^{13}-Tb^{3+}-cryptate] PTH 1-34, at a concentration of 100 pM, induced generation of 14.5 ± 0.9 nM cAMP (CI_{95} 10.5 – 18.5 nM), whereas 100 pM PTH 1-34 induced generation of 12.5 ± 1.5 nM cAMP (CI_{95} 6.0-19.0 nM) per well of a 6-well plate.

Activation of the PTHR, in general, induces internalization of the receptor-ligand-G protein complex. However, internalization is not obligatory since PTH analogues may bind to PTHR without inducing receptor desensitization **(1.3.2)**. Consequently, the ability of [C^{13}-d2] PTH 1-34 to induce internalization was confirmed by confocal microscopy **(Figure 22b)**. Imaging experiments confirmed intact binding properties for [C^{13}-d2] PTH 1-34, and in addition, demonstrated PTH-induced receptor internalization for appropriate time intervals at 15 min. Taken together, these data provide evidence that the fluorescent PTH analogues exhibit properties of native PTH in terms of receptor activation towards cAMP generation and receptor internalization.

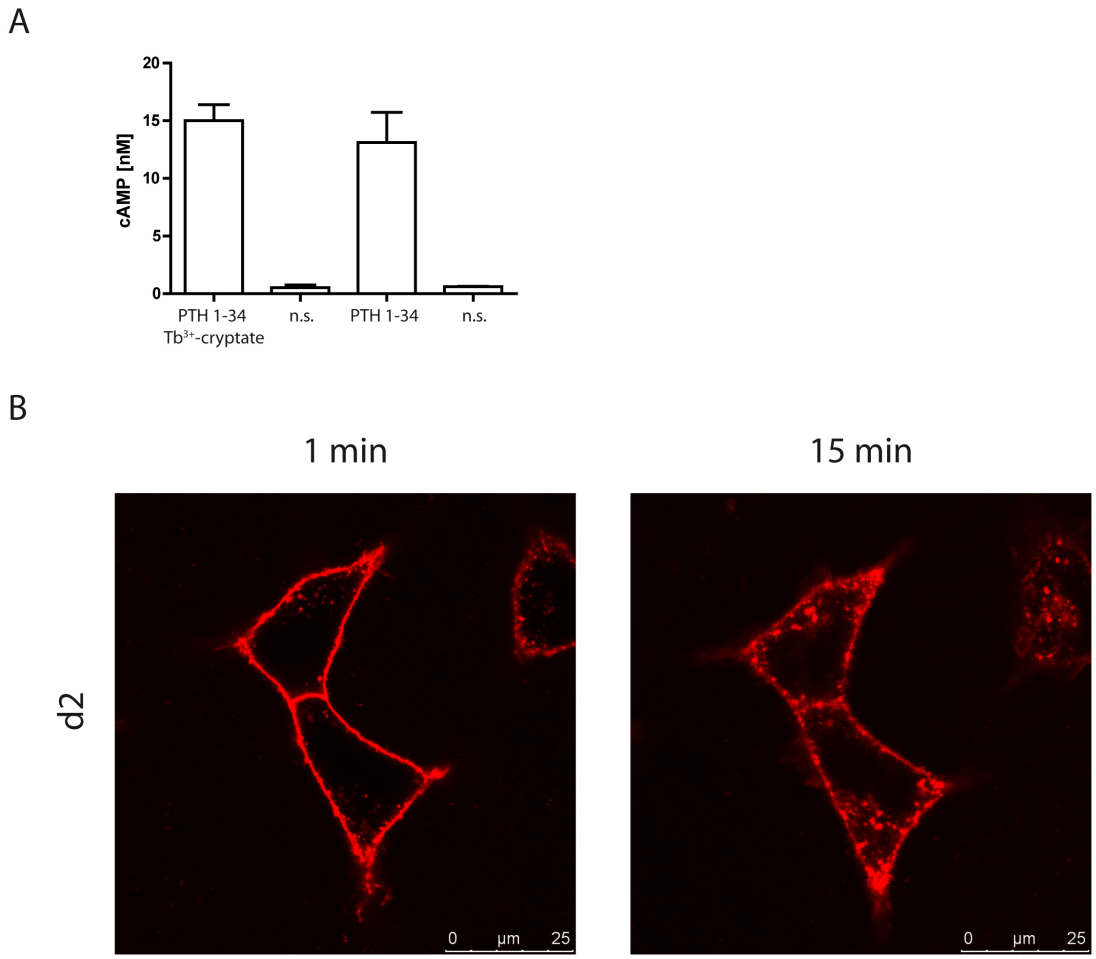

Figure 22. Integrity of labeled PTH analogues. (a) Radioimmuno assays for measurements of cAMP generation were performed in HEK 293 ad cells which transiently expressed PTHRs. Cells were incubated for 20 min with 100 pM [C^{13}-Tb^{3+}-cryptate] PTH 1-34, PTH 1-34 or pure buffer, indicated as non-stimulated (n.s.). Error bars represent SD of triplicates. **(b)** Imaging of [C^{13}-d2] PTH 1-34 was performed in living HEK 293 ad cells by confocal microscopy. Confocal pictures of HEK 293 ad cells expressing HA-PTHR1 were taken after incubation with 100 nM [C^{13}-d2] PTH 1-34 at indicated time points.

4.3.4. Time-resolved fluorescence separation assay (TRFS)

Development of labeled and fully functional PTH analogues was the prerequisite for ligand-binding assays with fluorescent PTH. At first instance, a ligand-binding approach that is analogous to classical ligand-binding was developed.

In more detail, a time-resolved fluorescence separation assay (TRFS) was established on adherent living cells by utilizing the labeled PTH analogues [C^{13}-Tb^{3+}-cryptate] PTH 1-34 and [C^{35}-Tb^{3+}-cryptate] PTH 1-34. To prevent receptor internalization, competition binding assays were performed at 4 °C. Using TRFS, affinities of [C^{13}-Tb^{3+}-cryptate] PTH 1-34 and [C^{35}-Tb^{3+}-

cryptate] PTH 1-34 to human PTHR1s were determined in saturation binding experiments resulting in dissociation constants of 39.5 (CI_{95} 28.7 nM to 50.3 nM) and 37.1 (CI_{95} 24.8 nM to 49.3 nM), respectively **(Figure 23a-b) (Table 6)**. To demonstrate the experimental precision and signal to noise ratio of saturation binding by TRFS, a single saturation binding experiment using [C^{35}-Tb^{3+}-cryptate] PTH 1-34 is shown in **(Figure 23c)**. These data indicate that the time-resolved fluorescence separation assay format allows saturation binding with adequate inter- and intra-experimental deviations.

Next, competition binding experiments were conducted at the TRFS assay format to determine inhibitory constants of PTH derivates. For this purpose, [C^{35}-Tb^{3+}-cryptate] PTH was used as tracer compound. For competition binding, the curve fit was adjusted for sigmoidal concentration-response at non-linear regression. These competition binding experiments provided Ki values for [$Nle^{8,18}$, Y^{34}] human PTH 1-34 16.4 nM (CI_{95} 12.2 to 21.9 nM), hPTH 1-34 wild-type 6.4 nM (CI_{95} 4.7 to 8.8 nM), [$Nle^{8,18}$, Y^{34}] bovine PTH 3-34 amide 5.7 nM (CI_{95} 4.0 to 8.1 nM) and hPTHrP 7-34 amide 221.0 nM (CI_{95} 165.7 to 294.8 nM) **(Figure 23d) (Table 6)**. Experimental precision and signal to noise ratio of competition binding in TRFS assays is shown in a single competition binding experiment **(Figure 23e)**. Thus, competition binding by TRFS enables determination of binding properties for ligands to the PTHR with sufficient assays windows and assay precision.

To choose an appropriate incubation time for saturation and competition binding, initial kinetic binding experiments had to be conducted. Since washing needs to be performed before data collection, each time point was measured in separated wells. However, kinetics were measured with acceptable standard deviations **(Figure 23f)**. Analysis using one-phase exponential association revealed an observed time constant of k_{ob} 0.021 min^{-1} and approximate equilibrium after 3 h **(Figure 23f, Table 6)**. The rate constant (k) was calculated according to the following equation: $counts = counts_{max} \times \left(1 - e^{(-k \times t)}\right)$. This result, once more, indicates that binding mechanism of PTH underlies slow binding kinetics.

In sum, the TRFS assay format was utilized to establish the fundamental pharmacological assays, namely saturation, competition and kinetic ligand-binding. Thereby, the presented data validated the TRFS method and characterized the labeled PTH analogues.

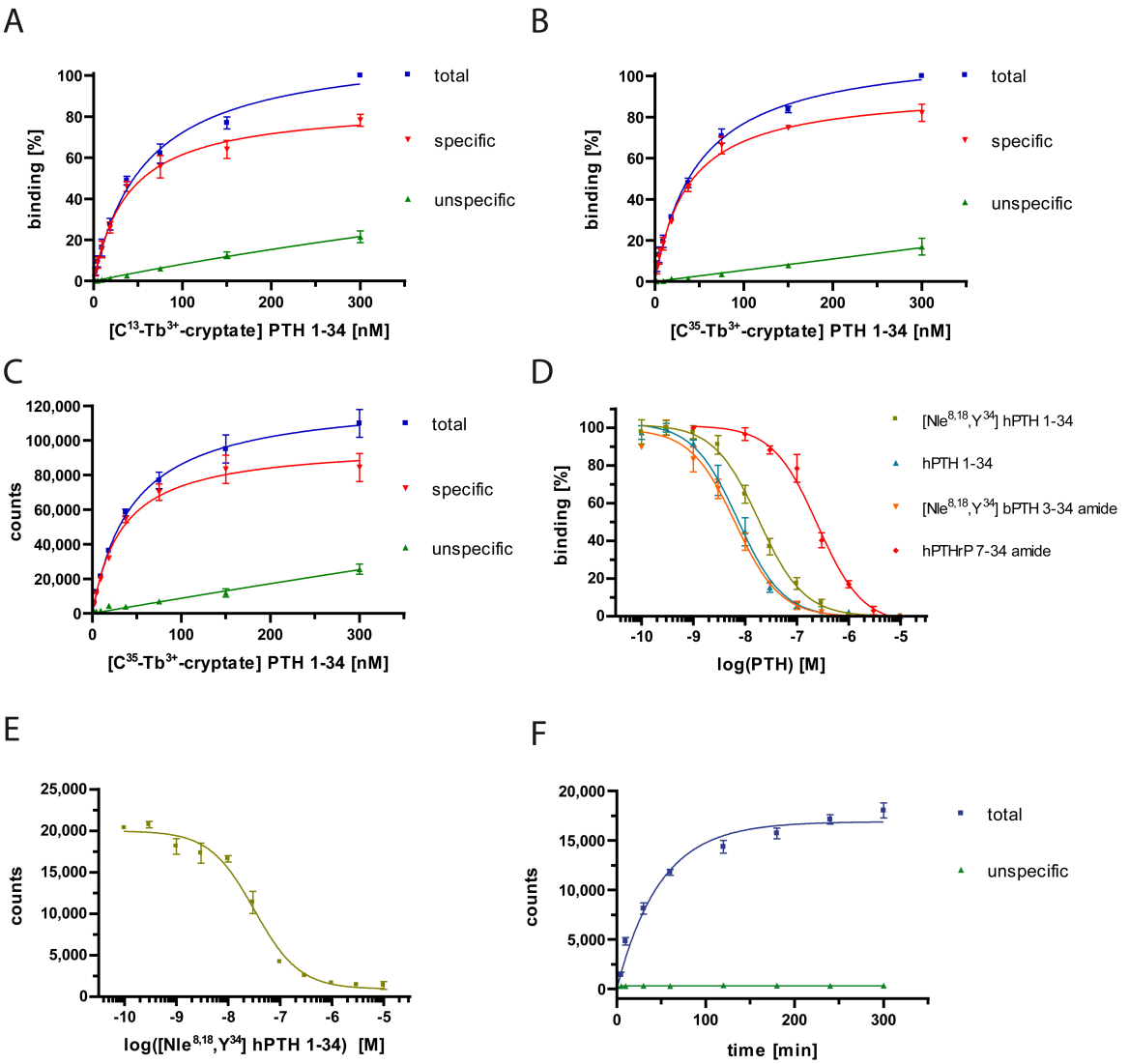

Figure 23. Time-resolved fluorescence separation assay (TRFS). Adherent HEK 293 ad cells were transiently transfected with human HA-PTHR1 in a 96-well plate format. Normalized saturation binding using [C^{13}-Tb^{3+}-cryptate] PTH 1-34 is shown in **(a)** or [C^{35}-Tb^{3+}-cryptate] PTH 1-34 in **(b)**. Error bars represent SEM, n=3. **(c)** A single saturation binding experiment using [C^{35}-Tb^{3+}-cryptate] PTH 1-34 demonstrates experimental precision. Error bars represent SD of triplicates. **(d)** Competition binding experiments were carried out with 5 nM [C^{35}-Tb^{3+}-cryptate] PTH 1-34 and PTH derivates at indicated concentrations. Error bars represent SEM, n=3-6. **(e)** One competition experiment is presented using hPTH 1-34, thus illustrating signal to noise ratio and precision. Error bars represent SD of quadruplicates. **(f)** Binding kinetics of 5 nM [C^{13}-Tb^{3+}-cryptate] PTH 1-34 is represented by one-phase exponential association fit. Error bars represent SD of triplicates.

Compound	Kd (CI_{95}) [nM]	Bmax ± SEM [%]	k_{ob} (CI_{95}) [min^{-1}]
[C^{13}-Tb^{3+}-cryptate] PTH 1-34	39.5 (28.7 to 50.3)	85.9 ± 4.0	0.021 (0.017 to 0.024)
[C^{35}-Tb^{3+}-cryptate] PTH 1-34	37.1 (24.8 to 49.3)	93.6 ± 3.3	
Compound	**Ki (CI_{95}) [nM]**		
[$Nle^{8,18}$, Y^{34}] hPTH 1-34	16.4 (12.2 to 21.9)		
hPTH 1-34 wild-type	6.4 (4.7 to 8.8)		
[$Nle^{8,18}$, Y^{34}] bPTH 3-34 amide	5.7 (4.0 to 8.1)		
hPTHrP 7-34 amide	221.0 (165.7 to 294.8)		

Table 6. Statistical summary of PTH binding to hPTHR1 obtained from TRFS. Mean values and standard error of the mean (SEM) or 95 % confidence intervals (CI_{95}) are listed for dissociation constants (Kd), inhibition constants (Ki), maximum binding (Bmax) and observed rate constants (k_{ob}). For Bmax values, the experiment giving the highest fluorescent signal was normalized to 100 %.

4.3.5. Homogeneous time-resolved fluorescence by tag-lite technology

In previous studies labeling of the PTHR with large fluorescent proteins at the extracellular domain did not significantly impair ligand-receptor binding [74]. Thus, it appeared that large proteins do not necessarily interfere with conformational movements of the extracellular domain, nevertheless the position for the fluorescent proteins may be critical.

In this work, a SNAP-tag was fused to the N-terminus of the PTHR for labeling of the receptor with O^6-benzylguanine-Tb^{3+}-cryptate. Consequently, [C^{13}-d2] PTH 1-34 or [C^{35}-d2] PTH 1-34 was used for HTRF assays on SNAP-PTHR. Thus the energy transfer of the HTRF takes place between the donor Tb^{3+}-cryptate and the acceptor d2. Saturation binding experiments were performed to determine affinities of labeled PTH to the SNAP-PTHR. Saturation binding obtained dissociation constants for [C^{13}-d2] PTH 1-34 of 46.3 nM (CI_{95} 20.4 to 72.1 nM) and for [C^{35}-d2] PTH 1-34 of 35.4 nM (CI_{95} 25.6 to 45.1 nM) **(Figure 24a-b, Table 7)**. These results are in accordance to values derived from TRFS **(Table 6)**.

Furthermore, competition binding assays confirmed that HTRF can be used for determination of binding studies with unlabeled ligands for PTHR. These competition assays were conducted with adherent cells on a 96-well plate format and cell suspension using 384-well plates. Curves were fitted using sigmoidal dose-response non-linear regression. Mean inhibition constants derived from tag-lite-based HTRF on adherent cells for [$Nle^{8,18}$, Y^{34}] hPTH 1-34 were 26.4 nM (CI_{95} 19.7 to 35.5 nM), for hPTH 1-34 wild-type 5.8 nM (CI_{95} 4.7 to 7.2 nM), for [$Nle^{8,18}$, Y^{34}] bPTH 3-34 amide 7.3 nM (CI_{95} 5.7 to 9.4 nM) and for hPTHrP 7-34 amide 446.3 nM (CI_{95} 335.3 to 594.0 nM) **(Table 7, Table 9c)**. These results are in accordance with literature [167-169]. Mean inhibition constants obtained from tag-lite HTRF on cell suspensions for [$Nle^{8,18}$, Y^{34}] hPTH 1-34 were 38.1

nM (CI_{95} 32.1 to 45.2 nM), for hPTH 1-34 wild-type 7.9 nM (CI_{95} 6.5 to 9.7 nM), for [$Nle^{8,18}$, Y^{34}] bPTH 3-34 amide 2.4 nM (CI_{95} 1.9 to 3.3 nM), and for hPTHrP 7-34 amide 230.0 nM (CI_{95} 192.3 to 275.2 nM) **(Table 7, Figure 24d)**. Homogeneous TRF competition assays were performed with suspension cells, thus offering time-saving protocols which are suitable for high-throughput screenings. HTRF experiments utilizing SNAP-PTHR for competition binding obtained signal-to-noise ratios of 30 **(Figure 24e**, **Table 9)**. This assay window and the homogeneous assay procedure highlight the convenience of HTRF.

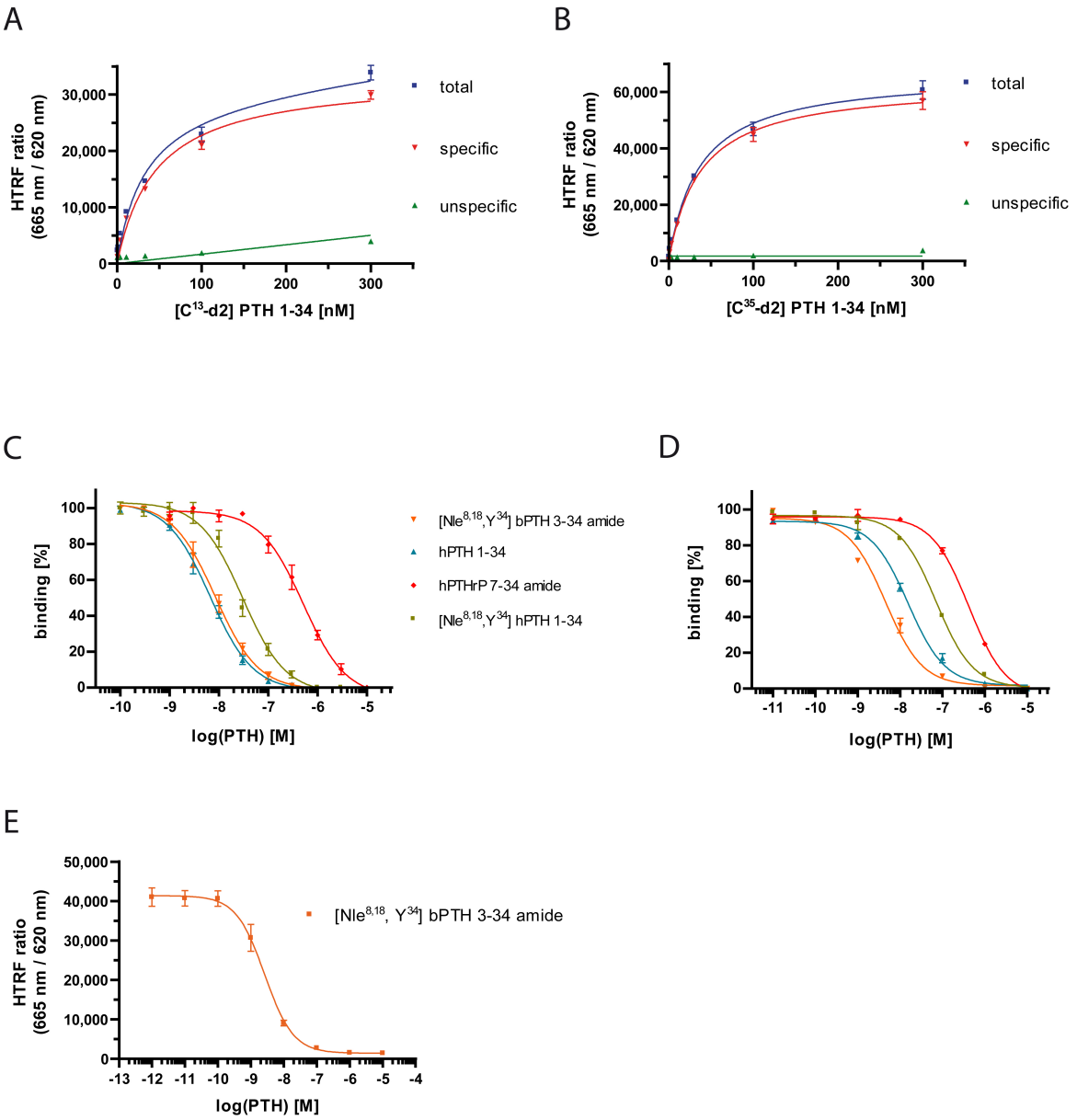

Figure 24. Homogeneous time-resolved fluorescence (HTRF) based on tag-lite technology. Adherent HEK293T cells were transiently transfected with SNAP-hPTHR1 and labeled by benzylguanine-Tb^{3+}-cryptate in a 96-well plate format. A representative saturation experiment is shown in **(a-b)**. For that, [C^{13}-d2] PTH 1-34 **(a)** or [C^{35}-d2] PTH 1-34 **(b)** was utilized. Error bars represent SD of triplicates, n=3. Three independent experiments of competition with [C^{35}-d2] PTH 1-34 and PTH derivatives using adherent cells are shown in **(c)** and using cell suspension in **(d)**. Error bars represent SEM, n=3-10. One competition experiment using [$Nle^{8,18}$, Y^{34}] bovine PTH 3-34 amide demonstrates signal to noise ratio and precision **(e)**. Error bars represent SD of triplicates. Tag-lite-based homogeneous time-resolved fluorescence (HTRF) ligand-binding studies were performed in cooperation with Cis bio.

Compound	Kd (CI_{95}) [nM]	Bmax ± SEM [%]
[C^{13}-d2] PTH 1-34	46.3 (20.4 to 72.1)	102.0 ± 5.5
[C^{35}-d2] PTH 1-34	35.4 (25.6 to 45.1)	101.6 ± 4,0
	Ki (CI_{95}) [nM] adherent cells	**Ki (CI_{95}) [nM] cell suspension**
[$Nle^{8,18}$, Y^{34}] hPTH 1-34	26.4 (19.7 to 35.5)	38.1 (32.1 to 45.2)
hPTH 1-34 wild-type	5.8 (4.7 to 7.2)	7.9 (6.5 to 9.7)
[$Nle^{8,18}$, Y^{34}] bPTH 3-34 amide	7.3 (5.7 to 9.4)	2.4 (1.9 to 3.3)
hPTHrP 7-34 amide	446.3 (335.3 to 594.0)	230.0 (192.3 to 275.2)

Table 7. PTH-binding statistics to SNAP-hPTHR1 obtained from HTRF based on tag-lite technology. Mean values and standard error of the mean or 95 % confidence intervals (CI_{95}) are listed for dissociation constants, inhibition constants and maximum binding. For Bmax values, the experiment giving the highest fluorescent signal was normalized to 100 %.

4.3.6. Antibody-based homogeneous time-resolved fluorescence

As demonstrated above, the advantages of homogeneous time-resolved fluorescence assay (HTRF) are represented by high signal-to-noise ratios and suitable assay procedures. Nevertheless, a significant drawback of HTRF based on tag-lite technology is the requirement for receptors which are fused to a SNAP-tag. This drawback may not have an impact on high-throughput screening, since ligand-binding was not impaired **(ref. 4.3.5)**. However, for ligand-binding experiments which are conducted for the investigation of molecular properties of receptors, the use of SNAP-tag-fused receptors is disadvantageous. Investigations of molecular properties are preferentially conducted on native receptors. To combine the usage of native receptors and the advantages of HTRF, an antibody-based HTRF assay format for the PTHR was designed. For that, the insertion of a small antibody epitope in the PTHR is necessary for ligand-binding experiments. For this HTRF based on antibodies, a Flag epitope was inserted at Exon E2, in the extracellular domain of the PTHR, which is known to be dispensable for ligand binding **(ref. 1.3.1)** [46]. In contrast to tag-lite-based HTRF, antibodies were used for labeling of PTHR with the acceptor fluorophore d2. Subsequently, PTH was labeled with the donor fluorophore Tb^{3+}-cryptate. Thus antibodies directed to the Flag epitope provide the acceptor fluorophore, d2, in proximity to ligand binding side. Whereas, terbium attached to PTH acts as the donor. Initially, three PTHR constructs were generated to determine whether the position of Flag-epitopes got an impact on FRET efficiency **(Figure 25a)**. S2-PTHR, S3-PTHR and Flag-PTHR carry Flag-epitopes at different positions and thus may obtain different FRET efficiency due to altered proximity of donor and acceptor fluorophores. However, in pre-tests for HTRF based on d2-labeled Flag-antibodies all three constructs displayed similar signal to noise ratios **(Figure 25b)**.

In addition, Flag-PTHR was tested in a radioligand binding experiment, with ^{125}I-PTH 1-34, to confirm the integrity of the receptor. Receptor integrity was confirmed, as PTH 1-34 had an EC_{50} of 10 nM for the Flag-PTHR (data not shown). For further experiments, the Flag-PTHR was used to obtain optimized protocols, because it represented the most native construct. Competition binding assays were established with the tracer compounds [C^{13}-Tb^{3+}-cryptate] PTH 1-34 or [C^{35}-Tb^{3+}-cryptate] PTH 1-34 **(Figure 26a)**. Notably, signal to noise ratios of 5-9 for the HTRF based on antibodies were lower than those of TRFS or HTRF based on tag-lite **(Table 9)**. Homogeneous procedure of HTRF allowed measurements of binding kinetics before saturation binding. For that, competition binding experiments were performed, and data were collected by measurements after indicated time intervals **(Figure 26b)**. Using sigmoidal concentration-response curve fits with variable slopes, this experiment illustrates binding kinetics as increasing intensity of competitions binding curves. For analysis of binding kinetics, the data set was plotted in a time-dependent manner for [C^{13}-Tb^{3+}-cryptate] PTH 1-34 or [C^{35}-Tb^{3+}-cryptate] PTH 1-34 **(Figure 26d-e)**. For this plot, curves can be fitted with one-phase exponential association equation that enables the calculation of observed rate constants (k_{ob}) **(Figure 26d-e, Table 8)**. Observed rate constants in antibody HTRF of 0.0085 min^{-1} (0.0071 to 0.0099 min^{-1}) for [C^{13}-Tb^{3+}-cryptate] PTH 1-34 and 0.018 min^{-1} (0.016 to 0.021 min^{-1}) for [C^{35}-Tb^{3+}-cryptate] PTH 1-34 were similar to binding kinetics for [C^{13}-Tb^{3+}-cryptate] PTH 1-34 of 0.021 min^{-1} (0.017 to 0.024 min^{-1}) in TRFS **(Figure 23f)**. Notably, PTH 1-34 affinities were slightly higher in HTRF antibody assay than in TRFS **(Table 8)**. Thus, antibody-based HTRF represent a useful alternative to HTRF based on tag-lite and TRFS, however lower signal to noise ratios need to be accepted.

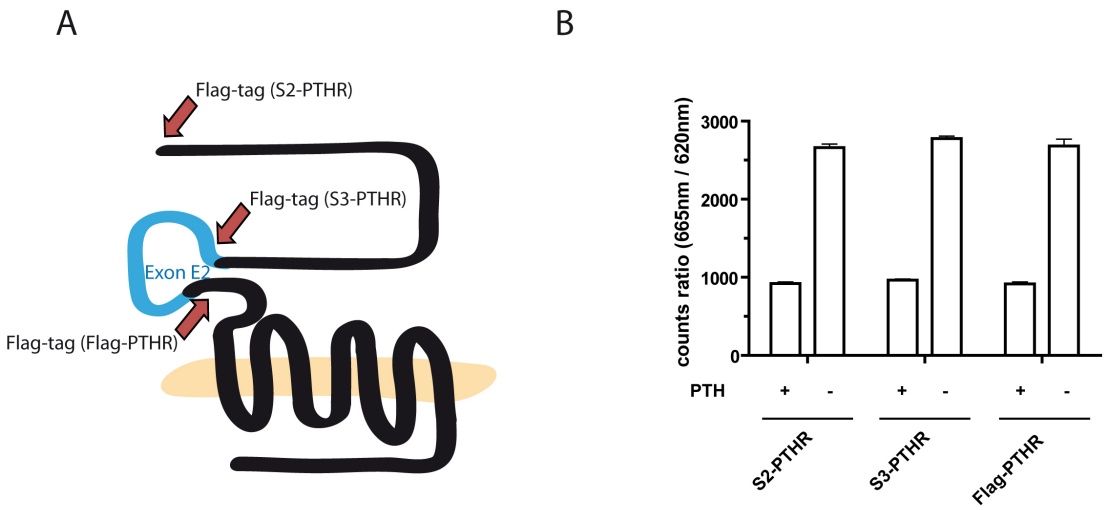

Figure 25. Optimization of Flag-tagged PTHR for antibody-based HTRF. (a) For S2-PTHR (ref. 2.5), a Flag-epitope was inserted at the N-terminal end of the human PTHR. S3-PTHR contains a Flag-epitope at residue 61, whereas exon E2 was deleted. For Flag-PTHR, a Flag epitope substituted residues 94-101, whereas Exon E2 was not changed. **(b)** S2-PTHR, S3-PTHR and Flag-PTHR were transfected in HEK 293 ad cells and HTRF assays were performed. For these HTRF assays, receptors were labeled by 4 nM D2-Flag-antibodies and 1 nM [C^{13}-Tb^{3+}-cryptate] PTH 1-34 in presence or absence of unlabeled [$Nle^{8,18}$, Y^{34}] bovine PTH 3-34 (PTH), as indicated (n=3, error bars represent SEM).

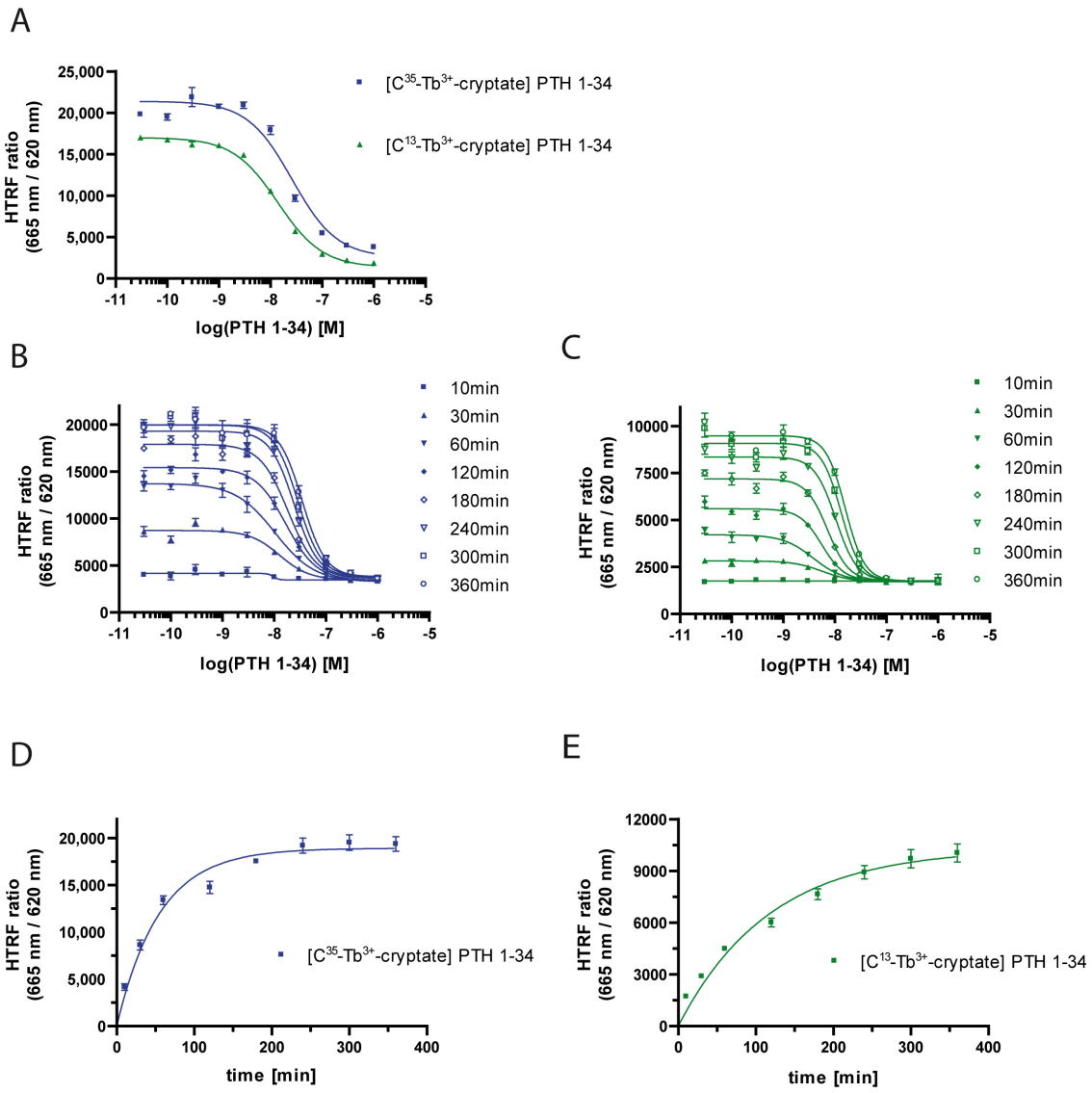

Figure 26. Homogeneous time-resolved fluorescence (HTRF) based on antibodies. Adherent HEK293 ad cells were transiently transfected with human Flag-PTHR1 in a 96-well plate format. **(a)** One representative competition binding experiments demonstrates precision and signal to noise of HTRF based on antibodies. PTHR was labeled with 4 nM D2-Flag-antibodies and 5 nM [C^{13}-Tb^{3+}-cryptate] PTH 1-34 or 5 nM [C^{13}-Tb^{3+}-cryptate] PTH 1-34 was competed with PTH 1-34 at indicated concentrations. Error bars represent SD of triplicates, n=3. **(b-c)** Competition binding curves illustrate PTH-binding in antibody HTRF as an increasing FRET signal in a time dependent manner. 4 nM d2 Flag antibody and 5 nM [C^{13}-Tb^{3+}-cryptate] PTH 1-34 **(b)** or 5 nM [C^{35}-Tb^{3+}-cryptate] PTH 1-34 **(c)** were incubated in presence of PTH 1-34. **(d-e)** Binding kinetics of [C-Tb^{3+}-cryptate] PTH 1-34 in antibody-based HTRF experiments on Flag-hPTHR1 reveal observed rate constants (k_{ob}) of 0.0085 min^{-1} (CI_{95} 0.0071 to 0.0099 min^{-1}) for [C^{13}-Tb^{3+}-cryptate] PTH 1-34 and 0.018 min^{-1} (CI_{95} 0.016 to 0.021 min^{-1}) for [C^{35}-Tb^{3+}-cryptate] PTH 1-34. Curve fitting was achieved via one-phase association of 5 nM [C^{35}-Tb^{3+}-cryptate] PTH 1-34 **(d)** or [C^{13}- Tb^{3+}-cryptate] PTH 1-34 **(e)**. Error bars represent SEM.

tracer	Ki (CI_{95}) [$Nle^{8,18}$, Y^{34}] hPTH 1-34 [nM]	k_{ob} (CI_{95}) [min^{-1}]
[C^{13}-Tb^{3+}-cryptate] PTH 1-34	9.0 (6.5 to 12.5)	0.0085 (0.0071 to 0.0099)
[C^{35}-Tb^{3+}-cryptate] PTH 1-34	25.0 (15.8 to 39.6)	0.018 (0.016 to 0.021)

Table 8. Statistical summary of PTH binding to Flag-hPTHR1 obtained from HTRF based on antibodies. Mean values and 95% confidence intervals (CI_{95}) are shown for inhibition constants (Ki) and observed rate constants (k_{ob}).

Assay format	Signal to noise	High through-put	Assay duration	Hands-on time	Receptor label
TRFS	14	No	4 d	8 h	label-free
HTRF (tag-lite)	30	Yes	3 d	7 h	SNAP-tag
HTRF (antibody)	5-9	Yes	3 d	6 h	antibody epitope

Table 9. Comparison of time-resolved ligand binding assays. Overview of three presented assay formats in respect to signal/noise ratio, high through-put capability, assay duration, hands-on time (working time) and degree of receptor (receptor label) modification.

5. Discussion

5.1. Identification of adaptor proteins for the PTHR

A proteomic approach was established to identify novel PTHR interacting proteins in cytosolic fractions of tissue or cell lysates. This method allows screening for protein interactions in any tissue or cell type and is not limited to proteins that are provided by cDNA libraries. In the case of PTHR, lysates of kidney and bone-related cell-types were used as a basis for the interaction screening. Identification of proteins that interacted with PTHR CT was done by mass spectrometry. High sensitivity of mass spectrometry allows detection of interacting proteins that occur at very low concentration or with low affinities to PTHR. As in many other screening approaches, using samples with high protein background such as cell lysates may result in false positive hits. These false-positive hits are due to unspecific interactions of proteins to material of the experiments as well as to MBP. In addition, high sensitivity of mass spectrometry leads to enormous amounts of positive hits. Three key features of the here presented proteomic approach reduce the probability of detecting false-positive interacting proteins for PTHR. (i) All experiments were conducted utilizing MBP constructs lacking a fusion protein in parallel to MBP-PTHR CT fusion constructs **(Figure 8)**. The experiments using MBP served as a negative control to recognize proteins which exhibit unspecific interactions to the support itself or MBP. Subsequently, differential mass spectrometry analysis revealed numerous true-positive PTHR CT interactions. However, differential data processing procedure after mass spectrometry is limited by the fact that solely protein fragments are detected. Detected fragments need to be correlated to specific proteins. This computational operation determines probabilities for correct correlation of peptide to protein, and thus, does not lead to 100 percent certainty. (ii) The enterokinase cleavage specifically elutes interacting proteins bound to PTHR CT but not unspecific-bound proteins to MBP or resin. Theoretically, enterokinase cleavages should not elute proteins of the MBP control sample. In reality, proteins were eluted even from the MBP control. This is due to the incubation at room temperature and the law of mass that causes dissociation of proteins. (iii) Appropriate washing buffers are critical for an ideal compromise between depletion of unbound, or unspecific bound proteins and the conservation of interaction to the PTHR CT. Thus, washing buffers need to be optimized for every type of tissue or cell lysate. Incubation with bovine kidney lysate required wash buffer containing 1 % Triton X-100; whereas, incubated ROS lysates must not be washed with detergents. By washing with 100-column volumes of washing buffer and appropriate concentration of detergent, a high stringency and subsequent low background was achieved **(Figure 10)**. Using these three features, identification of PTHR CT interacting proteins with low background was possible. As a

confirmation of the integrity of PTHR CT, mass spectrometry identified subtypes of the NHERF family as specific PTHR interacting proteins. In addition, this identification confirms the reliability of the whole screening approach. NHERF is known to bind to PDZ binding cassette of the very C-terminal residues of PTHR **(ref. 1.4)**. A drawback of the approach is based on the use of the isolated C-terminal domain of the PTHR (PTHR CT). The PTHR CT construct includes residues from 463 to 593, thus, intracellular loops of the PTHR are not present. Consequently, proteins interacting solely with intracellular loops of the PTHR will not be discovered, and proteins interacting with the C-terminal domain and intracellular loops will likely display decreased affinities. The absence of interactions to intracellular loops might be an explanation why β-arrestin was not detected as a PTHR CT interacting protein in the here presented screening approach.

Data processing of proteomic approaches was a critical step for the successful identification of novel PTHR interacting proteins. Thus, the readout values of the mass spectrometry analysis were represented by *number of unique peptides* which were specifically assigned to single proteins. Thereof, specificity ratios were calculated as a degree for the specificity of the interaction **(ref. 3.4.4)**. For NHERF3 and for NHERF1 a specificity ratio of 15 and 8 were determined, respectively. Especially for NHERF3 a drawback of specificity ratios becomes obvious. When ratiometric data analysis was used, peptides that were identified in the control sample but not in the PTHR CT interaction gave false results, as the numerator equals 0, and thus were excluded from the calculation. On the other hand, ratio calculations are beneficial for rankings representing the quality of hits for interacting proteins. For example, unique peptides of vav2, which specifically occur in samples of PTHR CT, e.g. *number of unique peptides* 4 to 0, benefit from ratios **(3.4.4)**. In contrast, peptides which occur in a more unspecific pattern, as 10 to 6, are ranked lower in a ratiometric calculation. Using differential data processing, very specific proteins with low intensities would not profit more than unspecific proteins with higher intensities.

The specificity ratios of independent experiments for each protein were added and used for ranking of all identified proteins. For vav2, a quite specific interaction pattern with low intensities was found in samples incubated with kidney lysate, and data processing led to high ranking of vav2. Vav2 had a cumulative specificity ratio of 4, but unique peptides of vav2 occurred very specifically in two experiments which were conducted with kidney lysates (3 to 0 and 1 to 0).

In contrast to the screenings in kidney lysate, screening in cytosolic fractions of rat osteosarcoma cells did not reveal any peptides of vav2. Immunoblotting experiments using anti-vav2 antibodies indicated that rat osteosarcoma cells do not express vav2 in detectable amounts

(data not shown). However, coimmunoprecipitation of the transiently expressed PTHR and vav2 proved that the interaction of vav2 and PTHR is also possible in rat osteosarcoma cells.
In sum, from a newly developed interaction screening vav2 was identified to bind to the PTHR-CT with high specificity.

5.2. Vav2 affects PTHR signaling

5.2.1. Vav2 binds to intracellular domains of PTHR

Vav2 was identified as a PTHR CT interacting protein from the described screening approach. It was further investigated whether vav2 interacts with full-length PTHR. Co-immunoprecipitation experiments confirmed that transfected vav2 binds to full-length PTHR **(Figure 13a-b)**. In addition, endogenously expressed vav2 was shown to co-precipitate with the PTHR in HEK cells, which may indicate a relevance of the PTHR vav2 interaction at physiological conditions **(Figure 13 d-e)**. Co-immunoprecipitations were washed with buffers containing the detergent NP40 to reduce unspecific binding proteins **(3.5.1)**. However, the vav2 PTHR interaction was even stable in the presence of more aggressive detergents, such as SDS (data not shown). In addition to stringent washing, cells were incubated with latrunculin A prior lysis. Latrunculin A inhibits unspecific interactions with the actin-cytoskeleton by depolymerization of F-actin. Usage of latrunculin A assured that vav2 did not co-precipitate due to unspecific cytoskeleton-mediated interactions. Consequently, it can be claimed that results obtained from immunoprecipitations are due to specific protein-protein interactions of vav2 with PTHR.
Notably, the interaction of vav2 to the PTHR in co-immunoprecipitation experiments was not affected by the activation of PTHR with PTH 1-34, and the subsequent signaling and trafficking events **(Figure 13a)**. These data suggests that vav2 and the PTHR exhibit a robust interaction. Remarkably, the binding capacity of transiently transfected or endogenous vav2 significantly decreased in absence of the PTHR C-terminal domain **(Figure 13a, d-e)**. Thus, a significant amount of binding capacity of vav2 to PTHR is determined by components of the PTHR up-stream of residue 480. These components may be represented by intracellular loops or residues in the C-terminal tail between amino acid 463 and 480. This relation could not be explored further in a cellular model as truncations of the PTHR CT upstream of residues 480 resulted in receptor mutants that were retained in the cell and thus were not functional **(Figure 15c-d)**.
Taken together, the observation of a decreased binding capacity of vav2 to PTHR T480 is in accordance with the interaction screening, as the isolated PTHR CT domain was used as bait for the screen.

Intriguingly, also truncated myc-vav2$^{188-512}$ co-precipitated with the HA-PTHR **(Figure 13c)**. As myc-vav2$^{188-512}$ solely consists of the Dbl homology domain (GEF domain) and the Pleckstrin homology domain, these data imply that these two domains constitute components of the binding interface to the PTHR. Moreover, information about the relevance of the GEF activity of vav2 for the interaction to the PTHR is provided by the shown experiments. Since myc-vav2$^{188-512}$ is known to exhibit constitutively active GEF activity, the autoinhibitory effects of calponin-homology (CH) region and acidic-rich (Ac) region are absent **(ref. 1.6)**. Consequently, it may be claimed that the GEF activity of vav2 does not diminish the interaction to PTHR. This hypothesis is supported by co-immunoprecipitation experiments which were performed in presence of C_8-PIP_3. By addition of C_8-PIP_3 the GEF activity of full-length endogenous vav2 was increased which did not affect binding of vav2 to PTHR **(Figure 14)**. As mentioned above, GEF activity of vav2 tightly regulates activity of RhoA GTPases, which themselves stimulate reorganization of actin cytoskeleton **(ref. 1.6)**. Thus, vav2 might bind to the PTHR and regulate the reorganization of the actin cytoskeleton simultaneously. Thereby, vav2 might facilitate the assembly of microdomains for compartmentalized PTHR signaling as it has been described for NHERF and PTHR at apical patches of opossum kidney cells [117].

Finally, it may be hypothesized that Rho GTPases can be activated by vav2 in close proximity to PTHR. In turn this may lead to reorganization of cytoskeleton in the close environment of PTHR.

5.2.2. Vav2 phosphorylation is regulated by PTH-induced PTHR activation

This work provides evidence that activity of vav2, monitored by tyrosine phosphorylation on key residues, is regulated by PTH **(Figure 16)**. For PTH-induced vav2 phosphorylation and vav2 regulation, several molecular mechanisms are possible. First, PTHR is known to transactivate EGFRs, and receptor tyrosine kinase activity could then activate vav2 through direct phosphorylation **(1.3.4)**. Second, a scaffolding complex of β-arrestin and Src was reported to interact with the PTHR. The involvement of Src in this complex may be responsible for vav2 phosphorylation. Consequently, PTH-mediated vav2 phosphorylation may be regulated through a PTHR-associated kinase.

Compared to EGF-induced vav2 phosphorylation, the PTH-mediated phosphorylation of vav2 was less intense **(Figure 16)**. This may indicate an indirect and less effective mechanism for PTH-mediated vav2 phosphorylation.

Notably, weak vav2 phosphorylation was also observed at basal conditions **(Figure 16)**. Basal phosphorylation of vav2 occurs, since vav2 can be phosphorylated even upon small mechanical

triggers. In some cases, medium exchange can also affect the phosphorylation state of vav2 proteins, which may be due to nutrients-induced growth.

In sum, the observed PTH-mediated vav2 phosphorylation links PTHR activation with effects of activated vav2, as cytoskeleton reorganization, proliferation and morphological alterations. This link may lead to the hypothesis that PTH-mediated effects on osteoblasts and osteoclasts may cause altered migration properties and consequently altered osteo-metabolic effects in bone matrices. Such a mechanism could be synergistic to well described effects of PTH on proliferation, differentiation and function of osteoblasts. Obtaining a molecular mechanism for PTH-induced vav2 phosphorylation could explain macroscopic observations on cell morphology and migration of PTHR expressing cell-types.

5.2.3. Vav2 competes with $G\alpha_q$ for coupling to PTHR

Studies on the G protein binding interface for PTHR suggest critical components for G protein-coupling to be present at residues 468-491 of the C-terminal tail of PTHR [77]. The coupling of heterotrimeric G proteins to activated receptors leads to activation of G protein. Subsequently, active $G\alpha_q$ subunits are supposed to dissociate from the heterotrimeric G protein receptor complex to activate PLC and thereby downstream pathways. In addition, it is claimed that, besides $G\alpha_q$, coupling of $G\beta\gamma$ is necessary for PLC signaling. Other studies on PTHR-signaling with the C-terminally truncated PTHR T480 revealed $G\alpha_q$-mediated IP generation to be even more efficient for the truncated T480 mutant [167, 170]. Identification of the interaction interface of $G\alpha_q$ on the PTHR by crystal structures of the complex would be supportive. Unfortunately, crystal structures obtained of the ternary beta2-adrenergic receptor complex with $G\alpha_s$ can be hardly transferred on the $G\alpha_q$-PTHR complex [18].

In sum, literature provides evidence that C-terminal residues between 468 and 480 of the PTHR are essential for G protein coupling, however, it is not fully understood which components of the PTHR serves for coupling of $G\alpha_q$.

Since vav2 is capable to coprecipitate with PTHR T480, vav2 may also interact with residues upstream of amino acids 480 of the PTHR **(Figure 13)**. Since G proteins likely interact with residues 468-480 to couple to the PTHR, both proteins, vav2 and G proteins, may share a common binding interface on PTHR.

In this work it is demonstrated that vav2 preferentially binds to activated $G\alpha_q$, but not $G\alpha_s$ subunits **(Figure 17)**. Interestingly, the amount of activated $G\alpha_q$ bound to vav2 was dramatically decreased by co-expression of PTHR **(Figure 17)**. As vav2 most likely interacts with the C-

terminal tail and presumably with parts of intracellular loops of the PTHR, it is conceivable that this interaction might sterically interfere with $G\alpha_q$-coupling.

Since this work reports, for the first time, that vav2 interacts with proteins of the PTHR-signaling cascade, the domains of vav2 that are required for these interactions are unknown. However, for other RhoA GEFs an interaction with G proteins, via RGS domains, is well described **(ref. 1.6.2)**. Notably, vav2 proteins do not harbor RGS domains, thus a different interface for the interaction to GPCRs is likely. Structural studies on the PTHR vav2 interaction interface would be necessary to pinpoint the binding mechanism.

Further experiments to elucidate the competitive nature of $G\alpha_q$ and vav2 for PTHR interaction were conducted by altering vav2 expression levels **(Figure 18a)**. Remarkably, overexpression of vav2 proteins lead to decreased interaction between PTHR and activated $G\alpha_q$. This is in accordance with results on the interaction between $G\alpha_q$ and vav2, which appeared to be competitive to the PTHR **(Figure 17)**. On the other hand, down-regulation of vav2 expression by si vav2 RNA did not alter the PTHR-$G\alpha_q$ interaction. Theoretically, upon down-regulation of endogenous vav2 expression, the PTHR-$G\alpha_q$ interaction should be increased and co-immunoprecipitated amounts of $G\alpha_q$ should be increased. A likely explanation to this could be that due to low expression levels of PTHR the capacity of PTHR binding to $G\alpha_q$ is saturated. Thus, decreased vav2 expression did not result in further interactions of PTHR and $G\alpha_q$ **(Figure 18a)**.

To support the hypothesis of a competitive mechanism of $G\alpha_q$ and vav2 for coupling to PTHR, it was investigated whether vav2 interacts preferentially with active or inactive $G\alpha_q$ subunits **(Figure 18b)**. These experiments remarkably confirmed the hypothesis, as the vav2-$G\alpha_q$ interaction displayed a significant dependence on the activation state of $G\alpha_q$ subunits. Interactions of vav2 and $G\alpha_q$ were dramatically increased upon PTH-induced activation of $G\alpha_q$ **(Figure 18b)**. This experiment indicates that binding of vav2 to $G\alpha_q$ depends on the PTHR-mediated activation of $G\alpha_q$.

In sum, co-immunoprecipitations of PTHR, vav2 and $G\alpha_q$ provide evidence for competitive action of vav2 with activated $G\alpha_q$ subunits for coupling to PTHR.

5.2.4. Vav2 affects IP generation dependent on NHERF MERM domains

In this work it was demonstrated that vav2 negatively regulates PTH-induced IP generation, whereas cAMP generation is not affected **(Figure 19)**. This effect of vav2 was obtained from siRNA-knockdown of endogenously expressed vav2. Vav2 knockdown did not affect the viability of HEK cells or the PTHR expression levels as it was assessed by Western blots. Thus, it can be concluded that vav2 affects specifically PTHR-mediated signaling cascades. In respect the

competitive interaction of PTHR, vav2 and $G\alpha_q$, it can be concluded that vav2 interferes with the PTHR/PLC signaling cascade on the level of G protein-coupling **(Figure 17) (Figure 18)**.

In contrast to knock-down of vav2 expression, overexpression of vav2 interfered with cellular integrity and viability. Thus, basal IP levels were altered, and levels of IP accumulation after receptor stimulation varied strongly. However, experiments using overexpression of vav2 do have the tendency to decrease IP generation although changes in IP productions are less pronounced than by knockdown of vav2 (data not shown). A reason might be the already high levels of endogenous vav2 which may saturate involved signaling mechanisms. Thus, further increase of vav2 expression would not affect these processes in addition.

Previous studies provided evidence that PTHR signaling is directed by the assembly of microdomains [117, 171]. In addition, the existence of NHERF-dependent microdomains for PTHR signaling complex has been reported to affect PTHR trafficking and were observed at apical patches of opossum kidney cells [117, 171]. These microdomains are assembled by NHERF proteins which link signaling complexes to the cytoskeleton via the MERM domain. The two PDZ domains of NHERF are capable to join PLCs and PTHR as signaling complexes that lead to more effective signaling. Hence, NHERF1 establishes interactions with the PTHR and specific signaling proteins, as PLC, within membrane microdomains to coordinate receptor signaling in a temporal and spatial manner. In addition, the relation between PTHR and NHERF seem to be similar to the relation of PTHR and vav2, since both assemble independently of receptor activation and affect the balance between AC and PLC signaling. Consequently, in this work the impact of the NHERF-mediated microdomain-assembly on the effect of vav2 for PTHR-signaling was investigated. Interestingly, overexpression of dominant-negative $NHERF1^{1-326}$ blocked the increase of IP generation which was provoked by vav2 knockdown **(Figure 20)**. As $NHERF1^{1-326}$ (dnNHERF1) still carries both PDZ domains, scaffolding of PLC and PTHR remains possible. However, $NHERF1^{1-326}$ is lacking the MERM domain, therefore the signaling complex cannot be linked to the actin cytoskeleton. It may thus be concluded that microdomains with the actin skeleton may be a prerequisite for effects vav2 imposes on PTHR-mediated PLC signaling.

In contrast to PLC, the presence of $G\alpha_q$ subunits in this microdomain context was not investigated in detail. However, it may be claimed that interaction of vav2 and $G\alpha_q$ play a role within microdomain-assembled signaling via PLCs.

5.2.5. Vav2 and bone metabolism

Here, the first link between vav2, a GEF for Rho GTPases, and a GPCR is reported. Moreover, for the first time a relation between vav2 and PTHR was observed. However, the effects of vav2 on known physiological functions of PTHR are not known.

The results from this work provide evidence for vav2 as a negative regulator of $G\alpha_q$-mediated IP generation. $G\alpha_q$ signaling, which consequently leads to IP generation, is believed to inhibit osteoanabolic effects of PTH [102]. Consequently, as vav2 affects $G\alpha_q$ signaling, an effect of vav2 on bone metabolism might be possible. However, the relevance of vav2 for bone metabolism was not investigated in this work. The mass-spectrometry-based screening did not reveal vav2 as a PTHR-interacting protein in osteosarcoma cells. Though, an absent interaction to PTHR does not exclude relevance for PTHR-related $G\alpha_q$ signaling of vav2. Thus, the impact of vav2 on PTHR-signaling in bone-related cells should be investigated.

A bone-phenotype of vav2 knockout mice is not known. In general, for vav2 knockout mice no significantly changed phenotype was reported, which may be explained by redundant action of vav isoforms [127]. However, distinct expression patterns of vav subtypes and differences in phenotypes of tissue-specific vav knockout mice strongly question the hypothesis of complete redundancy between vav subtypes. In contrast to no obvious phenotypes of vav2 knockout mice, previous studies reported a clear phenotype for $vav3^{-/-}$ mice [172]. These homozygote vav3 knockout mice exhibit increased bone mass and were less sensitive to bone resorption induced by PTH or RANKL [172]. Furthermore, vav3 was identified as a prerequisite for osteoclast function and subsequently for bone metabolism [172]. Osteoclasts, lacking vav3, exhibit dysfunctional cytoskeleton organization, polarization, spreading and resorptive activity.

Taken together, it may be hypothesized that vav2 promotes osteoanabolic bone metabolism by inhibiting $G\alpha_q$-signaling, whereas vav3 was reported to negatively regulate osteoanabolic metabolism **(Figure 27)**.

In addition to endocrine stimuli on bone metabolism, mechanical stimuli are known to promote bone formation. As vav2 represents a protein linked to the cytoskeleton which is sensitive to mechanical stress, future studies may unravel, whether vav2 mediates between PTHR activation and mechanical stress.

Another aspect, which needs to be taken into account, is the requirement of mobility of osteoblasts and osteoclasts for bone metabolism. Since, bone metabolism is determined by interplay of osteoblasts as well as osteoclasts, and the tight regulation of their motility, proliferation and differentiation. Therefore, regulation of cytoskeleton reorganization and cell migration by vav2 may play a role on the well-known effects of PTH on cell morphology and migration.

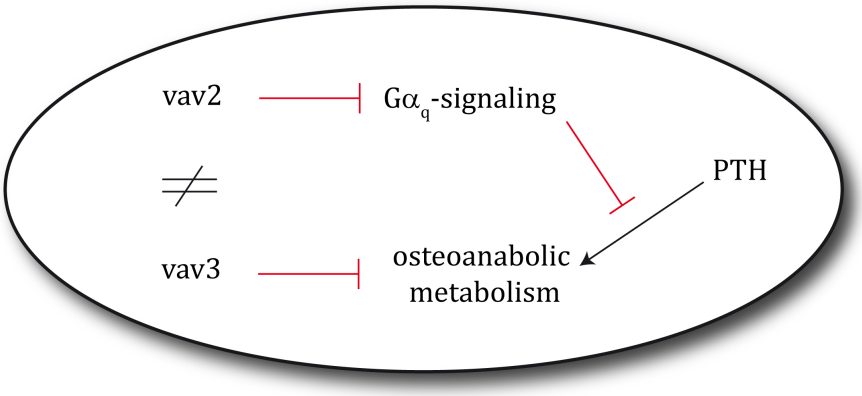

Figure 27. Contrary effects of vav2 and vav3 may be hypothesized. Vav2 inhibits $G\alpha_q$-mediated signaling, which was reported to inhibit PTH-induced anabolic bone metabolism [102]. Consequently, presence of vav2 may support osteoanabolic effects. In contrast, vav3 is believed to decrease anabolic bone metabolism [172].

5.3. Time-resolved ligand binding assays for PTHR

5.3.1. Time-resolved fluorescence separation assay (TRFS)

In this work, labeled parathyroid hormones (PTH) facilitated the development of the first non-radioactive ligand binding assays for the PTHR. A set of three time-resolved fluorescence ligand binding assays were established. TRFS, an approach similar to classical ligand binding assays, benefits from measuring time-resolved fluorescence. Time-resolved measurements significantly reduce background fluorescence. Thereby, signal to noise ratios, provided by TRFS, offer assay windows that are sufficient for common ligand binding applications **(Table 9)**. The signal to noise ratio represents a critical parameter for ligand-binding studies and is a weak point for fluorescence-based methods compared to methods based on radioactivity **(ref. 4.3)**. Using low concentrations of [C^{13}-Tb^{3+}-cryptate], e.g. 5 nM, TRFS provided signal-to-noise ratios of 14 and acceptable standard deviations **(Figure 23e).** Application of higher tracer concentrations elevated the observed signal to noise ratios up to 30 (data not shown) but consequently lead to increased standard deviations. Consequently, a tracer concentration of 5 nM was chosen as a compromise between assay intensity and precision. To further increase precision of TRFS assays, a lysis protocol was used prior TRFS measurements. On the one hand, this procedure decreases signal intensity and signal to noise ratios, on the other hand the precision of TRFS is significantly increased. Lysis has impact on assay precision, because TRFS assays are sensitive to inhomogeneity of signal intensities within a well. This means that any cell loss, difference in cell growth or receptor density within a well lead to high variability of one-point measurements.

This crucial sensitivity of TRFS is not as high in HTRF assays, since for HTRF ratiometric readouts by two fluorescence intensities are used **(ref. 4.3.5, 4.3.6)**. Lysis homogenizes receptor density and potential cell loss is averaged for the whole well, subsequently leading to more precise measurements. In addition to lysis protocols, the precision is increased by multiple point measurement, hereafter named as x-fold scan.

As mentioned above, in TRFS experiments saturation and competition binding with labeled PTH analogues allows determination of binding affinities for ligands of the PTHR **(Figure 23, Table 6)**. The Kd values for labeled PTH 1-34, derived by saturation binding are similar to Kd of the unlabeled PTH 1-34 analogue ([$Nle^{8,18}$, Y^{34}] hPTH 1-34) **(ref. 2.9)** that is provided by literature (28 ± 3.4 nM) [167]. In addition, the inhibition constants derived by competition binding in TRFS assays are similar to radioligand binding experiments in literature **(Figure 23d)** [167-169]. These data suggest that labeling of PTH did not significantly impair affinities to HA-PTHR and validate the obtained by TRFS assays.

Additionally to similar affinities, [C^{13}-Tb^{3+}-cryptate] PTH 1-34 is able to induce cAMP generation with comparable efficacy as unlabeled PTH 1-34 **(Figure 22b)**. This result suggested that the ability of [C^{13}-Tb^{3+}-cryptate] to activate PTHR was not affected by the fluorescent label and, furthermore, indicates the integrity of binding to PTHR. Moreover, Tb^{3+}-cryptate represents the largest of fluorescent labels utilized here and therefore theoretically had the highest probability of causing steric hindrance for PTH-binding. Furthermore, it was confirmed that labeled PTH analogues induced internalization of PTHR **(Figure 22b)**. Consequently, fluorescent PTH analogues exhibit properties of native PTH in terms of receptor activation towards cAMP generation and receptor internalization.

As mentioned above, a complex mechanism underlies the PTH binding kinetics. This mechanism consists of two distinct binding steps; thus kinetics of PTH binding are known to be slow **(1.3.3)** [59, 74]. However, the equation of one-phase exponential association can be used for calculation of the rate constant (k): $counts = counts_{max} \times \left(1 - e^{(-k \times t)}\right)$ **(Figure 23f, Table 6)**. Since association and dissociation occur simultaneously, the observed rate constant (k_{ob}) represents a mixture of k_{on} and k_{off} rates, underlying association and dissociation, respectively. The calculated rate constant (k) confirmed the assumed slow binding kinetics of PTH. Moreover, with respect to binding affinities of low nanomolar range, low k_{off} rates can be assumed.

The main advantage of TRFS is the possibility to detect native receptors and all receptor-mutants which are capable of binding the fluorescent ligand. The disadvantages of the TRFS evolve from the heterogeneity, since washing steps are time consuming and decrease robustness.

Taken together, TRFS represents a less harmful substitution for classical radioligand competition binding. Moreover, TRFS assays provide the first PTH saturation binding that is suitable for high expression levels as achieved by recombinant expression.

5.3.2. Homogeneous time-resolved fluorescence tag-lite technology

Homogeneous time-resolved fluorescence (HTRF) assays are based on fluorescence resonance energy transfer (FRET). The readout for HTRF is represented by a ratio between acceptor emission and donor emission. FRET efficacy, and subsequently the FRET ratio, increases upon increasing proximity of fluorophores. By binding of the labeled ligand to the labeled receptor, the fluorophores are located in close proximity, which leads to a change of the ratio of acceptor and donor emission. These ratiometric readouts are insensible to cell-loss and inhomogeneous receptor densities within a well **(ref. 4.3.4)**. Additionally, proximity-based readouts do not require depletion of unbound ligand. Though, for tag-lite technology, a SNAP-tag needs to be fused to the PTHR that allows enzymatic labeling of SNAP-fusion receptor with O^6-benzylguanine-tagged fluorophores. Hence, native PTHR or other generic PTHR constructs cannot be detected. In general the requirement of SNAP-fusion receptors represents a drawback of HTRF. However, for the PTHR and many other GPCRs, SNAP-tag did not impair ligand-binding. The affinities of labeled PTH to the SNAP-PTHR were determined by saturation binding experiments in the HTRF tag-lite assay format **(Figure 24 a-b, Table 7)**. Referring to similar values for the wild-type hPTHR1 which were derived from TRFS **(Table 6)**, it can be hypothesized that the SNAP-tag did not impair affinity of labeled PTH to the PTHR. As shown in **(Figure 24d)**, the signal to noise ratio of 30 offers adequate assay windows **(Table 9)**.

HTRF, based on tag-lite technology, represents the most robust and suitable of here presented assays. The homogeneous TRF avoids washing steps and is predestinated for high-throughput experiments. Additionally, the miniaturization of suspension cultures supports high-scale screenings for the PTHR and substitutes tedious radioligand binding.

5.3.3. Antibody-based homogeneous time-resolved fluorescence

HTRF, based on antibodies, offers signal to noise ratios of about 5 to 9 **(Table 9)**. Notably, these signal to noise ratios are lower than those of TRFS or HTRF based on tag-lite **(Table 9)**. The improvement relies on the combination of advantages of HTRF and TRFS. Performing antibody-based HTRF is suitable, as tag-lite HTRF, because of the homogeneous protocols which avoid washing steps. Since no washing steps are required, high-throughput experiments and measurements of kinetics are achievable. Additionally, just a small epitope is necessary for detection via antibodies. The FLAG epitope did not impair receptor function for the PTHR. Nevertheless, the structure of antibodies need to be considered to explain the lower FRET efficiency and subsequently lower signal to noise ratios of antibody-based HTRF. One parameter might be the large distances between donor and acceptor fluorophores which were attached to antibodies. Foerster-radius for terbium and red-acceptors, like d2 and Alexa633, are approximately 60Å [173]. Immense immunoglobulin size of about 50 x 50 x 200 Å indicates large distances between fluorophores. Moreover, disorder of the Exon E2, containing the Flag-epitope, lead to flexibility of antibody-bound acceptor fluorophore [42]. Thus, probabilities of proximity between acceptor and donor fluorophore are lower which results in low energy-transfer efficiencies.

Kinetic binding experiments by antibody HTRF revealed observed rate constants of about 0.01 to 0.02 min^{-1} **(Figure 26, Figure 25, Table 8)**. In HTRF using antibodies, the observed rate constant can be theoretically determined by ligand-binding and antibody-binding steps, whereas in TRFS solely ligand-binding determines kinetics. This indicates that the rate determining step is dominated by ligand binding rather than the antibody binding. The state of equilibrium may be almost reached after 3 to 4 h. PTH 1-34 affinities are slightly higher in HTRF antibody assay which may be due to antibody association to the extracellular domain of the PTHR **(Table 8)**.

6. Conclusions

In this work, it was demonstrated that the guanine nucleotide exchange factor vav2 interacts with intracellular domains of the PTHR independently of receptor activation **(Figure 28)**. Experiments with truncated vav2 mutants suggest that the Rho GEF domain and the pleckstrin homology domain of vav2 are required for binding to the PTHR. Moreover, PTHR activation by PTH 1-34 increased the phosphorylation of vav2. Especially, phosphorylation of Tyr^{172}, which directly leads to GEF activity, suggests a PTH-mediated activation mechanism for vav2. Furthermore, evidence was provided that vav2 affects PTHR signaling. Vav2 competes with PTHR for interaction with $G\alpha_q$, but not $G\alpha_s$, in an activation-dependent manner. Remarkably, vav2 negatively regulates PTH-induced inositol phosphate generation, whereas cAMP signaling was not affected **(Figure 28)**. This inhibitory effect of vav2 requires scaffold function of NHERF1 MERM domain. The data suggest that vav2 contributes to PTHR-related signaling complexes and is assembled with $G\alpha_q$ and NHERF1 in microdomains **(Figure 28)**.

It can be concluded that vav2 is an adaptor protein for PTHR-mediated signal transduction which may have impact on bone metabolism. Therefore, ternary interactions might be present for PTHR, vav2 and $G\alpha_q$ **(Figure 29)**. This novel interaction might help in the understanding of PTH-induced effects on osteoclasts and osteoblast, thereby supporting the development of novel therapeutics for treatment of osteoporosis.

Furthermore, novel ligand binding assays based on time-resolved fluorescence for PTHR were established. Three different variants were developed that showed superior features compared to traditional radioligand binding assays and thus may facilitate drug development and fundamental research on the PTHR.

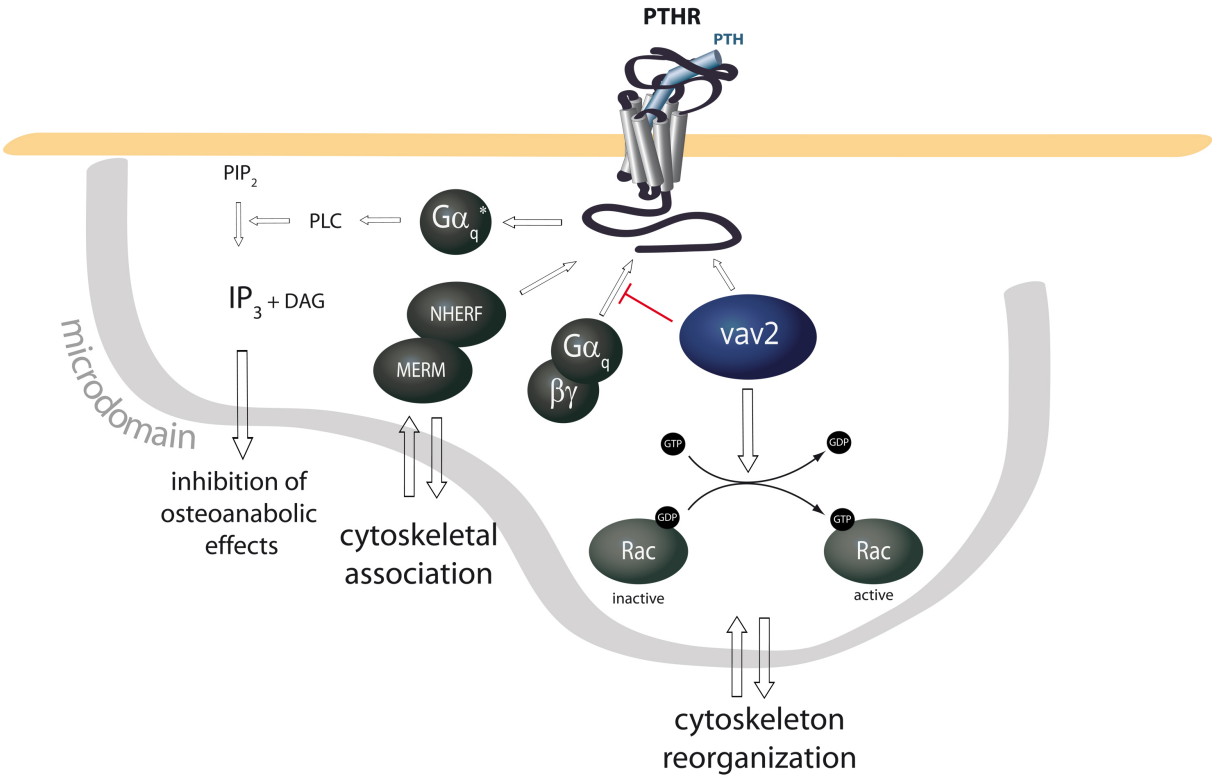

Figure 28. Illustration of PTHR-related signaling complexes in microdomains. NHERF assembles PTHR-linked signaling complexes, which include heterotrimeric G proteins and PLC, in microdomains. These microdomains are assembled by cytoskeletal association via interactions to MERM and actin by NHERF. Vav2 is associated in microdomains in proximity to PTHR, whereby GEF activity for Rho/Rac GTPases may contribute to cytoskeleton reorganizations for microdomains. Additionally, presence of vav2 blocks the inhibitory effects of the $G\alpha_q$/PLC/IP_3-signaling cascade for anabolic bone metabolism.

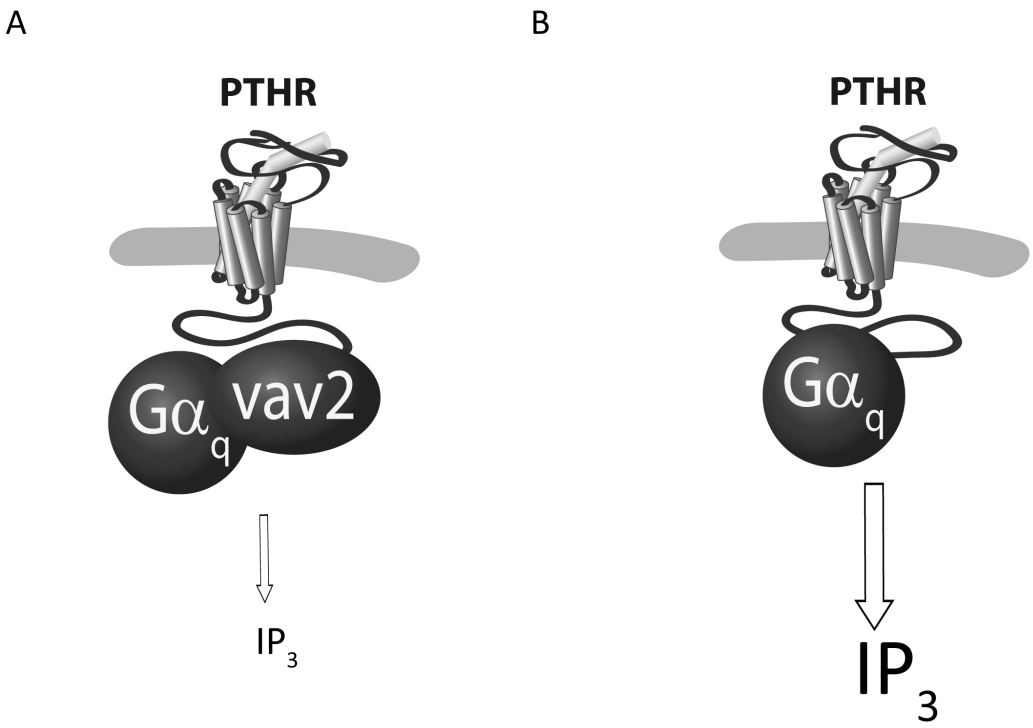

Figure 29. Scheme for ternary interactions between PTHR, vav2 and $G\alpha_q$. (a) At basal conditions, vav2 competes with $G\alpha_q$ for coupling to PTHR, thereby decreasing efficiency of the $G\alpha_q$-mediated generation of IP. **(b)** At reduced expression levels of vav2, coupling of $G\alpha_q$ to PTHR is more efficient or more frequent and subsequently PTH-mediated IP generation is promoted.

7. Abbreviations

Abbreviation	Long form
%	percent
° C	degree Celsius
aa	amino acids
AC	adenylate cyclases
Bmax	maximum binding
BMD	bone mineral density
C_8-PIP_3	phosphatidylinositol-3,4,5-triphosphate, dioctanoyl
cAMP	cyclic 3’-5’-cyclic adenosine monophosphate
CaSR	extracellular calcium-sensing receptor-related
Cdc42	cell division control protein 42 homolog
CI_{95}	confidence interval 95 %
Cy2	Cyanine 2
D2	red fluorescent dye
DAG	diacylglycerol
DMEM	Dulbecco's Modified Eagle Medium
DTT	dithiothreitol
EBP50	ezrin binding protein 50
EC50	half maximal effective concentration
EDTA	ethylenediaminetetraacetic acid
EGFR	epidermal growth factor receptor
EtOH	ethanol, ethyl alcohol
FRET	fluorescence resonance energy transfer
G protein	guanine nucleotide-binding protein
GABA	gamma-aminobutyric acid receptors
GDP	guanosine-5'-diphosphate
GEFs	nucleotide exchange factors
GIRK	G protein-coupled inwardly-rectifying potassium channels
GPCR	G protein-coupled receptor
GTP	Guanosine-5'-triphosphate
GTPase	guanine nucleotide triphosphate hydrolyzing proteins
Gα	guanine nucleotide-binding protein alpha-subunit
h	hour(s)
HEPES	4-(2-hydroxyethyl)-1-piperazineethanesulfonic acid
TRFS	time-resolved fluorescence separation assay
HTRF®	homogeneous time-resolved fluorescence
IB	immunoblotting
IBMX	3-isobutyl-1-methylxanthine
IC_{50}	half-maximal inhibitory concentration
IP	immunoprecipitation
$IP_{(3)}$	inositol 1,4,5 trisphosphate (inositol phosphates)
kb	kilo bases
kBq	kilo Becquerel

Kd	dissociation constant
kDa	kilo Dalton
Ki	inhibitory constant
k_{ob}	observed rate constant
k_{off}	dissociation rate
k_{on}	association rate
LB medium	lysogeny broth medium
m/v	mass per volume
M_3	muscarinic acetylcholine receptors 3
MAPK	Mitogen-activated protein kinase
MBP	maltose-binding protein
mGlu	metabotropic glutamate receptor
min	minute
msec	millisecond(s)
MWCO	molecular weight cut-off
NHE3	Na^+/H^+ exchanger 3
NHERF	Na^+/H^+ Exchanger Regulatory Factor
nm	nanometer(s)
OPG	osteoprotegerin
PBS	phosphate buffer saline
Pi	inorganic phosphate
PI3Kγ	phosphoinositol-3-kinases gamma
PIP_2	phosphatidylinositol-4,5-bisphosphate
PIP_3	phosphatidylinositol-3,4,5-trisphosphate
PLC	phospholipase C
PLCβ	phospholipase Cβ
PLD	phospholipase D
PTH	parathyroid hormone
PTHR, hPTHR1	human parathyroid hormone receptor 1
PTHrP	parathyroid hormone-related peptide
Rac1	Ras-related C3 botulinum toxin substrate 1
RANKL	receptor activator of nuclear factor kappa B ligand
RGS	Regulators of G protein signaling
Rho	rat sarcoma (Ras) homology gene family
RIPA	radio immuno precipitation assay buffer
ROS	rat osteosarcoma cells
SDS	sodium dodecyl sulfate
SDS-PAGE	sodium dodecyl sulfate polyacrylamide gel electrophoresis
sec	second(s)
SED	standard error of difference
SEM	standard error of the mean
TEMED	N, N, N‘, N‘,-tetramethylethylenediamine
TNF-receptor	tumor necrosis factor receptor
TR-FRET	time-resolved fluorescence resonance energy transfer
TRIS	tris(hydroxymethyl)aminomethane

V	volt
v/v	volume per volume
β_2AR	beta-adrenergic receptor 2
τ	rate constant (tau or k)

8. Literature

1. Wess, J., *G-protein-coupled receptors: molecular mechanisms involved in receptor activation and selectivity of G-protein recognition.* FASEB J, 1997. **11**(5): p. 346-54.
2. Pierce, K.L., R.T. Premont, and R.J. Lefkowitz, *Seven-transmembrane receptors.* Nat Rev Mol Cell Biol, 2002. **3**(9): p. 639-50.
3. Rask-Andersen, M., M.S. Almen, and H.B. Schioth, *Trends in the exploitation of novel drug targets.* Nat Rev Drug Discov, 2011. **10**(8): p. 579-90.
4. Van Eps, N., et al., *Interaction of a G protein with an activated receptor opens the interdomain interface in the alpha subunit.* Proc Natl Acad Sci U S A, 2011. **108**(23): p. 9420-4.
5. Downes, G.B. and N. Gautam, *The G protein subunit gene families.* Genomics, 1999. **62**(3): p. 544-52.
6. Peleg, S., et al., *G(alpha)(i) controls the gating of the G protein-activated K(+) channel, GIRK.* Neuron, 2002. **33**(1): p. 87-99.
7. Boyer, J.L., G.L. Waldo, and T.K. Harden, *Beta gamma-subunit activation of G-protein-regulated phospholipase C.* J Biol Chem, 1992. **267**(35): p. 25451-6.
8. Camps, M., et al., *Isozyme-selective stimulation of phospholipase C-beta 2 by G protein beta gamma-subunits.* Nature, 1992. **360**(6405): p. 684-6.
9. Tang, W.J. and A.G. Gilman, *Type-specific regulation of adenylyl cyclase by G protein beta gamma subunits.* Science, 1991. **254**(5037): p. 1500-3.
10. Pitcher, J.A., et al., *Role of beta gamma subunits of G proteins in targeting the beta-adrenergic receptor kinase to membrane-bound receptors.* Science, 1992. **257**(5074): p. 1264-7.
11. Stephens, L., et al., *A novel phosphoinositide 3 kinase activity in myeloid-derived cells is activated by G protein beta gamma subunits.* Cell, 1994. **77**(1): p. 83-93.
12. Logothetis, D.E., et al., *The beta gamma subunits of GTP-binding proteins activate the muscarinic K+ channel in heart.* Nature, 1987. **325**(6102): p. 321-6.
13. Neubig, R.R., *Membrane organization in G-protein mechanisms.* FASEB J, 1994. **8**(12): p. 939-46.
14. Gross, W. and M.J. Lohse, *Mechanism of activation of A2 adenosine receptors. II. A restricted collision-coupling model of receptor-effector interaction.* Mol Pharmacol, 1991. **39**(4): p. 524-30.
15. Neubig, R.R., R.D. Gantzos, and W.J. Thomsen, *Mechanism of agonist and antagonist binding to alpha 2 adrenergic receptors: evidence for a precoupled receptor-guanine nucleotide protein complex.* Biochemistry, 1988. **27**(7): p. 2374-84.
16. Seifert, R., et al., *Functional differences between full and partial agonists: evidence for ligand-specific receptor conformations.* J Pharmacol Exp Ther, 2001. **297**(3): p. 1218-26.
17. De Lean, A., J.M. Stadel, and R.J. Lefkowitz, *A ternary complex model explains the agonist-specific binding properties of the adenylate cyclase-coupled beta-adrenergic receptor.* J Biol Chem, 1980. **255**(15): p. 7108-17.
18. Rasmussen, S.G., et al., *Crystal structure of the beta(2) adrenergic receptor-Gs protein complex.* Nature, 2011.
19. Roberts, D.J. and M. Waelbroeck, *G protein activation by G protein coupled receptors: ternary complex formation or catalyzed reaction?* Biochem Pharmacol, 2004. **68**(5): p. 799-806.

20. Waelbroeck, M., L. Boufrahi, and S. Swillens, *Seven helix receptors are enzymes catalysing G protein activation. What is the agonist Kact?* J Theor Biol, 1997. **187**(1): p. 15-37.
21. Lohse, M.J., et al., *beta-Arrestin: a protein that regulates beta-adrenergic receptor function.* Science, 1990. **248**(4962): p. 1547-50.
22. Lohse, M.J., et al., *Receptor-specific desensitization with purified proteins. Kinase dependence and receptor specificity of beta-arrestin and arrestin in the beta 2-adrenergic receptor and rhodopsin systems.* J Biol Chem, 1992. **267**(12): p. 8558-64.
23. Lohse, M.J. and C. Klenk, *Blocking them all: beta-arrestins inhibit cellular signaling.* Mol Cell, 2008. **31**(5): p. 619-21.
24. Pierce, K.L., L.M. Luttrell, and R.J. Lefkowitz, *New mechanisms in heptahelical receptor signaling to mitogen activated protein kinase cascades.* Oncogene, 2001. **20**(13): p. 1532-9.
25. Dhanasekaran, N., L.E. Heasley, and G.L. Johnson, *G protein-coupled receptor systems involved in cell growth and oncogenesis.* Endocr Rev, 1995. **16**(3): p. 259-70.
26. Luttrell, L.M., Y. Daaka, and R.J. Lefkowitz, *Regulation of tyrosine kinase cascades by G-protein-coupled receptors.* Curr Opin Cell Biol, 1999. **11**(2): p. 177-83.
27. Rajagopal, S., K. Rajagopal, and R.J. Lefkowitz, *Teaching old receptors new tricks: biasing seven-transmembrane receptors.* Nat Rev Drug Discov, 2010. **9**(5): p. 373-86.
28. Shukla, A.K., et al., *Distinct conformational changes in beta-arrestin report biased agonism at seven-transmembrane receptors.* Proc Natl Acad Sci U S A, 2008. **105**(29): p. 9988-93.
29. Kenakin, T., *Inverse, protean, and ligand-selective agonism: matters of receptor conformation.* FASEB J, 2001. **15**(3): p. 598-611.
30. Kolakowski, L.F., Jr., *GCRDb: a G-protein-coupled receptor database.* Receptors Channels, 1994. **2**(1): p. 1-7.
31. Foord, S.M., et al., *International Union of Pharmacology. XLVI. G protein-coupled receptor list.* Pharmacol Rev, 2005. **57**(2): p. 279-88.
32. Cadigan, K.M. and R. Nusse, *Wnt signaling: a common theme in animal development.* Genes Dev, 1997. **11**(24): p. 3286-305.
33. Juppner, H., et al., *A G protein-linked receptor for parathyroid hormone and parathyroid hormone-related peptide.* Science, 1991. **254**(5034): p. 1024-6.
34. Ponten, F., et al., *A global view of protein expression in human cells, tissues, and organs.* Mol Syst Biol, 2009. **5**: p. 337.
35. Urena, P., et al., *Parathyroid hormone (PTH)/PTH-related peptide receptor messenger ribonucleic acids are widely distributed in rat tissues.* Endocrinology, 1993. **133**(2): p. 617-23.
36. Gelbert, L., et al., *Chromosomal localization of the parathyroid hormone/parathyroid hormone-related protein receptor gene to human chromosome 3p21.1-p24.2.* J Clin Endocrinol Metab, 1994. **79**(4): p. 1046-8.
37. Kong, X.F., et al., *The rat, mouse and human genes encoding the receptor for parathyroid hormone and parathyroid hormone-related peptide are highly homologous.* Biochem Biophys Res Commun, 1994. **200**(3): p. 1290-9.
38. Usdin, T.B., C. Gruber, and T.I. Bonner, *Identification and functional expression of a receptor selectively recognizing parathyroid hormone, the PTH2 receptor.* J Biol Chem, 1995. **270**(26): p. 15455-8.

39. Panda, D., et al., *TIP39/Parathyroid Hormone Type 2 Receptor Signaling is a Potent Inhibitor of Chondrocyte Proliferation and Differentiation.* Am J Physiol Endocrinol Metab, 2009.
40. Usdin, T.B., *The PTH2 receptor and TIP39: a new peptide-receptor system.* Trends Pharmacol Sci, 2000. **21**(4): p. 128-30.
41. Shimada, M., et al., *Purification and characterization of a receptor for human parathyroid hormone and parathyroid hormone-related peptide.* J Biol Chem, 2002. **277**(35): p. 31774-80.
42. Pioszak, A.A. and H.E. Xu, *Molecular recognition of parathyroid hormone by its G protein-coupled receptor.* Proc Natl Acad Sci U S A, 2008. **105**(13): p. 5034-9.
43. Pioszak, A.A., et al., *Structural basis for parathyroid hormone-related protein binding to the parathyroid hormone receptor and design of conformation-selective peptides.* J Biol Chem, 2009. **284**(41): p. 28382-91.
44. Pioszak, A.A., et al., *Dimeric arrangement of the parathyroid hormone receptor and a structural mechanism for ligand-induced dissociation.* J Biol Chem, 2010.
45. Klenk, C., et al., *Agonist-regulated cleavage of the extracellular domain of parathyroid hormone receptor type 1.* J Biol Chem, 2010. **285**(12): p. 8665-74.
46. Lee, C., et al., *Role of the extracellular regions of the parathyroid hormone (PTH)/PTH-related peptide receptor in hormone binding.* Endocrinology, 1994. **135**(4): p. 1488-95.
47. Bisello, A., et al., *Role of glycosylation in expression and function of the human parathyroid hormone/parathyroid hormone-related protein receptor.* Biochemistry, 1996. **35**(49): p. 15890-5.
48. Iida-Klein, A., et al., *Mutations in the second cytoplasmic loop of the rat parathyroid hormone (PTH)/PTH-related protein receptor result in selective loss of PTH-stimulated phospholipase C activity.* J Biol Chem, 1997. **272**(11): p. 6882-9.
49. Huang, Z., et al., *The N-terminal region of the third intracellular loop of the parathyroid hormone (PTH)/PTH-related peptide receptor is critical for coupling to cAMP and inositol phosphate/Ca2+ signal transduction pathways.* J Biol Chem, 1996. **271**(52): p. 33382-9.
50. Tawfeek, H.A., F. Qian, and A.B. Abou-Samra, *Phosphorylation of the receptor for PTH and PTHrP is required for internalization and regulates receptor signaling.* Mol Endocrinol, 2002. **16**(1): p. 1-13.
51. Malecz, N., et al., *Identification of phosphorylation sites in the G protein-coupled receptor for parathyroid hormone. Receptor phosphorylation is not required for agonist-induced internalization.* Mol Endocrinol, 1998. **12**(12): p. 1846-56.
52. Miedlich, S.U. and A.B. Abou-Samra, *Eliminating phosphorylation sites of the parathyroid hormone receptor type 1 differentially affects stimulation of phospholipase C and receptor internalization.* Am J Physiol Endocrinol Metab, 2008. **295**(3): p. E665-71.
53. Qian, F., A. Leung, and A. Abou-Samra, *Agonist-dependent phosphorylation of the parathyroid hormone/parathyroid hormone-related peptide receptor.* Biochemistry, 1998. **37**(18): p. 6240-6.
54. Gardella, T.J. and H. Juppner, *Molecular properties of the PTH/PTHrP receptor.* Trends Endocrinol Metab, 2001. **12**(5): p. 210-7.
55. Calvi, L.M. and E. Schipani, *The PTH/PTHrP receptor in Jansen's metaphyseal chondrodysplasia.* J Endocrinol Invest, 2000. **23**(8): p. 545-54.

56. Ferrari, S.L. and A. Bisello, *Cellular distribution of constitutively active mutant parathyroid hormone (PTH)/PTH-related protein receptors and regulation of cyclic adenosine 3',5'-monophosphate signaling by beta-arrestin2.* Mol Endocrinol, 2001. **15**(1): p. 149-63.
57. Carter, P.H., et al., *Selective and nonselective inverse agonists for constitutively active type-1 parathyroid hormone receptors: evidence for altered receptor conformations.* Endocrinology, 2001. **142**(4): p. 1534-45.
58. Mahon, M.J., et al., *Na(+)/H(+) exchanger regulatory factor 2 directs parathyroid hormone 1 receptor signalling.* Nature, 2002. **417**(6891): p. 858-61.
59. Potts, J.T., *Parathyroid hormone: past and present.* J Endocrinol, 2005. **187**(3): p. 311-25.
60. Brewer, H.B., Jr. and R. Ronan, *Bovine parathyroid hormone: amino acid sequence.* Proc Natl Acad Sci U S A, 1970. **67**(4): p. 1862-9.
61. Keutmann, H.T., et al., *Complete amino acid sequence of human parathyroid hormone.* Biochemistry, 1978. **17**(26): p. 5723-9.
62. Martin, K.J., et al., *The peripheral metabolism of parathyroid hormone.* N Engl J Med, 1979. **301**(20): p. 1092-8.
63. Abou-Samra, A.B., et al., *Expression cloning of a common receptor for parathyroid hormone and parathyroid hormone-related peptide from rat osteoblast-like cells: a single receptor stimulates intracellular accumulation of both cAMP and inositol trisphosphates and increases intracellular free calcium.* Proc Natl Acad Sci U S A, 1992. **89**(7): p. 2732-6.
64. Raisz, L.G., et al., *Comparison of the effects of a potent synthetic analog of bovine parathyroid hormone with native bPTH-(1-84) and synthetic bPTH-(1-34) on bone resorption and collagen synthesis.* Calcif Tissue Int, 1979. **29**(3): p. 215-8.
65. Potts, J.T., Jr., et al., *Synthesis of a biologically active N-terminal tetratriacontapeptide of parathyroid hormone.* Proc Natl Acad Sci U S A, 1971. **68**(1): p. 63-7.
66. Yasuda, T., et al., *Characterization of the human parathyroid hormone-like peptide gene. Functional and evolutionary aspects.* J Biol Chem, 1989. **264**(13): p. 7720-5.
67. Mangin, M., et al., *Two distinct tumor-derived, parathyroid hormone-like peptides result from alternative ribonucleic acid splicing.* Mol Endocrinol, 1988. **2**(11): p. 1049-55.
68. Chung, U.I., et al., *The parathyroid hormone/parathyroid hormone-related peptide receptor coordinates endochondral bone development by directly controlling chondrocyte differentiation.* Proc Natl Acad Sci U S A, 1998. **95**(22): p. 13030-5.
69. Vortkamp, A., et al., *Regulation of rate of cartilage differentiation by Indian hedgehog and PTH-related protein.* Science, 1996. **273**(5275): p. 613-22.
70. Vilardaga, J.P., et al., *Molecular basis of parathyroid hormone receptor signaling and trafficking: a family B GPCR paradigm.* Cell Mol Life Sci, 2011. **68**(1): p. 1-13.
71. Gardella, T.J. and H. Juppner, *Interaction of PTH and PTHrP with their receptors.* Rev Endocr Metab Disord, 2000. **1**(4): p. 317-29.
72. Luck, M.D., P.H. Carter, and T.J. Gardella, *The (1-14) fragment of parathyroid hormone (PTH) activates intact and amino-terminally truncated PTH-1 receptors.* Mol Endocrinol, 1999. **13**(5): p. 670-80.
73. Vilardaga, J.P., et al., *Measurement of the millisecond activation switch of G protein-coupled receptors in living cells.* Nat Biotechnol, 2003. **21**(7): p. 807-12.

74. Castro, M., et al., *Turn-on switch in parathyroid hormone receptor by a two-step parathyroid hormone binding mechanism.* Proc Natl Acad Sci U S A, 2005. **102**(44): p. 16084-9.
75. Singh, A.T., M.A. Frohman, and P.H. Stern, *Parathyroid hormone stimulates phosphatidylethanolamine hydrolysis by phospholipase D in osteoblastic cells.* Lipids, 2005. **40**(11): p. 1135-40.
76. Singh, A.T., et al., *G alpha12/G alpha13 subunits of heterotrimeric G proteins mediate parathyroid hormone activation of phospholipase D in UMR-106 osteoblastic cells.* Endocrinology, 2005. **146**(5): p. 2171-5.
77. Mahon, M.J., et al., *A docking site for G protein betagamma subunits on the parathyroid hormone 1 receptor supports signaling through multiple pathways.* Mol Endocrinol, 2006. **20**(1): p. 136-46.
78. Nutt, R.F., et al., *Removal of partial agonism from parathyroid hormone (PTH)-related protein-(7-34)NH2 by substitution of PTH amino acids at positions 10 and 11.* Endocrinology, 1990. **127**(1): p. 491-3.
79. Horiuchi, N., et al., *A parathyroid hormone inhibitor in vivo: design and biological evaluation of a hormone analog.* Science, 1983. **220**(4601): p. 1053-5.
80. Carter, P.H., H. Juppner, and T.J. Gardella, *Studies of the N-terminal region of a parathyroid hormone-related peptide (1-36) analog: receptor subtype-selective agonists, antagonists, and photochemical cross-linking agents.* Endocrinology, 1999. **140**(11): p. 4972-81.
81. Friedman, P.A., et al., *Cell-specific signaling and structure-activity relations of parathyroid hormone analogs in mouse kidney cells.* Endocrinology, 1999. **140**(1): p. 301-9.
82. Dean, T., et al., *Mechanisms of ligand binding to the parathyroid hormone (PTH)/PTH-related protein receptor: selectivity of a modified PTH(1-15) radioligand for GalphaS-coupled receptor conformations.* Mol Endocrinol, 2006. **20**(4): p. 931-43.
83. Dean, T., et al., *Altered selectivity of parathyroid hormone (PTH) and PTH-related protein (PTHrP) for distinct conformations of the PTH/PTHrP receptor.* Mol Endocrinol, 2008. **22**(1): p. 156-66.
84. Hoare, S.R., et al., *Conformational states of the corticotropin releasing factor 1 (CRF1) receptor: detection, and pharmacological evaluation by peptide ligands.* Peptides, 2003. **24**(12): p. 1881-97.
85. Perry, S.J., et al., *Targeting of cyclic AMP degradation to beta 2-adrenergic receptors by beta-arrestins.* Science, 2002. **298**(5594): p. 834-6.
86. Okazaki, M., et al., *Prolonged signaling at the parathyroid hormone receptor by peptide ligands targeted to a specific receptor conformation.* Proc Natl Acad Sci U S A, 2008. **105**(43): p. 16525-30.
87. Ferrandon, S., et al., *Sustained cyclic AMP production by parathyroid hormone receptor endocytosis.* Nat Chem Biol, 2009. **5**(10): p. 734-42.
88. Calebiro, D., et al., *Signaling by internalized G-protein-coupled receptors.* Trends Pharmacol Sci, 2010. **31**(5): p. 221-8.
89. Sneddon, W.B., et al., *Ligand-selective dissociation of activation and internalization of the parathyroid hormone (PTH) receptor: conditional efficacy of PTH peptide fragments.* Endocrinology, 2004. **145**(6): p. 2815-23.

90. Gesty-Palmer, D., et al., *Distinct beta-arrestin- and G protein-dependent pathways for parathyroid hormone receptor-stimulated ERK1/2 activation.* J Biol Chem, 2006. **281**(16): p. 10856-64.
91. Ahmed, I., et al., *Transactivation of the epidermal growth factor receptor mediates parathyroid hormone and prostaglandin F2 alpha-stimulated mitogen-activated protein kinase activation in cultured transgenic murine osteoblasts.* Mol Endocrinol, 2003. **17**(8): p. 1607-21.
92. Gentili, C., S. Morelli, and A. Russo De Boland, *Involvement of PI3-kinase and its association with c-Src in PTH-stimulated rat enterocytes.* J Cell Biochem, 2002. **86**(4): p. 773-83.
93. Yamamoto, T., et al., *Parathyroid hormone activates phosphoinositide 3-kinase-Akt-Bad cascade in osteoblast-like cells.* Bone, 2007. **40**(2): p. 354-9.
94. Singh, A.T., et al., *Regulation of parathyroid hormone-stimulated phospholipase D in UMR-106 cells by calcium, MAP kinase, and small G proteins.* J Bone Miner Res, 2003. **18**(8): p. 1453-60.
95. Body, J.J., et al., *A randomized double-blind trial to compare the efficacy of teriparatide [recombinant human parathyroid hormone (1-34)] with alendronate in postmenopausal women with osteoporosis.* The Journal of clinical endocrinology and metabolism, 2002. **87**(10): p. 4528-35.
96. Neer, R.M., et al., *Effect of parathyroid hormone (1-34) on fractures and bone mineral density in postmenopausal women with osteoporosis.* N Engl J Med, 2001. **344**(19): p. 1434-41.
97. Bos, M.P., et al., *Expression of the parathyroid hormone receptor and correlation with other osteoblastic parameters in fetal rat osteoblasts.* Calcif Tissue Int, 1996. **58**(2): p. 95-100.
98. Huang, J.C., et al., *PTH differentially regulates expression of RANKL and OPG.* J Bone Miner Res, 2004. **19**(2): p. 235-44.
99. Nakagawa, N., et al., *RANK is the essential signaling receptor for osteoclast differentiation factor in osteoclastogenesis.* Biochem Biophys Res Commun, 1998. **253**(2): p. 395-400.
100. Simonet, W.S., et al., *Osteoprotegerin: a novel secreted protein involved in the regulation of bone density.* Cell, 1997. **89**(2): p. 309-19.
101. Goltzman, D., *Studies on the mechanisms of the skeletal anabolic action of endogenous and exogenous parathyroid hormone.* Arch Biochem Biophys, 2008. **473**(2): p. 218-24.
102. Ogata, N., et al., *G{alpha}q Signal in Osteoblasts Is Inhibitory to the Osteoanabolic Action of Parathyroid Hormone.* J Biol Chem, 2011. **286**(15): p. 13733-40.
103. Ferrari, S.L. and M.L. Bouxsein, *Beta-arrestin-biased parathyroid hormone ligands: a new approach to the development of agents that stimulate bone formation.* Sci Transl Med, 2009. **1**(1): p. 1ps1.
104. Gesty-Palmer, D. and L.M. Luttrell, *'Biasing' the Parathyroid Hormone Receptor: A Novel Anabolic Approach to Increasing Bone Mass?* Br J Pharmacol, 2011.
105. Tashjian, A.H., Jr. and R.F. Gagel, *Teriparatide [human PTH(1-34)]: 2.5 years of experience on the use and safety of the drug for the treatment of osteoporosis.* Journal of bone and mineral research : the official journal of the American Society for Bone and Mineral Research, 2006. **21**(3): p. 354-65.

106. Rosen, C.J. and J.P. Bilezikian, *Clinical review 123: Anabolic therapy for osteoporosis.* J Clin Endocrinol Metab, 2001. **86**(3): p. 957-64.
107. Rosen, C.J., *The cellular and clinical parameters of anabolic therapy for osteoporosis.* Crit Rev Eukaryot Gene Expr, 2003. **13**(1): p. 25-38.
108. Bohinc, B.N. and D. Gesty-Palmer, *beta-Arrestin-Biased Agonism at the Parathyroid Hormone Receptor Uncouples Bone Formation from Bone Resorption.* Endocr Metab Immune Disord Drug Targets, 2011. **11**(2): p. 112-9.
109. Gesty-Palmer, D., et al., *A beta-arrestin-biased agonist of the parathyroid hormone receptor (PTH1R) promotes bone formation independent of G protein activation.* Sci Transl Med, 2009. **1**(1): p. 1ra1.
110. Kennedy, M.B., *Origin of PDZ (DHR, GLGF) domains.* Trends Biochem Sci, 1995. **20**(9): p. 350.
111. Tsunoda, S., J. Sierralta, and C.S. Zuker, *Specificity in signaling pathways: assembly into multimolecular signaling complexes.* Curr Opin Genet Dev, 1998. **8**(4): p. 419-22.
112. Aronson, P.S., *Role of ion exchangers in mediating NaCl transport in the proximal tubule.* Kidney Int, 1996. **49**(6): p. 1665-70.
113. Schultheis, P.J., et al., *Renal and intestinal absorptive defects in mice lacking the NHE3 Na+/H+ exchanger.* Nat Genet, 1998. **19**(3): p. 282-5.
114. Yun, C.H., et al., *Mammalian Na+/H+ exchanger gene family: structure and function studies.* Am J Physiol, 1995. **269**(1 Pt 1): p. G1-11.
115. Weinman, E.J., D. Steplock, and S. Shenolikar, *CAMP-mediated inhibition of the renal brush border membrane Na+-H+ exchanger requires a dissociable phosphoprotein cofactor.* J Clin Invest, 1993. **92**(4): p. 1781-6.
116. Reczek, D., M. Berryman, and A. Bretscher, *Identification of EBP50: A PDZ-containing phosphoprotein that associates with members of the ezrin-radixin-moesin family.* J Cell Biol, 1997. **139**(1): p. 169--179.
117. Mahon, M.J. and G.V. Segre, *Stimulation by parathyroid hormone of a NHERF-1-assembled complex consisting of the parathyroid hormone I receptor, phospholipase Cbeta, and actin increases intracellular calcium in opossum kidney cells.* J Biol Chem, 2004. **279**(22): p. 23550-8.
118. Seidler, U., et al., *The role of the NHERF family of PDZ scaffolding proteins in the regulation of salt and water transport.* Ann N Y Acad Sci, 2009. **1165**: p. 249-60.
119. Cunningham, R., et al., *Role of NHERF and scaffolding proteins in proximal tubule transport.* Urol Res, 2010. **38**(4): p. 257-62.
120. Wennerberg, K. and C.J. Der, *Rho-family GTPases: it's not only Rac and Rho (and I like it).* J Cell Sci, 2004. **117**(Pt 8): p. 1301-12.
121. Etienne-Manneville, S. and A. Hall, *Rho GTPases in cell biology.* Nature, 2002. **420**(6916): p. 629-35.
122. Brown, J.H., D.P. Del Re, and M.A. Sussman, *The Rac and Rho hall of fame: a decade of hypertrophic signaling hits.* Circ Res, 2006. **98**(6): p. 730-42.
123. Henning, S. and S. Cleverley, *Small GTPases in lymphocyte biology: Rho proteins take center stage.* Immunol Res, 1999. **20**(1): p. 29-42.
124. Ridley, A.J., et al., *Rho family proteins and cell migration.* Biochem Soc Symp, 1999. **65**: p. 111-23.
125. Hornstein, I., A. Alcover, and S. Katzav, *Vav proteins, masters of the world of cytoskeleton organization.* Cell Signal, 2004. **16**(1): p. 1-11.

126. Tamas, P., et al., *Mechanism of epidermal growth factor regulation of Vav2, a guanine nucleotide exchange factor for Rac.* J Biol Chem, 2003. **278**(7): p. 5163-71.
127. Turner, M. and D.D. Billadeau, *VAV proteins as signal integrators for multi-subunit immune-recognition receptors.* Nat Rev Immunol, 2002. **2**(7): p. 476-86.
128. Schuebel, K.E., et al., *Isolation and characterization of murine vav2, a member of the vav family of proto-oncogenes.* Oncogene, 1996. **13**(2): p. 363-71.
129. Han, J., et al., *Role of substrates and products of PI 3-kinase in regulating activation of Rac-related guanosine triphosphatases by Vav.* Science, 1998. **279**(5350): p. 558-60.
130. Henske, E.P., et al., *Identification of VAV2 on 9q34 and its exclusion as the tuberous sclerosis gene TSC1.* Ann Hum Genet, 1995. **59**(Pt 1): p. 25-37.
131. Abe, K., et al., *Vav2 is an activator of Cdc42, Rac1, and RhoA.* J Biol Chem, 2000. **275**(14): p. 10141-9.
132. Liu, B.P. and K. Burridge, *Vav2 activates Rac1, Cdc42, and RhoA downstream from growth factor receptors but not beta1 integrins.* Mol Cell Biol, 2000. **20**(19): p. 7160-9.
133. Pandey, A., et al., *Analysis of receptor signaling pathways by mass spectrometry: identification of vav-2 as a substrate of the epidermal and platelet-derived growth factor receptors.* Proc Natl Acad Sci U S A, 2000. **97**(1): p. 179-84.
134. Tamas, P., Z. Solti, and L. Buday, *Membrane-targeting is critical for the phosphorylation of Vav2 by activated EGF receptor.* Cell Signal, 2001. **13**(7): p. 475-81.
135. Sah, V.P., et al., *The role of Rho in G protein-coupled receptor signal transduction.* Annu Rev Pharmacol Toxicol, 2000. **40**: p. 459-89.
136. Fukuhara, S., H. Chikumi, and J.S. Gutkind, *Leukemia-associated Rho guanine nucleotide exchange factor (LARG) links heterotrimeric G proteins of the G(12) family to Rho.* FEBS Lett, 2000. **485**(2-3): p. 183-8.
137. Fukuhara, S., et al., *A novel PDZ domain containing guanine nucleotide exchange factor links heterotrimeric G proteins to Rho.* J Biol Chem, 1999. **274**(9): p. 5868-79.
138. Mao, J., et al., *Guanine nucleotide exchange factor GEF115 specifically mediates activation of Rho and serum response factor by the G protein alpha subunit Galpha13.* Proc Natl Acad Sci U S A, 1998. **95**(22): p. 12973-6.
139. Moolenaar, W.H., *Bioactive lysophospholipids and their G protein-coupled receptors.* Exp Cell Res, 1999. **253**(1): p. 230-8.
140. Vogt, S., et al., *Receptor-dependent RhoA activation in G12/G13-deficient cells: genetic evidence for an involvement of Gq/G11.* J Biol Chem, 2003. **278**(31): p. 28743-9.
141. Lutz, S., et al., *The guanine nucleotide exchange factor p63RhoGEF, a specific link between Gq/11-coupled receptor signaling and RhoA.* J Biol Chem, 2005. **280**(12): p. 11134-9.
142. Lutz, S., et al., *Structure of Galphaq-p63RhoGEF-RhoA complex reveals a pathway for the activation of RhoA by GPCRs.* Science, 2007. **318**(5858): p. 1923-7.
143. Shankaranarayanan, A., et al., *Galpha q allosterically activates and relieves autoinhibition of p63RhoGEF.* Cell Signal, 2010. **22**(7): p. 1114-23.
144. Ming, W., et al., *The Rac effector p67phox regulates phagocyte NADPH oxidase by stimulating Vav1 guanine nucleotide exchange activity.* Mol Cell Biol, 2007. **27**(1): p. 312-23.

145. Lawson, C.D., et al., *P-Rex1 and Vav1 cooperate in the regulation of formyl-methionyl-leucyl-phenylalanine-dependent neutrophil responses.* J Immunol, 2011. **186**(3): p. 1467-76.
146. Kuder, K. and K. Kiec-Kononowicz, *Fluorescent GPCR ligands as new tools in pharmacology.* Current medicinal chemistry, 2008. **15**(21): p. 2132-43.
147. Albizu, L., et al., *Time-resolved FRET between GPCR ligands reveals oligomers in native tissues.* Nat Chem Biol, 2010. **6**(8): p. 587-94.
148. Alpha, B., J.M. Lehn, and G. Mathis, *Energy-Transfer Luminescence of Europium(Iii) and Terbium(Iii) Cryptates of Macrobicyclic Polypyridine Ligands.* Angewandte Chemie-International Edition in English, 1987. **26**(3): p. 266-267.
149. Bazin, H., E. Trinquet, and G. Mathis, *Time resolved amplification of cryptate emission: a versatile technology to trace biomolecular interactions.* J Biotechnol, 2002. **82**(3): p. 233-50.
150. de Jong, L.A., et al., *Receptor-ligand binding assays: technologies and applications.* J Chromatogr B Analyt Technol Biomed Life Sci, 2005. **829**(1-2): p. 1-25.
151. Gagne, A., P. Banks, and S.D. Hurt, *Use of fluorescence polarization detection for the measurement of fluopeptidetm binding to G protein-coupled receptors.* J Recept Signal Transduct Res, 2002. **22**(1-4): p. 333-43.
152. Albizu, L., et al., *Toward efficient drug screening by homogeneous assays based on the development of new fluorescent vasopressin and oxytocin receptor ligands.* J Med Chem, 2007. **50**(20): p. 4976-85.
153. Zwier, J.M., et al., *A fluorescent ligand-binding alternative using Tag-lite(R) technology.* J Biomol Screen, 2010. **15**(10): p. 1248-59.
154. Leyris, J.P., et al., *Homogeneous time-resolved fluorescence-based assay to screen for ligands targeting the growth hormone secretagogue receptor type 1a.* Anal Biochem, 2011. **408**(2): p. 253-62.
155. Jou, W.M., et al., *Complete structure of the hemagglutinin gene from the human influenza A/Victoria/3/75 (H3N2) strain as determined from cloned DNA.* Cell, 1980. **19**(3): p. 683-96.
156. Guan, X.M., T.S. Kobilka, and B.K. Kobilka, *Enhancement of membrane insertion and function in a type IIIb membrane protein following introduction of a cleavable signal peptide.* J Biol Chem, 1992. **267**(31): p. 21995-8.
157. Chen, C. and H. Okayama, *High-efficiency transformation of mammalian cells by plasmid DNA.* Mol Cell Biol, 1987. **7**(8): p. 2745-52.
158. Laemmli, U.K., *Cleavage of structural proteins during the assembly of the head of bacteriophage T4.* Nature, 1970. **227**(259): p. 680-5.
159. Shevchenko, A., et al., *Mass spectrometric sequencing of proteins silver-stained polyacrylamide gels.* Anal Chem, 1996. **68**(5): p. 850-8.
160. Vilardaga, J.P., et al., *Internalization determinants of the parathyroid hormone receptor differentially regulate beta-arrestin/receptor association.* J Biol Chem, 2002. **277**(10): p. 8121-9.
161. Vilardaga, J.P., et al., *Differential conformational requirements for activation of G proteins and the regulatory proteins arrestin and G protein-coupled receptor kinase in the G protein-coupled receptor for parathyroid hormone (PTH)/PTH-related protein.* J Biol Chem, 2001. **276**(36): p. 33435-43.
162. Fukuhara, S., H. Chikumi, and J.S. Gutkind, *RGS-containing RhoGEFs: the missing link between transforming G proteins and Rho?* Oncogene, 2001. **20**(13): p. 1661-8.

163. Booden, M.A., D.P. Siderovski, and C.J. Der, *Leukemia-associated Rho guanine nucleotide exchange factor promotes G alpha q-coupled activation of RhoA.* Mol Cell Biol, 2002. **22**(12): p. 4053-61.
164. Klenk, C., et al., *Formation of a ternary complex among NHERF1, beta-arrestin, and parathyroid hormone receptor.* J Biol Chem, 2010. **285**(39): p. 30355-62.
165. Jin, L., et al., *Crystal structure of human parathyroid hormone 1-34 at 0.9-A resolution.* J Biol Chem, 2000. **275**(35): p. 27238-44.
166. Rosenblatt, M. and J.T. Potts, Jr., *Design and synthesis of parathyroid hormone analogues of enhanced biological activity.* Endocr Res Commun, 1977. **4**(2): p. 115-33.
167. Dicker, F., et al., *Phosphorylation-independent inhibition of parathyroid hormone receptor signaling by G protein-coupled receptor kinases.* Proc Natl Acad Sci U S A, 1999. **96**(10): p. 5476-81.
168. Nagasaki, K., et al., *In vitro and in vivo antagonists against parathyroid hormone-related protein.* Biochem Biophys Res Commun, 1989. **158**(3): p. 1036-42.
169. Gardella, T.J., et al., *Transmembrane residues of the parathyroid hormone (PTH)/PTH-related peptide receptor that specifically affect binding and signaling by agonist ligands.* J Biol Chem, 1996. **271**(22): p. 12820-5.
170. Castro, M., et al., *Dual regulation of the parathyroid hormone (PTH)/PTH-related peptide receptor signaling by protein kinase C and beta-arrestins.* Endocrinology, 2002. **143**(10): p. 3854-65.
171. Ardura, J.A., et al., *Dynamic Na+-H+ exchanger regulatory factor-1 association and dissociation regulate parathyroid hormone receptor trafficking at membrane microdomains.* J Biol Chem, 2011.
172. Faccio, R., et al., *Vav3 regulates osteoclast function and bone mass.* Nat Med, 2005. **11**(3): p. 284-90.
173. Kupcho, K.R., et al., *Simultaneous monitoring of discrete binding events using dual-acceptor terbium-based LRET.* J Am Chem Soc, 2007. **129**(44): p. 13372-3.

9. Annex

Acknowledgments

I am gratefully indebted to Prof. Dr. Martin J. Lohse for the initialization and the supervision of this PhD thesis.
I am grateful to Prof. Dr. Michael Sendtner his support and for acting as the chairperson.
For her technical support and the enjoyable companionship, I am immensely thankful to Michaela Hoffmann.
I am particularly thankful to Dr. Christoph Klenk for supervision of this work and stimulating discussions.
For advises and support I am very grateful to Prof. Dr. Antje Gohla and Dr. Elisabeth Jeanclos.
I would like to thank Prof. Dr. Caroline Kisker and Prof. Dr. Thomas Müller for supervision and helpful advises.
For their professional technical support on projects that were not part of this thesis, I would like to thank Christian Dees and Annette Hannawacker.
I am very grateful to Dr. Asparouh Iliev and Dr. Ulrike Zabel for scientific advices and numerous lively debates.
My special thanks go to four workmates at the Department of Pharmacology. I am very grateful to them for motivating me and especially for the close friendship. Thank you, Marie, Manuela, Anni and Gunnar (for 12/02/11).
Finally, I would like to thank all colleagues of the Department of Pharmacology and Toxicology, as well as the Rudolf Virchow Center for the support and companionship.

Cooperation

Labeling of PTH analogues was achieved in cooperation with Cis bio (Marcoule, France). In addition, homogeneous time-resolved fluorescence ligand-binding studies, by tag-lite®, technology were obtained in cooperation with Cis bio GmbH.
Mass spectrometry analyses were performed in cooperation with Dr. Henning Urlaub, Bioanalytical Mass Spectrometry Group, Max Planck Institute for Biophysical Chemistry, Göttingen.

Publications

Emami-Nemini A., Gohla A., Urlaub H., Lohse M. J., Klenk C. (2012). *The guanine nucleotide exchange factor vav2 is a negative regulator of PTH-receptor / G_q-signaling*. Department of Pharmacology and Toxicology, Julius-Maximilian's-University of Würzburg. Mol Pharmacol; published ahead of print May 3, 2012.

International symposia and published conference participations

19 - 22 Mar 2012; **Conference of the *Deutsche Gesellschaft für experimentelle und klinische Pharmakologie und Toxikologie* (DGPT)**; Dresden, Germany
Contribution: Poster
Emami-Nemini A., Roux T., Leblay M., Bourrier E., Lamarque L., Trinquet E., Lohse M. J. (2012). *Time-resolved fluorescence ligand-binding assays for parathyroid hormone receptors*. Naunyn-Schmiedeberg´s Arch Pharmacol Volume 385, Number 1, page S24.

28 – 30 Jul 2011; **The International Symposium Molecular Pharmacology of Receptors, Channels and Transporters**; Sonderforschungsbereich 487, Würzburg, Germany
Contribution: Poster
Emami-Nemini A., Roux T., Leblay M., Bourrier E., Lamarque L., Trinquet E., Lohse M. J.. *Time-resolved fluorescence ligand-binding assays for parathyroid hormone receptors*.

30 Mar – 01 Apr 2011; **Conference of the *Deutsche Gesellschaft für experimentelle und klinische Pharmakologie und Toxikologie* (DGPT)**; Frankfurt, Germany
Contribution: Poster
Emami-Nemini A., Urlaub H., Lohse M.J., Klenk C. (2011). *The guanine nucleotide exchange factor vav2 acts as an adaptor for parathyroid hormone receptor signaling*. Naunyn-Schmiedeberg´s Arch Pharmacol Volume 381, Number 3, page 21-22.

Klenk C., **Emami-Nemini A.**, Lohse M. J. (2011). *Implications of the proteolytic cleavage of the extracellular domain of parathyroid hormone receptor 1*. Naunyn-Schmiedeberg´s Arch Pharmacol Volume 381, Number 3, page 70-71.

9 – 14 Jan 2011; **Gordon Research Conference (GRC) on Molecular Pharmacology**, Ventura, USA

Contribution: Poster

Emami-Nemini A., Urlaub H., Lohse M.J., Klenk C. *The guanine nucleotide exchange factor vav2 acts as an adaptor for parathyroid hormone receptor signaling*.

23 – 25 Mar 2010; **Conference of the *Deutsche Gesellschaft für experimentelle und klinische Pharmakologie und Toxikologie* (DGPT)**; Mainz, Germany

Contribution: Talk

Emami-Nemini A.D., Klenk C., Pérez Aso M., Urlaub H., Lohse M.J. (2010). *Identification of novel parathyroid hormone receptor interacting proteins*. Naunyn-Schmiedeberg´s Arch Pharmacol Volume 383, Number 4: page 12.

Deiss K., Fischer M., **Emami A.**, Lohse M.J., Lorenz K. (2010). *The substrate switch of RKIP from Raf1 to GRK2 involves RKIP-phosphorylation and –oligomerization*. Naunyn-Schmiedeberg´s Arch Pharmacol Volume 383, Number 4: page 31.

9 - 10 Oct 2009; **The GPCR Dimer Symposium**; Würzburg; Germany

Contribution: Poster

Emami-Nemini A., Klenk C., Pérez Aso M., Zahedi R.P., Lohse M.J. *Identification of novel parathyroid hormone receptor interacting proteins*.

Affidavit

I hereby confirm that my thesis entitled “Differential parathyroid hormone receptor signaling directed by adaptor proteins” is the result of my own work. I did not receive any help or support from commercial consultants. All sources and / or materials applied are listed and specified in the thesis.

Furthermore, I confirm that this thesis has not yet been submitted as part of another examination process neither in identical nor in similar form.

Würzburg,

Eidesstattliche Erklärung

Hiermit erkläre ich an Eides statt, die Dissertation „Steuerung differenzieller Signalgebung des Parathormon Rezeptors durch Adapterproteine“ eigenständig, d.h. insbesondere selbständig und ohne Hilfe eines kommerziellen Promotionsberaters, angefertigt und keine anderen als die von mir angegebenen Quellen und Hilfsmittel verwendet zu haben.

Ich erkläre außerdem, dass die Dissertation weder in gleicher noch in ähnlicher Form bereits in einem anderen Prüfungsverfahren vorgelegen hat.

Würzburg,

Trademarks and legal wording

HTRF® and Tag-lite® are registered trademarks of Cisbio Bioassays. Lumi4® (here named as Tb^{3+}-cryptate) is a registered trademark of Lumiphore, Inc. SNAP-tag® is a trademark of News England Biolabs, Inc.

Copyright

This thesis contains scientific data that is used for manuscripts which are in progress for publication in international peer-reviewed journals.